Energy Conversion and Management 366 (2026) 121856

Contents lists available at ScienceDirect

Energy Conversion and Management

journal homepage: www.elsevier.com/locate/enconman

Research Paper

Exploring the flexibility potential of office building with air-to-water heat pumps in the Mediterranean climate

Maurizio La Villetta [*], Pietro Catrini, Antonio Piacentino

Department of Engineering, University of Palermo, Viale Delle Scienze, Palermo, Italy

ARTICLE INFO

Keywords:
Demand-side management
Air-to-water heat pump
Photovoltaic-battery system
Human comfort
TRNSYS
IMST-ART

ABSTRACT

Buildings account for a significant share of energy consumption, making heat pumps and renewable energy key solutions for decarbonization. However, the variability of renewables poses challenges to grid stability and reliability. In this context, heat pumps, when coupled with other renewable systems, offer substantial potential for demand response programs by modulating their electricity consumption according to external signals such as energy prices and grid constraints. This study investigates the potential of demand response programs in a tertiary sector building. A dynamic simulation was conducted in TRNSYS, accurately modeling building envelopes with different insulation levels, the multi-stage heat pump, the photovoltaic-battery system and their integrated controls. The analysis evaluates both price-based and photovoltaic-driven demand response strategies by dynamically and statically varying the temperature setpoints of the thermal zones and the thermal energy storage. Four strategies are assessed against a reference scenario, and their impacts on electricity consumption and human comfort are evaluated. The most effective demand response approach is achieved by combining thermal energy storage setpoint adjustments with the enhanced insulation configuration and night-time ventilation, increasing annual acceptable thermal comfort to 81.22% and reducing annual electricity consumption by up to 28.22%. When coupled with a photovoltaic-battery system, the interaction between on-site solar generation and optimized thermal loads further enhances grid benefits, achieving a reduction in annual electricity drawn from the grid of up to 59.89%. These findings demonstrate the potential of integrated solutions for grid flexibility with limited comfort impacts.

1. Introduction

The building sector represents a major share of global energy consumption [1]. In 2023, it exceeded 120 EJ, accounting for 28% of global final energy. Between 2010 and 2023, demand increased at an average annual rate of 0.9%, and it is projected to surpass 130 EJ by 2030 [2]. The United States (US), the European Union (EU), and China collectively accounted for nearly half of the total building energy use in 2023. The European Commission reports that buildings are responsible for approximately 40% of the total energy, making them the largest contributors to final energy consumption across member states [3]. Electricity demand in buildings is expected to rise significantly due to improved living conditions, greater access to energy, and the growing use of household electrical devices [4]. The EU has highlighted electric heating, particularly through the deployment of Heat Pumps (HPs) and the use of Renewable Energy Sources (RES), as an essential measure to lower dependence on fossil fuels [5], and support the decarbonization of the building sector [6]. However, a growing share of distributed RES in the energy mix may compromise the reliability of the power system due to their variable and weather-dependent output [7]. High RES penetration levels are likely to introduce frequent fluctuations in electricity supply [8], making it more difficult to maintain grid stability and match energy production with consumption [9]. Furthermore, the increasing use of HPs and the shift toward electric mobility are expected to cause a notable increase in electricity demand, further challenging the resilience of the grid [10]. Without proper management, such changes could place considerable strain on the electrical grid and jeopardize the reliability of the power supply.

In this context, Demand-Side Management (DSM), combined with the intelligent operation of electrical devices, can improve energy efficiency and contribute to the reliability of the power grid [11]. When integrated into smart systems, certain appliances can also provide operational flexibility by enabling Demand Response (DR) strategies. Through digitalisation, these devices evolve from passive energy consumers to active, controllable loads that support grid stability and

* Corresponding author.
E-mail address: maurizio.lavilletta@unipa.it (M. La Villetta).

https://doi.org/10.1016/j.enconman.2026.121856

Available online 11 July 2026

Nomenclature

Acronyms/abbreviations

ACs	Air Conditioners
ASHP	Air-Source Heat Pump
BOPTEST	Building Optimization Testing Framework platform
COP	Coefficient of Performance
CTZ	Core Top Zone
DDR	Direct Demand Response
DHCN	District heating and cooling network
DR	Demand Response
DSM	Demand-Side Management
DSO	Distribution System Operator
EU	European Union
EPSC+	Extended Price Storage Control+
GTA	Grid-Triggered Adjustment
GSHP	Ground Source Heat Pump
HPs	Heat Pumps
HVAC	Heating, Ventilation, and Air Conditioning
IDR	Indirect Demand Response
ICFs	Insulated Concrete Forms
INS	Well-insulated building
MEF	Marginal Emission Factors
MLP	Multi-Layer Perceptron
MLR	Multiple Linear Regression
NB	Bottom Node of Thermal Energy Storage
NT	Top Node of Thermal Energy Storage
PSO	Particle Swarm Optimization
PMV	Predicted Mean Vote
PPD	Predicted Percentage Dissatisfied
PTZ	Perimeter Top Zone
PV	Photovoltaic plant
PV-B	Photovoltaic-Battery system
RES	Renewable Energy Source
RC	Resistance-Capacitance model
TES	Thermal Energy Storage
SAHP	Solar-Assisted Heat Pump
SVR	Support Vector Regression
ToU	Time-of-Use tariffs
VRE	Variable Renewable Energy
WWR	Window-Wall-Ratio
w/o PV	DR strategy referred to a poorly insulated building without the PV-battery system
w/o PV (INS)	DR strategy referred to a well-insulated building without the PV-battery system
w PV	DR strategy referred to a poorly insulated building with the PV-battery system
w PV (INS)	DR strategy referred to a well-insulated building with the PV-battery system

Variables

ACH	Air Changes per Hour (h^{-1})
CC	Cooling Capacity (kW_{frig})
CCR	Comfort Compliance Ratio (%)
COP	Coefficient Of Performance (-)
EER	Energy Efficiency Ratio (-)
E_t^{DR}	Energy consumption in the range $t = 0 - 8760$ h when the DR programs are in place (kWh)
E_t^{NODR}	Energy consumption in the range $t = 0 - 8760$ without DR programs (kWh)
HC	Heating Capacity (kW_{th})
I_0	Diode reverse saturation current (A)
I_L	Light current [A]
IDBT	Indoor Dry Bulb Temperature (°C)
IRH	Indoor Relative Humidity (%)
$K_{1,HC}$	Fitting coefficient for N_{CMP}, referred to the electric power in heating mode
$K_{2,HC}$	Fitting coefficient for *ODT*, referred to the electric power in heating mode
$K_{3,HC}$	Fitting coefficient for $T_{wr,CND}$, referred to the electric power in heating mode
$K_{1,CC}$	Fitting coefficient for N_{CMP}, referred to the electric power in cooling mode
$K_{2,CC}$	Fitting coefficient for *ODT*, referred to the electric power in cooling mode
$K_{3,CC}$	Fitting coefficient for $T_{wr,EVP}$, referred to the electric power in cooling mode
KPIs	Key Performance Indicators
KPI_{min}	Minimum value of KPI evaluated for *CCR*, $VarP_{t\_max}$, $VarP_{t\_max}$ and $Var\Delta t_{s\_last}$ across all investigated DR strategies (-)
KPI_{MAX}	Maximum value of KPI evaluated for *CCR*, $VarP_{t\_max}$, $VarP_{t\_max}$ and $Var\Delta t_{s\_last}$ across all investigated DR strategies (-)
KPI_{NORM}	Normalized key performance indicator evaluated for *CCR*, $VarP_{t\_max}$, $VarP_{t\_max}$ and $Var\Delta t_{s\_last}$ across all investigated DR strategies (-)
$L_{1,HC}$	Fitting coefficient for N_{CMP}, referred to heating capacity
$L_{2,HC}$	Fitting coefficient for *ODT*, referred to heating capacity
$L_{3,HC}$	Fitting coefficient for $T_{wr,CND}$, referred to heating capacity
$L_{1,CC}$	Fitting coefficient for N_{CMP}, referred to cooling capacity
$L_{2,CC}$	Fitting coefficient for *ODT*, referred to cooling capacity
$L_{3,CC}$	Fitting coefficient for $T_{wr,CND,EVP}$, referred to cooling capacity
N	Number of time steps in the daytime considered
N_{CMP}	Number of compressors
ODT	Dry-Bulb Temperature of the outdoor air (°C)
$P_{m,H}$	Electric power for an air-to-water HP (heating) (kW_{el})
$P_{m,C}$	Electric power for an air-to-water HP (cooling) (kW_{el})
P_t^{DR}	Maximum power consumption in the heating and cooling seasons when the DR is in place (kW_{el})
P_t^{NODR}	Power consumption at the time step *t* without DR programs (kW_{el})
$P_{t\_max}^{DR}$	Maximum power consumption in the heating and cooling seasons when the DR is in place (kW_{el})
$P_{t\_max}^{NODR}$	Maximum power consumption in the heating and cooling seasons in the reference case (kW_{el})
PMV_t^{DR}	Predicted Mean Vote evaluated from the corresponding instantaneous values at each time step *t* (-)
$PMV_{t\_mean}^{DR}$	Predicted Mean Vote evaluated over the daytime period comprising *N* time steps with DR (-)
$PMV_{t\_mean}^{NODR}$	Predicted Mean Vote evaluated over the daytime period comprising *N* time steps without any DR programs implemented (-)
PPD_t^{DR}	Predicted Percentage Dissatisfied evaluated from the corresponding instantaneous values at each time step *t* (-)
$PPD_{t\_mean}^{DR}$	Predicted Percentage Dissatisfied evaluated over the daytime period comprising *N* time steps with DR (%)
$PPD_{t\_mean}^{NODR}$	Predicted Percentage Dissatisfied evaluated over the daytime period comprising *N* time steps without any DR programs implemented (%)
PUN	Prezzo Unico Nazionale (€/MWh)
$\overline{PUN}$	Average value of Prezzo Unico Nazionale (€/MWh)
RH	Indoor Relative Humidity of the zone (%)
R_s	Series resistance (Ω)
R_{sh}	Shunt resistance (Ω)
$SCOP_{,T}$	Seasonal Coefficient of Performance (-)
$SEER_{,T}$	Seasonal Energy Efficiency Ratio (-)

SoC	State Of Charge (%)
t	Simulation time step (h)
T	Total analysed period over the same time span (h)
$t^{DR}_{s\_last}$	Latest hour obtained from electricity load duration curve when DR is in place (h)
$t^{NODR}_{s\_last}$	Latest hour obtained from electricity load duration curve without any DR (h)
$T_{set\text{-}TES}$	Set-point temperatures detected on NT in the heating season and in NB in the cooling season (°C)
$T_{set\text{-}th.zone}$	Set-point temperatures for heating or cooling of i-th air node (°C)
$T_{wr,CND}$	Temperature of the water returning from the building and entering the HP's condenser (°C)
$T_{wr,EVP}$	Temperature of the water returning from the building and entering the HP's evaporator (°C)
$VarP_{t\_max}$	Peak load shifting potential (%)
$VarE^{DR}_{t}$	Cumulative load shifting potential (%)
Var_{SCOP}	Annual season coefficient of performance variation (%)
Var_{SEER}	Annual season energy efficiency ratio variation (%)
$Var\Delta t_{s\_last}$	Variance percentage of time shifting (%)
x	Required degree of flexibility (%)
Greek Letters	
α	Ideality factor [-]
δ_t	Number of time steps t (or hours) during which the human comfort satisfies the criterion $PPD_t \leq 10\%$ (h)
Δt_{s_last}	Time shifting (h)
ΔT_{SP}	Setpoint variation of thermal zones according to PUN profile (°C)
ΔT_{SP_winter}	Setpoint variation of thermal zones in winter according to PUN profile (°C)
ΔT_{SP_summer}	Setpoint variation of thermal zones in summer according to PUN profile (°C)
Subscripts/superscript	
annual	Referred to the whole year
C	Referred to cooling
CMP	Referred to compressor
CND	Referred to condenser
EVP	Referred to evaporator
frig	Referred to fridge
H	Referred to heating
mean	Referred to the mean value evaluated over the daytime period comprising N time steps
NORM	Referred to the normalized KPIs
s_last	Referred to the time shifting
sp	Referred to setpoint variation
SP,summer	Referred to set-point of thermal zone in summer season
SP,winter	Referred to set-point of thermal zone in winter season
t	Referred to the time step used in the dynamic simulation
t_max	Referred to the maximum power
wr	Referred to water returning

enhance energy security. The smart and efficient use of electrical appliances thus plays a key role in improving system performance and reducing energy demand. This potential is especially evident in the building sector, where integrating digital technologies could lower energy use by as much as 30-40% [12]. When network-connected, devices such as those for Heating, Ventilation, Air Conditioning (HVAC), and water heating, both with HPs, can also enhance system flexibility by participating in DR schemes. Their energy consumption can be adjusted, either increased, decreased, or delayed, based on the needs of the electricity grid [13], helping to ease peak demand and maintain grid stability [14]. As a result, digitalisation allows modern electrical devices to become active, responsive loads that support energy security rather than strain the power system [12]. HVAC systems represent a key opportunity for DR in both commercial and residential buildings. They can be controlled via thermostats without compromising occupant comfort [15], especially when buildings are well-insulated [16] or equipped with Thermal Energy Storage (TES) systems [7]. Appliances that generate cyclical loads, such as HPs and Air Conditioners (ACs), can be temporarily reduced or set to different temperatures for brief periods (ranging from several minutes to a few hours), providing grid services like peak shaving or load shifting. These technologies are increasingly acknowledged for their capability to support DR strategies that facilitate the integration of Variable Renewable Energy (VRE) sources [17], by enabling load modulation during periods of surplus renewable electricity generation [18]. Similarly, HP-based preheating and precooling strategies leverage the thermal inertia of buildings to temporally shift energy demand toward grid-favorable operating conditions [19]. The flexibility provided by HPs is often enabled through smart meters that respond to dynamic pricing models like Time-of-Use tariffs (ToU) or through financial incentives offered to users who take part in DR programs. In particular, DR relies on sending economic signals to consumers to encourage modifications in their expected electricity consumption. By reacting to these signals, consumers offer flexibility services to grid operators, supporting functions such as congestion management, grid stability, fast frequency regulation, and reserve capacity. Depending on the nature of the signal, DR can be classified into Indirect Demand Response (IDR) and Direct Demand Response (DDR) [20]. IDR is a continuous demand-side management approach based on time-varying price signals that guide consumption toward periods of lower demand and/or higher renewable generation. Its main objectives include peak shaving and valley filling actions, contributing to reduced stress on distribution networks and increased use of local renewable energy. Conversely, DDR operates on an event-based basis through one-off incentive signals. In many countries, including those in the European Union, regulatory frameworks prevent grid operators from sending DDR signals directly to consumers. As a result, these incentives are issued through trading processes within flexibility markets [20].

Ongoing digitization is expected to accelerate the widespread deployment of smart buildings and HVAC systems combined with renewable energy sources, enabling them to act as flexible assets for the power grid by supporting load shifting, renewable integration, and grid-balancing services within a grid-interactive framework.

1.1. Literature review

The literature review focuses on studies investigating DR strategies in buildings equipped with HPs and TES systems, including their integration with RESs. The review is organised around four main themes: (i) the flexibility potential of DR strategies, (ii) the implementation of DR through dynamic pricing schemes, (iii) the impact of DR on occupants' thermal comfort, and (iv) DR applications in buildings operating under Mediterranean climate conditions.

A significant portion of the existing literature has examined the impact of DR in buildings on peak load reduction, electricity consumption, and cost savings through the use of HPs, often in combination with other RESs. Gao et al.[21] investigated the thermal imbalance and optimal operation of a hybrid Ground Source Heat Pump (GSHP) system in cold-winter and hot-summer climates using validated models and multi-objective optimization. The results showed that optimized DR strategies improve efficiency and limit ground thermal imbalance compared to continuous operation. Meng et al. [22] examined DR programs in both heating and cooling modes using an Air Source Heat Pump (ASHP) combined with a TES. Experimental results showed that flexible tank control reduces ASHP cycling, stabilizes return water temperature, and enables effective peak load shedding, demonstrating that small-scale thermal storage can improve both system efficiency and grid flexibility. Dengiz et al. [23] investigated HPs as flexible resources for power systems, proposing heuristic control strategies within a hybrid centralised-decentralised architecture to reduce heating costs and surplus energy in residential applications. Simulations showed that these methods reduce heating costs by 4.1-13.3% and surplus energy by 38.3-52.6%. Müller et al. [24] studied a large-scale DR program with over 300 residential buildings equipped with HPs. The results showed that controlled heat pump throttling achieves load reductions of 40-65% with high accuracy, maintaining a median absolute percentage error below 7%. Zhang et al. [25] analysed the DR flexibility of aggregated residential HPs in highly electrified future power systems. Using dedicated control algorithms and flexibility metrics that respect comfort constraints, they showed that flexibility and rebound effects depend on building thermal inertia, minimal in high-inertia homes and significant in low-inertia ones, while hybrid electric-gas heating reduces both energy payback and comfort loss. Kutlu et al. [26] investigated a Solar-Assisted Heat Pump (SAHP) system with controllable phase change material storage to shift demand from peak hours to periods of high solar availability. Component modelling was performed using quasi-steady-state assumptions for the collectors, simplified thermodynamic representations for the HP, and a detailed building thermal model developed in the integrated environmental solutions virtual environment platform, with overall system simulations implemented in MATLAB using real weather data. Results show that the control strategy efficiently manages storage charging and discharging, achieving a weekly Coefficient of Performance (COP) of 3.56 and reducing peak electricity consumption to 28.5% of total demand. Vivian et al. [27] analyzed the impact of heating electrification on distribution grids and evaluated a centralized optimization strategy for coordinating residential HPs with TES. The buildings were modeled using a modified lumped-capacitance approach based on ISO 13790, while the HP and TES were represented with simplified equations that capture their essential thermal and operational behaviour. Simulations showed peak reductions of up to 21% for space heating and 35% when including hot water storage, highlighting the effectiveness of coordinated control in mitigating grid stress. Koch et al. [28] investigated the use of HPs for frequency control as an advanced DR strategy. Single-zone residential building models implemented in the Building Optimization Testing Framework platform (BOPTEST) were used, and predictive control based on thermostat setpoints enabled flexible participation. Two-month simulation results indicated that 57-59% of the energy was available for flexibility, with tracking errors of 12-14%, while the integration of local batteries and the aggregation of multiple buildings significantly reduced these errors. Li et al. [29] analysed the importance of accounting for both building and air-conditioning system thermal inertia to enhance DR strategies in commercial buildings. The proposed DR strategy achieved up to 16.74% additional peak load reduction through on-off control and 1.93% via chilled water temperature control. Yin et al. [30] applied an optimized pre-cooling approach across 11 office buildings in a hot Californian climate, resulting in peak demand reductions ranging from 2.15 to 12.16 W/m^2, with the most effective method involving pre-cooling combined with a linear temperature reset. Zhao et al. [31] experimentally evaluated nine HVAC demand response strategies, including temperature reset, pre-cooling, active energy storage, and equipment control, using both physical tests on a central air-conditioning system and TRNSYS simulations [32]. Results showed that integrating a buffer tank reduces HP cycling from 46 to 6 times, while thermal inertia allows DR participation for 40-50 minutes with a power reduction of 8.9%-12.6%. Simulations reveal that active storage can extend DR participation to 120 minutes, cut peak power by 23.4%, and lower operating costs by 21.7%. Chen et al. [33] proposed two DR control strategies (pre-cooling, temperature setpoint adjustment with passive cooling and active storage) implemented through HVAC systems, aiming to assess their effectiveness in shifting cooling loads. The results demonstrate that the pre-cooling strategy effectively reduces load demand during the DR event and extends the chiller's off-cycle, while still satisfying the thermal comfort requirement. Liu et al. [34] examined the impact of DR strategies in an office building, considering the coordination between the alternating current system and a photovoltaic (PV) installation. Simulations indicate that the implemented DR measures reduce peak power by 45.2% while increasing the building's self-sufficiency and self-consumption ratios to 0.83 and 0.91, respectively. Lu et al. [35] investigated the potential for energy flexibility in nearly zero-energy office buildings equipped with HPs, considering factors such as building thermal mass, internal heat gains, and cooling systems. Results showed that an optimized control strategy can lower peak power by 55.6% during occupied hours and reduce peak energy consumption by 54.0%. Keskar et al. [36] analysed load-shifting DR via global thermostat adjustments, which reduces renewable energy curtailment while maintaining indoor temperature and humidity within occupant comfort limits. Key results indicate that fan power response increases with larger setpoint variations. However, because the response is asymmetric, being stronger during setpoint decreases than during increases, additional fan energy consumption occurs, particularly during symmetrical down-up setpoint adjustment events.

Other studies have investigated DR programs for HPs based on dynamic pricing schemes. In this respect, Kim and Braun [37] implemented a model predictive control strategy under different ToU scenarios to shift loads in commercial buildings with staged Rooftop Units (RTU), achieving more than 30% reduction in HVAC demand and 40% reduction during peak periods, while overall energy savings remained under 10%. Rocca et al. [20] presented an optimal scheduling framework for district-level HPs within energy management systems, addressing both IDR and DDR schemes. Using quadratic programming, the method was tested on real data, showing that IDR enables peak shaving and valley filling (reductions up to 13-34%), while DDR allows flexible load adjustments, with peak and average consumption varying significantly depending on flexibility prices, and moderate impacts on total energy costs. Söderholm et al. [38] assessed the DR potential of grocery stores by coordinating refrigeration and HP systems under variable Nord Pool spot prices. Exploiting thermal storage in refrigerated goods and heating buffers, their strategy achieved 5-13% annual cost savings, with a modest increase in winter electricity use and reduced district heating demand. Simulations showed that coordinated control and optimized heat recovery improved both economic performance and overall energy system efficiency. Wang et al. [39] analysed an optimal water temperature scheduling strategy to improve the DR capability of ASHPs under ToU tariffs. The approach combines a Resistance-Capacitance (RC)-based room thermal model with a fan coil and an artificial neural network-based model of the ASHP. Field tests in Beijing (China) showed that the proposed strategy significantly increases flexibility and reduces heating costs by 20.8-43%. Gradwohl et al. [40] assessed the theoretical potential of flexible HP operation in decentralised energy systems using a multi-objective optimisation model that minimises energy costs and grid stress. A data-driven household energy system with HPs, PV system, thermal and electrical storage was analysed across diverse buildings and load profiles, showing that day-ahead price-based DR effectively reduces costs and grid peaks, with HPs and TES delivering the greatest flexibility. Kovačević et al. [41] introduced the so-called Extended Price Storage Control+ (EPSC+) strategy for the flexible operation of clustered building heating systems under high renewable penetration. Buildings were represented using reduced-order RC thermal models, while HPs were described through simplified models allowing modulation between 20% and 100%. Winter simulations on a ten-building German cluster showed that the strategy shifts space heating and domestic hot water demand under dynamic pricing, reducing median peak load by 38.8% and electricity costs by 15%. Wang et al. [42] investigated the DR potential of SAHP drying systems under dynamic electricity pricing. The drying chamber heat demand was modeled using an RC network based on drying kinetics and equivalent thermal parameters, while a virtual energy storage model represents thermal flexibility. Simulation results showed that optimized scheduling can reduce the cost of a drying cycle by 13.8%, demonstrating effective load shifting and enhanced grid flexibility. Gupta et al. [43] assessed residential DR on a low-voltage feeder in the United Kingdom using coordinated HPs, home batteries, and PV systems. Field trials showed that short turn-down actions cut evening peak imports by up to 67% per dwelling, while turn-up actions substantially increase midday demand. The results highlighted the effectiveness of ToU tariffs and the importance of feeder-level coordination for scalable residential DR. Romero et al. [44] analysed DR strategies for a plus-energy dwelling equipped with an HP, a TES and a PV-Battery system (PV-B) under dynamic pricing. Using a TRNSYS model calibrated with manufacturer and measured data, they compared multiple control strategies and showed that dynamic price-based control achieves up to 25% cost savings, increases self-consumption and reduces grid peak demand. Alimohammadisagvand et al. [45] presented DR control in a detached house in a cold climate, comparing a GSHP with dual thermal storage to a water-based electric heating system. Four rule-based DR algorithms, driven by real-time and forecast electricity prices, were evaluated using the validated IDA ICE platform. Results showed that the sliding-maximum subarray-based control achieves the highest savings, reducing annual heating energy use and costs by up to 10% and 15% for the HP, with smaller reductions for the electric heating system. Hao et al. [46] simulated a market-driven control scheme that limited HVAC power to 10% below baseline peak demand, achieving peak load reductions of approximately 6.1%-6.3%. Birrer et al. [47] proposed a DR model for a service-sector building equipped with a HP and TES, driven by electricity tariffs. Their analysis demonstrates that scheduling heat production during low-tariff periods can achieve cost reductions of up to 34% and decrease overall energy consumption by 20%. Xiao et al. [48] developed an optimal load scheduling strategy for building clusters using a multi-agent system approach, aiming to balance electricity costs and carbon emissions under dynamic pricing and Marginal Emission Factors (MEF). Applied to a University Campus in Hong Kong across three DR schemes, the study found that price-based DR can sometimes increase emissions, whereas MEF-based DR may lead to higher costs, depending on the correlation between electricity prices and emission factors. The proposed hybrid strategy effectively mitigates these trade-offs, reducing peak load by 5.54% without increasing cost or emissions, even under unfavourable market conditions, offering a practical path for sustainable and cost-effective DR management.

Other works explored the flexibility potential of HPs, considering human comfort. Cheng et al. [49] developed a DR framework for clusters of electric HPs based on temperature-controlled loads while preserving occupant comfort. Thermal comfort was evaluated through a Predicted Mean Vote (PMV) and Predicted Percentage of Dissatisfied (PPD)-based model, and power allocation was optimized using an enhanced Particle Swarm Optimization (PSO) approach. HP behaviour was modeled through a second-order equivalent thermal parameter model, enabling effective integration within smart community operations. Pignatta et al. [50] investigated the effectiveness of pre-cooling in residential buildings of varying energy efficiency, construction weight, and AC unit sizes across four Australian cities. Results showed that higher-rated and lightweight buildings, as well as those with larger AC units, tend to achieve greater daily and seasonal cost savings. Pre-cooling significantly reduces thermal discomfort, especially in buildings with smaller AC units, though it may not always lead to cost savings. Peak demand reduction is more pronounced in well-insulated and heavier buildings, but is influenced by occupants' comfort expectations and may be limited in high-performance homes. Kaspar et al. [51] demonstrated that occupant behaviour significantly impacts the effectiveness of DR with HPs in residential communities. A reinforcement learning-based control applied to a 10-home neighbourhood showed that incorporating adaptive thermostat setbacks with occupant override options reduces electricity use by 17% and costs by 12% during DR events, while maintaining comfort.

Finally, an overview of DR applications in buildings operating under Mediterranean and similar warm climates was carried out. The combination of high cooling demand, strong solar potential, and seasonal variability makes DR particularly relevant and effective in these areas. According to the European climatic zoning framework and the Köppen-Geiger climate classification [52], these Mediterranean and similar warm climates typically correspond to Mediterranean climates (Csa-Mediterranean hot summer climate, Csb-Mediterranean warm summer climate), warm temperate coastal climates with dry summers, as well as transitional warm-temperate zones with hot or warm summers and mild winters. These conditions are commonly found in Southern Europe (e.g., Italy, Spain, Greece, southern France, and the Balkans), parts of the eastern Mediterranean (e.g., Turkey, Israel and Palestine, Lebanon), North Africa (e.g., Tunisia, Algeria, Morocco, Libya), and other comparable regions characterized by pronounced summer cooling demand and relatively mild heating seasons. Similar climatic conditions are also observed in the west coast of the US, particularly in California, which is frequently considered a representative reference region due to its Mediterranean-type climate and comparable seasonal energy demand patterns. In these contexts, price-based DR strategies, ventilation control, and thermal mass utilization are often highlighted as key enablers of energy flexibility, complementing active HVAC-based control approaches. Catrini et al. [53] investigated price-based DR strategies in a standardized commercial building equipped with RTUs located in Palermo (Southern Italy). The analyzed strategies included cooling system deactivation and indoor temperature setpoint modulation. Partial deactivation achieved up to 50% peak shaving and 22.72% seasonal energy savings, while a +2 °C setpoint increase provided an additional 5.2% reduction in energy use. Conversely, a -2 °C setpoint shift increased peak demand from 7.7 to 25.3 kW and raised seasonal consumption by 43.6%. Di Silvestre et al. [54] developed a blockchain-based DR platform for Mediterranean island energy systems, including experimental applications in Palermo. The proposed strategy relied on customized smart contracts to remunerate users participating in DR and vehicle-to-grid programs. The approach aimed to reduce diesel fuel dependence and increase renewable energy penetration in isolated island grids. Tina et al. [55] investigated DR strategies for a shopping centre located in Catania (Southern Italy) equipped with an HP, considering measures such as adjusting thermal zone setpoints and reducing HP power. Comfort was evaluated using the PMV and PPD indices. The study reports energy savings of 128-160 kWh during the summer and 40-160 kWh in other periods, although comfort levels deteriorated significantly in the summer, with PPD reaching up to 40%. Morrone et al. [56] investigated thermal mass-based DR strategies in Mediterranean residential buildings located in Italy, constructed with Insulated Concrete Forms (ICFs) and conventional brick masonry. The flexibility strategy relied on exploiting building thermal inertia for load shifting. ICF systems achieved up to 56% heating energy savings compared to brick masonry and contributed to reducing summer peak cooling demand. Massana et al. [57] investigated short-term load forecasting techniques for DR applications in a non-residential university building located in Girona (Spain). The study evaluated Multiple Linear Regression (MLR), Multi-Layer Perceptron (MLP) and Support Vector Regression (SVR) forecasting models considering weather, occupancy, and indoor environmental data. The proposed methodology achieved high prediction accuracy with low computational cost, supporting smart-grid-oriented energy management strategies. Chantzis et al. [58] assessed thermal mass-based DR strategies in a typical office building located in Greece. The study evaluated load shifting through variable-speed HPs controlled by electricity price and CO_2 intensity signals. The results demonstrated that suitable control strategies can reduce both operational costs and emissions, although energy consumption may increase depending on the adopted flexibility schedule. Novosel et al. [59] evaluated district heating and cooling systems as DR tools for renewable integration in Croatia. The strategy exploited power-to-heat flexibility to improve wind and PV utilization within urban energy systems. Results showed that RESs could cover up to 73% of total electricity demand, while annual excess electricity generation was limited to only 5%. Hadded et al. [60] analyzed passive and hybrid ventilation-based DR strategies in residential buildings located in Tunisian Mediterranean climates. Optimized natural ventilation reduced annual energy consumption by 38.4-42.6% and CO_2 emissions by 6-10.8%, while hybrid ventilation improved thermal comfort, increasing comfortable occupied hours to nearly 76%. Economic savings reached up to 42.96 Tunisian dinars per square metre in the analyzed Mediterranean regions. Tellache et al. [61] evaluated adaptive thermal comfort and mixed-mode ventilation strategies in Mediterranean residential buildings located in Algiers. The study highlighted that indoor discomfort already affects more than one-third of annual hours, with summer overheating expected to dominate by 2100 under the Representative Concentration Pathway 8.5 scenario. Passive and mixed-mode ventilation strategies were identified as key solutions for improving resilience and reducing cooling demand. Noorollahi et al. [62] developed a DR-oriented energy system model for a Mediterranean-climate region in north-eastern Iran. The proposed strategy combined renewable energy integration with DR management in future scenarios. The wind-based scenario reduced CO_2 emissions by 93.87 and 227.78 kt/year, while annual system costs decreased by €8.27 million and €156.06 million, respectively, compared to the business-as-usual scenario. Clark et al. [63] proposed DR strategies based on the modulation of building ventilation systems in commercial and residential buildings located in the US. This study showed that ventilation curtailment can significantly contribute to peak demand reduction, particularly in warm California climates. Simulations revealed that ventilation can be paused for up to five hours without compromising health or comfort, enabling up to 30% peak power demand reduction and energy savings of around 10%, with higher savings in hotter regions. de Chalendar et al. [64] experimentally investigated cooling setpoint-based DR strategies in six commercial buildings operating under a warm-summer Mediterranean climate in the US. Increasing the cooling setpoint by 2 °F reduced daily cooling loads by 13-28% in office buildings and by 3-4% in laboratory buildings, while indoor temperatures remained within acceptable comfort ranges. The study confirmed the effectiveness of temperature-based load shifting for commercial Mediterranean buildings. Oxizidis et al. [65] reviewed DR solutions for Mediterranean climate buildings designed according to zero energy building principles. The study focused on the integration of HPs, TES, PVs, solar thermal systems and combined heat and power units to enhance building flexibility. The analysis highlighted that energy storage technologies are essential to significantly increase DR capability in high-performance buildings.

A summary table of the proposed literature review is provided in the Appendix (Table A.1). The contents are organised by year, building/plant type, geographic location, DR strategies, constraints, and main results, in order to provide a structured and comparative overview of the main approaches investigated. The analysis revealed a wide range of strategies, from rule-based and price-driven control of HPs, often combined with thermal and electrical storage, building thermal mass exploitation, and renewable energy integration. Overall, the evidence shows that significant flexibility can be achieved in terms of peak load reduction, cost savings, and emission reduction, particularly when HPs, TES, RESs and smart control strategies are jointly implemented. Results also highlight that performance and human comfort are highly dependent on building characteristics, climate conditions, tariff structures, and the level of modeling detail.

1.2. Knowledge gaps and scope

Despite the growing body of research on DR approaches, the following gaps remain insufficiently analysed:

- DR programs addressed by HPs with TES and combined with PV-B systems in Southern Mediterranean countries, involving pricing strategies, setpoint adjustments, and occupant comfort, remain largely unexplored. For example, the studies in [53] and [55] neglected the influence of building insulation levels and the integration of HPs with other RESs. Given the high solar radiation in cooling-dominated regions and the potential for energy surpluses and deficits, understanding how building envelopes with different insulation levels and associated HPs combined with PV-B systems can support grid operators in managing these fluctuations is crucial.
- Several works employ simplified building models for DR applications [41], commonly represented through RC modeling approaches [39]. It is widely recognized that the accuracy of simulation outcomes depends heavily on the selected modeling method. RC models offer a simplified representation of heat transfer and storage, making them computationally efficient and relatively straightforward to implement. However, they may not fully capture the influence of thermal mass and other dynamic thermal behaviours. Conversely, detailed simulation platforms, such as TRNSYS, offer an accurate description of system behaviour under dynamic operating conditions. These advanced models enable the capture of transient thermal responses, stratification effects, and interactions within hydronic systems, albeit at the cost of increased computational effort. In contrast, reduced-order approaches, such as RC models, enable faster simulations but may introduce discrepancies when applied to DR scenarios, particularly in the presence of complex control strategies. In this context, the use of detailed modelling approaches appears beneficial to ensure consistency in DR analyses. This assumption is supported by previous studies in which RC building models were validated against the TRNSYS TYPE 56 environment [66] through comparisons of indoor air temperature profiles and the evaluation of mean squared errors [67]. While the present study does not include a direct comparison between modelling approaches, these findings from the literature suggest that higher-fidelity models can provide improved reliability when assessing building flexibility and control performance.
- Research exploring the effects of flexibility strategies on HP operation remains scarce, primarily because most studies employ very simplified modeling approaches (e.g., [49]), which neglects the logic used to modulate the delivered heating/cooling capacity. Ignoring these aspects may lead to the selection of flexibility strategies that appear promising from an energy perspective but ultimately result in unsustainable ON-OFF cycling of HPs, increasing the risk of compressor failure.
- Finally, only a few studies performed a flexibility analysis by using HP models validated from detailed data (e.g., [44]).

In this context, the work investigates the implementation of DR strategies in a tertiary building situated in Palermo, representative of a cooling-dominated Mediterranean climate. A dynamic office building characterised by different insulation levels is implemented in TRNSYS and coupled with a reversible air-to-water HP, a PV-B system, a thermally stratified water tank, and a hydronic distribution network with circulation pumps, fan coils, and associated control strategies. A detailed reversible HP is modeled in IMST-ART v4.0, accounting for one-dimensional thermo-hydraulic simulations of the condenser and evaporator, with the compressor described through performance maps. Model performance is validated using data supplied by the manufacturer. Starting from a baseline scenario (No DR), the study evaluates both price-based and PV-driven DR strategies by dynamically and statically varying the temperature setpoints of the thermal zones and the TES. In particular, the analysis considers a price-based approach, defined according to the Italian wholesale market's Prezzo Unico Nazionale (PUN), and a PV-driven DR program, aimed at enhancing the integration of VRE sources. Their impacts on energy consumption and occupants' comfort are examined considering daily and yearly timescales. Additionally, the effect of building envelope insulation was incorporated into the analysis to ensure a comprehensive assessment. The developed model also explicitly accounts for night-time natural ventilation as a passive cooling strategy to mitigate the risk of overheating, a common challenge in well-insulated buildings during the summer months.

This study provides the following contributions to the current body of knowledge:

- The development of a fully integrated simulation framework based on TRNSYS, capable of simultaneously modelling a poorly and well-insulated multizone office building with a reversible ASHP and TES combined with a PV-B system under transient conditions. The simultaneous assessment of energy performance and indoor thermal comfort enables a more holistic evaluation of the effectiveness of DR strategies.
- In contrast to several published studies that assume a single thermal zone and simplified HP representations, this study adopts a detailed multizone building model developed in TRNSYS, coupled with an advanced hydronic system. The thermodynamic behaviour of the reversible HP is modeled through one-dimensional thermo-hydraulic simulations of its main components using IMST-ART v4.0. The model's accuracy was validated against catalog data provided by Magellano (AERMEC). The performances are assessed as functions of outdoor Dry-Bulb Temperature (ODT), number of compressors (N_{CMP}), and the water temperature entering the reversible HP. Moreover, the control logic governing compressor modulation under both full-load and part-load conditions is considered. This approach provides more reliable results than simplified models for the effective implementation of the DR program.
- Flexibility strategies (namely, a price-based and a PV-driven approach) are analyzed for cooling-dominated climates, with a focus on adjusting the temperature setpoints of the thermal zones and the thermal energy storage. This analysis provides valuable insights for grid operators into the flexibility potential of building envelopes with different insulation levels equipped with HPs combined with a PV-B system, demonstrating their ability not only to reduce electricity demand but also to increase it during periods of surplus electricity from RES. Meantime, details on the effects of these strategies on occupants' comfort are provided.
- The work enables a deeper understanding of the role of control logic, system integration, and building characteristics in determining the achievable flexibility, thus contributing to bridging the gap between simplified modelling approaches and real system behaviour.

The paper is organized as follows: *Materials and Methods* details the numerical model and case study, *Results and Discussion* presents and interprets the findings, and *Conclusions* summarizes the main outcomes.

2. Materials and method

This section presents the numerical approach adopted in the study, including the models developed for the standardized building, the HP with TES, the hydronic distribution system, and the PV-B system. The DR strategies implemented in the analysis are also described.

2.1. Office building modeling

The standard office building model defined in ASHRAE 90.1-2016 [68] was adapted to the Italian context by considering two scenarios: (i) a poorly insulated envelope, characterized according to UNI/TR 11552:2014 [69], and (ii) a well-insulated envelope, designed to comply with current regulations prescribing high thermal performance standards [70]. Details on the geometrical and thermal properties are summarized in Table 1. Note that the term *"code entity"* refers to the construction materials used within the wall assembly, as specified in the UNI/TR 11552:2014 Standard, whereas the U-values assumed for the well-insulated envelope refer to buildings located in climate zone B, such as the city of Palermo. The office building consists of three aboveground floors and includes 15 conditioned thermal zones. Each floor presents one core zone and four perimeter zones. The building features 652.87 m^2 of window glass area, 30% of which is located on the south façades, and 1977.92 m^2 of gross wall area, resulting in a Window-to-Wall Ratio (WWR) of 33%. The building geometry was created using Google SketchUp and subsequently imported into TRNSYS utilizing TYPE 56.

The model incorporates air infiltration rates, expressed in Air Changes per Hour (ACH), and internal heat gains from occupants, lighting, and electrical equipment. These inputs were scheduled with monthly and weekly variations, following ASHRAE 90.1-2016 guidelines and adapted to the specifics of the case study. Fig. 1 shows infiltration and internal gains schedules implemented on TYPE 56.

The thermal comfort of the building zones was simulated using TYPE 56. In accordance with UNI EN ISO 7730 [71], two indices were

Table 1
Properties of office chosen according to ASHRAE 90.1 and UNI/TR 11552:2014.

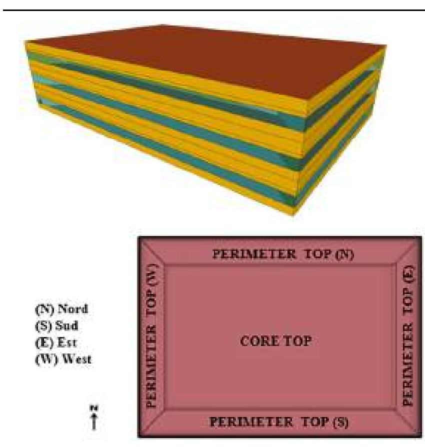

Geometrical properties and internal gains of the building according to ASHRAE 90.1	
Net conditioned floor [m^2]	4982.2
Number of floors	3
Window-Wall-Ratio (WWR) [%]	33
Number of thermal zones	18
Lighting [W/m^2]	11
Electric equipment [W/m^2]	8
Occupants [m^2/person]	19
Thermal properties for the *poorly-insulated envelope* according to UNI/TR 1552: 2014	
Ground [W/m^{2}K] – Code entity	2.02 – SOL13
External wall [W/m^{2}K] – Code entity	2.82 – MPI01
External roof [W/m^{2}K] – Code entity	1.45 – COP04
Adjacent wall [W/m^{2}K] – Code entity	1.18 – MLP03
Adjacent ceiling [W/m^{2}K] – Code entity	1.68 – SOL02
Windows [W/m^{2}K] – Code entity	5.80 –WinID 1001TRNSYS library
Thermal properties for the *well-insulated envelope according to the current Italian regulation [70]**	
Ground [W/m^{2}K]	0.40
External wall [W/m^{2}K]	0.43
External roof [W/m^{2}K]	0.35
Adjacent wall [W/m^{2}K] – Code entity	1.18 – MLP03
Adjacent ceiling [W/m^{2}K] – Code entity	1.68 – SOL02
Windows [W/m^{2}K]	3.00

* Details on the physical properties of each construction layer are provided in the Supplementary Material.

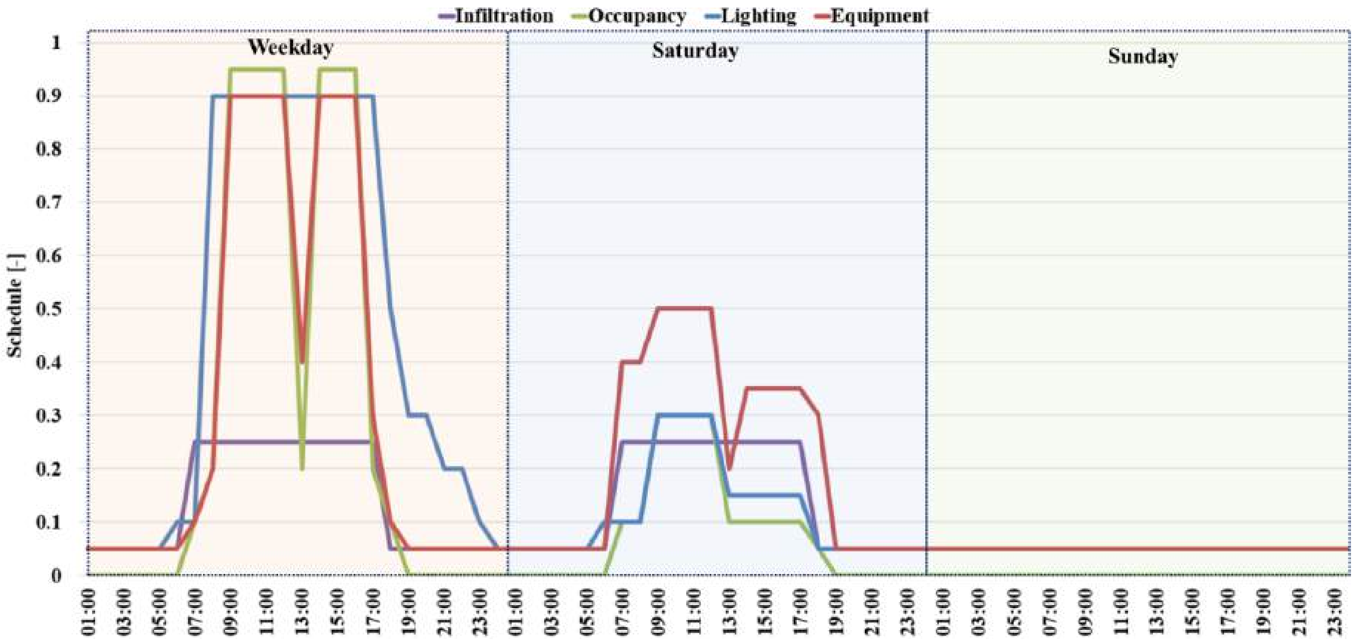

Fig. 1. ASHRAE 90.1-2016: schedules implemented on TYPE 56 [68].

employed to assess comfort: the PMV and the PPD. PMV represents an index that predicts the mean thermal sensation reported by a group of occupants on a seven-point comfort scale, while PPD estimates the proportion of users likely to be dissatisfied with the indoor thermal conditions (Table 2).

The UNI EN ISO 7730 defines three comfort levels (A, B, and C), each associated with specific acceptability criteria. More recently, the European standards EN 16798-1 and CEN/TR 16798-2 [73] have expanded this framework by introducing four comfort categories (I, II, III, and IV) based on PMV values: Category I ($|PMV| \leq 0.2$), corresponding to very high comfort expectations; Category II ($|PMV| \leq 0.5$), generally recommended for office buildings; Category III ($|PMV| \leq 0.7$), representing acceptable comfort conditions for existing buildings or situations with operational constraints; and Category IV ($|PMV| \leq 1.0$), applicable to conditions that may be tolerated for limited periods of occupancy (Table 3).

Regarding the implementation of the thermal comfort model, the following parameters were set for the simulation: clothing factor 1.0 in winter and 0.6 in summer, metabolic rate: 1.0, external work: 0.0, and relative air velocity: 0.1 m/s.

The dynamic simulation for the entire year using a *timestep* equal to 0.05 h (3 minutes) with a *timebase* equal to 1, was realised for Palermo according to the weather files in the *Meteonorm* directory from TRNSYS. Fig. 2a illustrates the annual heating and cooling demand obtained from simulations for the No DR scenario. Fig. 2b depicts the weekly electricity demand of lighting and equipment loads (mandatory electricity demand from the thermal zones), as defined by ASHRAE 90.1-2016 schedules.

Table 3
Limits of acceptability for thermal comfort [73].

Comfort Category	PMV Range	Description
Category I	$-0.2 \leq PMV \leq +0.2$	High level of thermal expectation. Recommended for spaces occupied by sensitive and vulnerable users, where very high indoor environmental quality is required.
Category II	$-0.5 \leq PMV \leq +0.5$	Normal level of thermal expectation. Recommended for new and renovated office buildings and represents the target comfort range for most mechanically conditioned buildings.
Category III	$-0.7 \leq PMV \leq +0.7$	Moderate level of thermal expectation. Acceptable for existing buildings or situations where operational, technical, or energy constraints limit the achievement of Category II conditions
Category IV	$-1.0 \leq PMV \leq +1.0$	Lowest acceptable level of thermal expectation. Intended for limited periods of occupancy or transient conditions and may be used when Categories I-III cannot be achieved.

2.2. Hydronic network modeling

The hydronic system was developed considering the following subsystems. The *primary circuit* (Figs. 3-a.b) is composed of an air-to-water HP (modelled by TYPE Equation Editor) coupled with a TES (TYPE 534-NoHX:TES, TANK macro, Fig. 3a). The TANK macro preserves water stratification throughout the heating (winter and spring) and cooling (summer and autumn) periods. In the TRNSYS model, the control system actively manages diverting valves to reverse the water flow, ensuring optimal thermal performance under varying operational conditions (Fig. 3b).

During the heating season, water is introduced at the Top Node (NT) of the TES, whereas in the cooling season, the flow is directed to the Bottom Node (NB). This configuration, controlled dynamically within TRNSYS, ensures effective thermal stratification and optimal performance of the storage tank (Figs. 4-a.b).

The total control of the hydronic plant according to the specific seasonal, daily, and hourly schedules using TYPE 515, TYPE 516 and

Table 2
Level of PMV and PPD [72].

PMV	[-3, -2.5]	[-2.5, -1.5]	[-1.5, -0.5]	[-0.5, +0.5]	[+0.5, +1.5]	[+1.5, +2.5]	[+2.5, +3]
PPDThermal perception	95-100% Cold	50-95% Cool	10-50% Slightly cool	0-10% Neutral (Comfortable)	10-50% Slightly warm	50-95% Warm	95-100% Hot

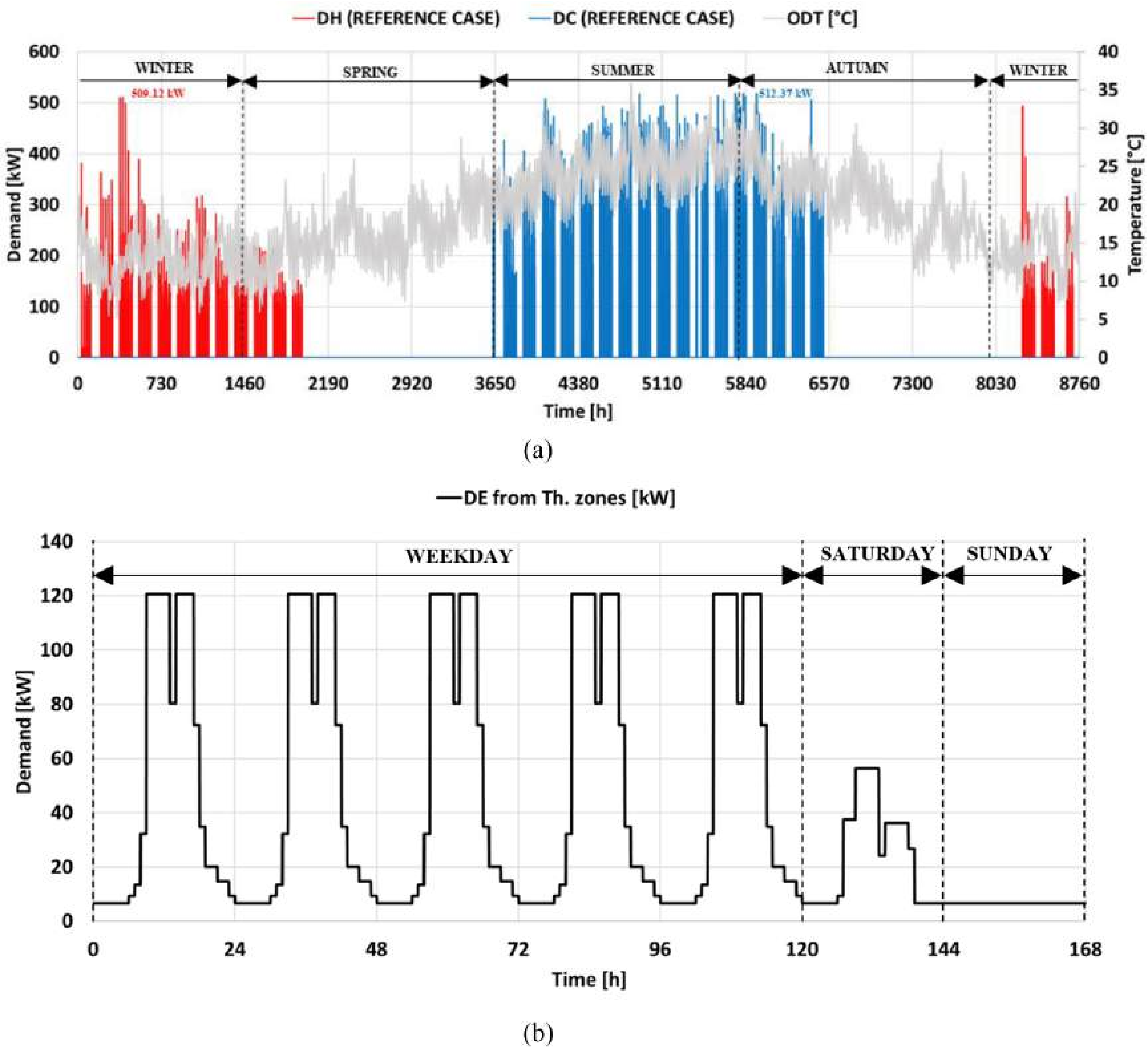

Fig. 2. Energy demands from the office building: (a) yearly thermal and cooling demands, (b) weekly electricity demand in winter.

TYPE 519a was provided. The operation of the heat pump was coordinated with seasonal, daily, and hourly schedules through a hysteresis controller (TYPE 2b). The HP operates across four stages, corresponding to the number of active compressors, based on the temperature measured at NT or NB of the TES. The ON_HM - ON_CM macro (Fig. 3a) maintains the node temperature at the setpoint $T_{set\text{-}TES}$ (50°C for heating, 7°C for cooling) within a ± 1°C dead band. Figs. 5-a.b provides a detailed representation of the four modulation stages, which adjust the heating and cooling capacity according to the measured temperature on the TES Node.

The *secondary circuit* (Figs. 6-a.b) was represented as a hydronic distribution network within TRNSYS (USER macro, Fig. 3a). The macro includes diverting and mixing valves (TYPE 647 and TYPE 649) to regulate water delivery to the different thermal zones, along with piping (TYPE 31), circulation pumps (TYPE 114), and fan coil units. The THERMAL ZONES macro (Fig. 6a) models the fan coils installed in the thermal zones. This macro was developed by combining several TRNSYS components, specifically TYPE 11, TYPE 33, TYPE 112, TYPE 508c, and TYPE 753e. Each fan coil, equipped with its own pump and fan, is controlled by the corresponding zone air temperature and operates to maintain the zone setpoint $T_{set\text{-}th.zone}$ at 20°C during the heating season and 26°C during the cooling season, with a ±1°C dead band (Fig. 6b).

As highlighted in Fig. 6a, the price-based approach was implemented using TYPE 21 to generate dynamic time-dependent signals at each simulation step, together with TYPE 62 to enable data exchange with Excel. A Fortran routine facilitates rapid communication with Excel through a component object model interface, ensuring efficient data transfer.

As explained in more detail later, Fig. 7 illustrates the PUN profile for the year 2023, as implemented by TYPE 62.

The PV-driven DR strategies were addressed by static time-dependent signals at each simulation step, configured according to specific daily and hourly schedules using TYPE 516 (Figs. 3a and 6b), and based on PV-Battery system production (Fig. 3a). Details on the PV-Battery system model in Section 2.4 are provided.

2.3. *Reversible heat pump modeling & validation*

The air-to-water HP, operating in both heating and cooling modes, was performed in IMST-ART v4.0 [74]. IMST-ART is a physics-based, component-level simulation environment for vapour compression systems. It explicitly resolves the thermodynamic cycle through the

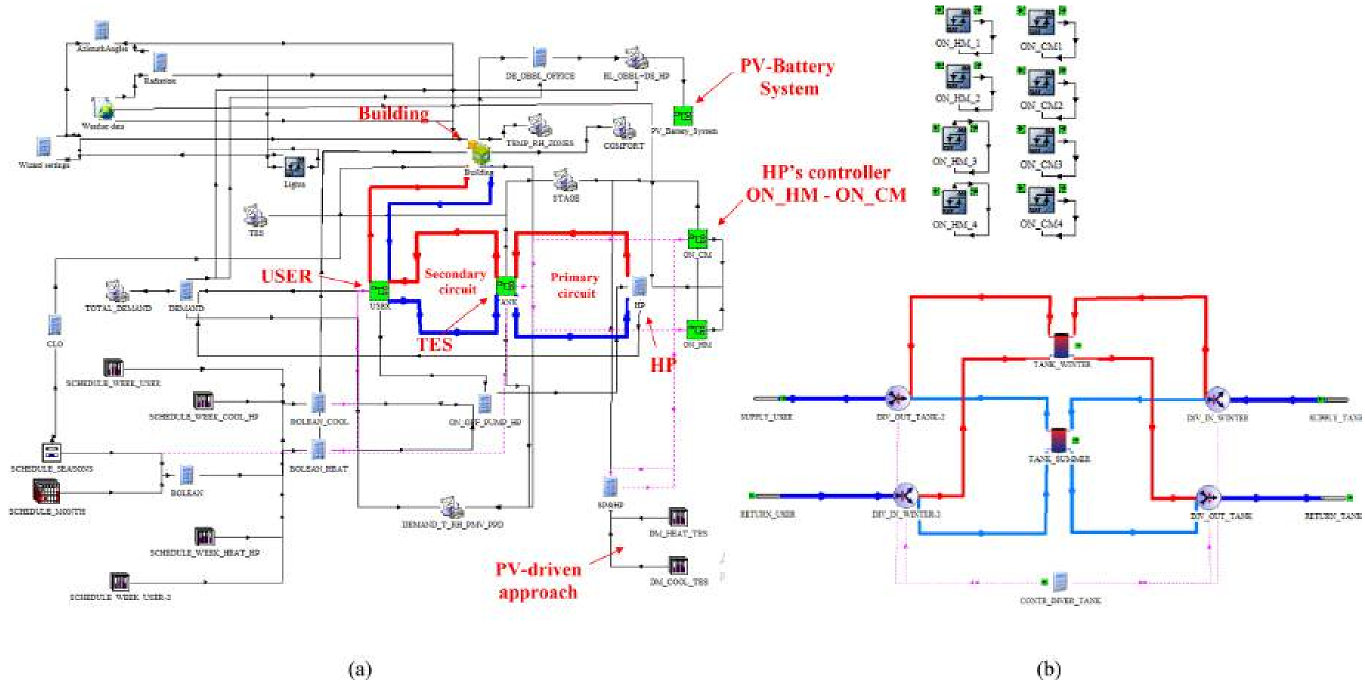

Fig. 3. Simulation Studio flowchart: (a) overall project with the detailed hydronic plant, (b) TES and HP's controller modelled in heating and cooling seasons.

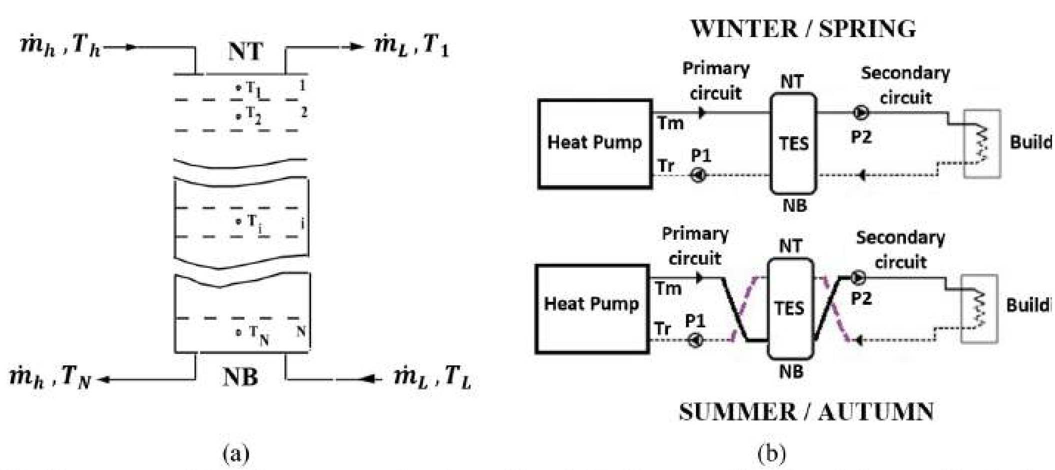

Fig. 4. Thermal energy storage modelled in TRNSYS: (a) tank segments and node positions [32], (b) reverse direction of the mass flow in the heating and cooling seasons.

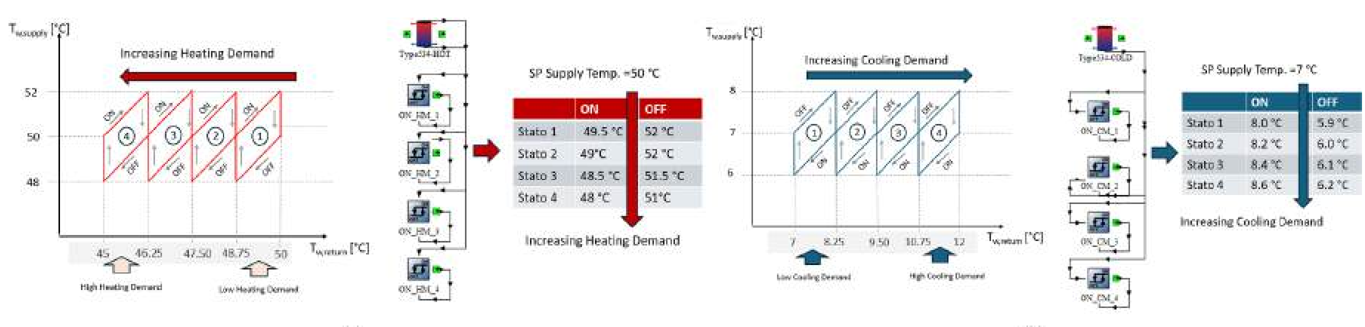

Fig. 5. TES modeled in TRNSYS: (a) stage activations based on NT temperature in heating season, (b) stage activations based on NB temperature in cooling season

coupled modelling of compressors, heat exchangers, expansion devices, and connecting lines, with one-dimensional discretisation of heat exchangers enabling local resolution of heat transfer and pressure losses. This high-fidelity formulation allows accurate prediction of non-uniform

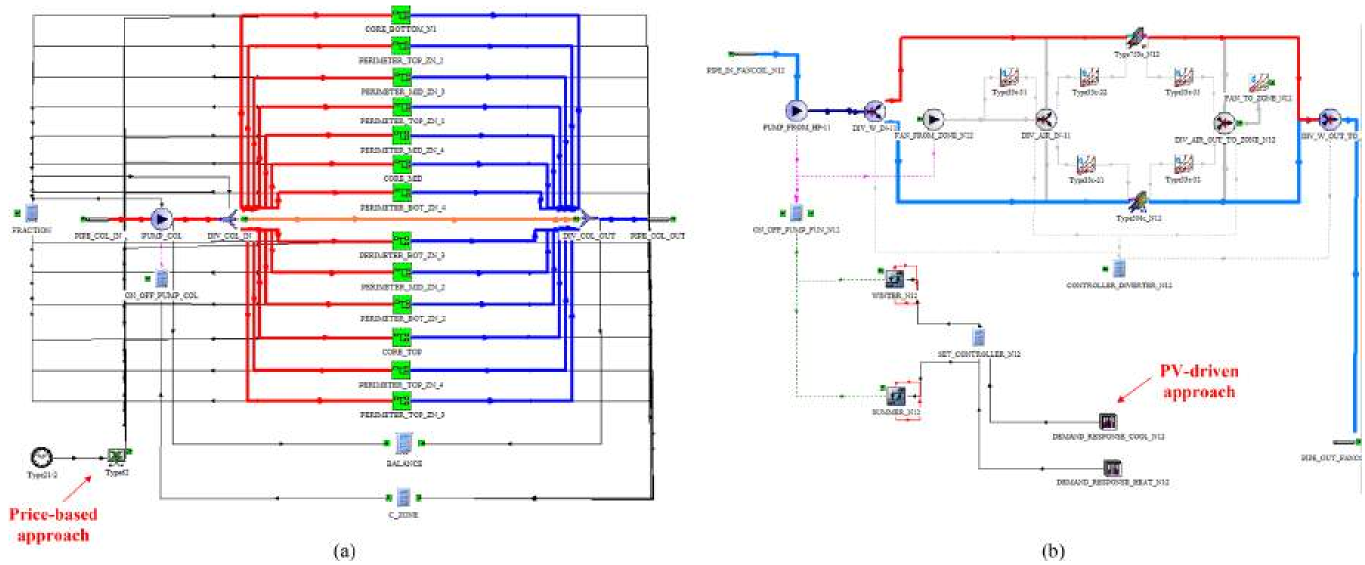

Fig. 6. The numerical model developed in TRNSYS: (a) secondary circuit (hydronic network) for supply water to thermal zones, (b) fan coil.

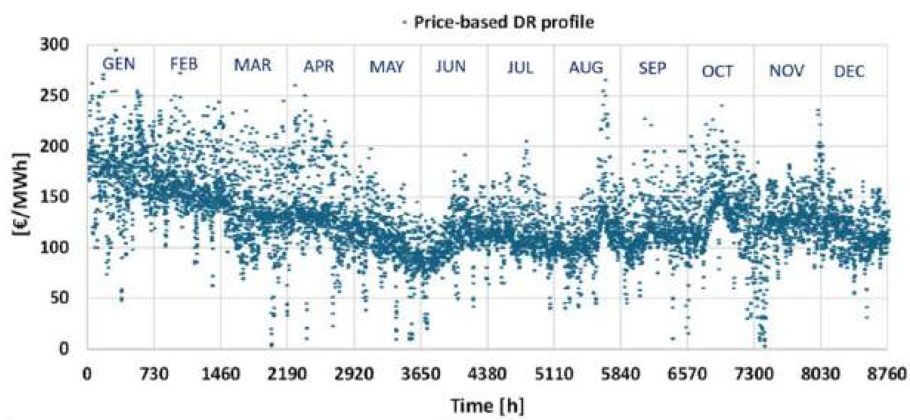

Fig. 7. Price-based DR profile implemented on Excel file by Type 62.

effects such as superheating and subcooling. The platform was validated against experimental data. As a result, IMST-ART is widely used in the literature for the design [75], optimisation [76], and off-design analysis of advanced heat pump systems [77].

In this study, the condenser and evaporator were simulated considering detailed geometric and material properties, including tube arrangement, heat exchanger dimensions, and surface characteristics (Fig. 8). The condenser was represented as a tube-and-fin heat exchanger with copper tubes and aluminium fins, while the evaporator was modeled as a plate heat exchanger with stainless steel plates, allowing for precise simulation of flow arrangements (co-current or counter-current) and pressure losses. The refrigerant used in the cycle was R410A. Compressor performance was represented by converting manufacturer-provided operating maps into polynomial correlations. The methodology adopted to define the test matrix for characterizing the HP is detailed in [78].

Equations 1-8 describe the main variables governing the performance of the air-to-water HP: the delivered Heating Capacity (HC), Cooling Capacity (CC) and the required electric power ($P_{m,H}$, $P_{m,C}$) are dependent on the ODT, N_{CMP} and the temperature of the water returning from the TES and entering the HP's condenser ($T_{wr,CND}$) and evaporator ($T_{wr,EVP}$) in heating and cooling seasons, respectively.

$$HC = f\left(N_{CMP}, ODT, T_{wr,CND}\right) \tag{1}$$

$$P_{m,H} = g\left(N_{CMP}, ODT, T_{wr,CND}\right) \tag{2}$$

$$CC = f\left(N_{CMP}, ODT, T_{wr,EVP}\right) \tag{3}$$

$$P_{m,C} = g\left(N_{CMP}, ODT, T_{wr,EVP}\right) \tag{4}$$

The parameters HC, $P_{m,H}$, CC and $P_{m,C}$ were expressed as linear functions of the main governing variables:

$$HC = L_{1,HC}N_{CMP} + L_{2,HC}ODT + L_{3,HC}T_{wr,CND} \tag{5}$$

$$P_{m,H} = K_{1,HC}N_{CMP} + K_{2,HC}ODT + K_{3,HC}T_{wr,CND} \tag{6}$$

$$CC = L_{1,CC}N_{CMP} + L_{2,CC}ODT + L_{3,CC}T_{wr,EVP} \tag{7}$$

$$P_{m,C} = K_{1,CC}N_{CMP} + K_{2,CC}ODT + K_{3CC}T_{wr,EVP} \tag{8}$$

where $L_{1,HC}, L_{1,CC}, K_{1,HC}, K_{1,CC}, L_{2,HC}, L_{2,CC}, K_{2,HC}, K_{2,CC}$, $L_{3,HC}, L_{3,CC}, K_{3,HC}$, $K_{3,CC}$, are fitting coefficients for N_{CMP}, ODT, $T_{wr,CND}$ and $T_{wr,EVP}$.

To assess the energy performance of the HP, the instantaneous $COP_{,t}$ and the Seasonal Coefficient of Performance ($SCOP_{,T}$) were defined as reported in Eqs. (9) and (10). Here, $HC_{,t}$ and $P_{m,H,t}$ denote the heating capacity and the electrical power input at timestep t, respectively. The $SCOP_{,T}$ was determined by integrating both quantities over the same reference period T, equal to 8760 h [78].

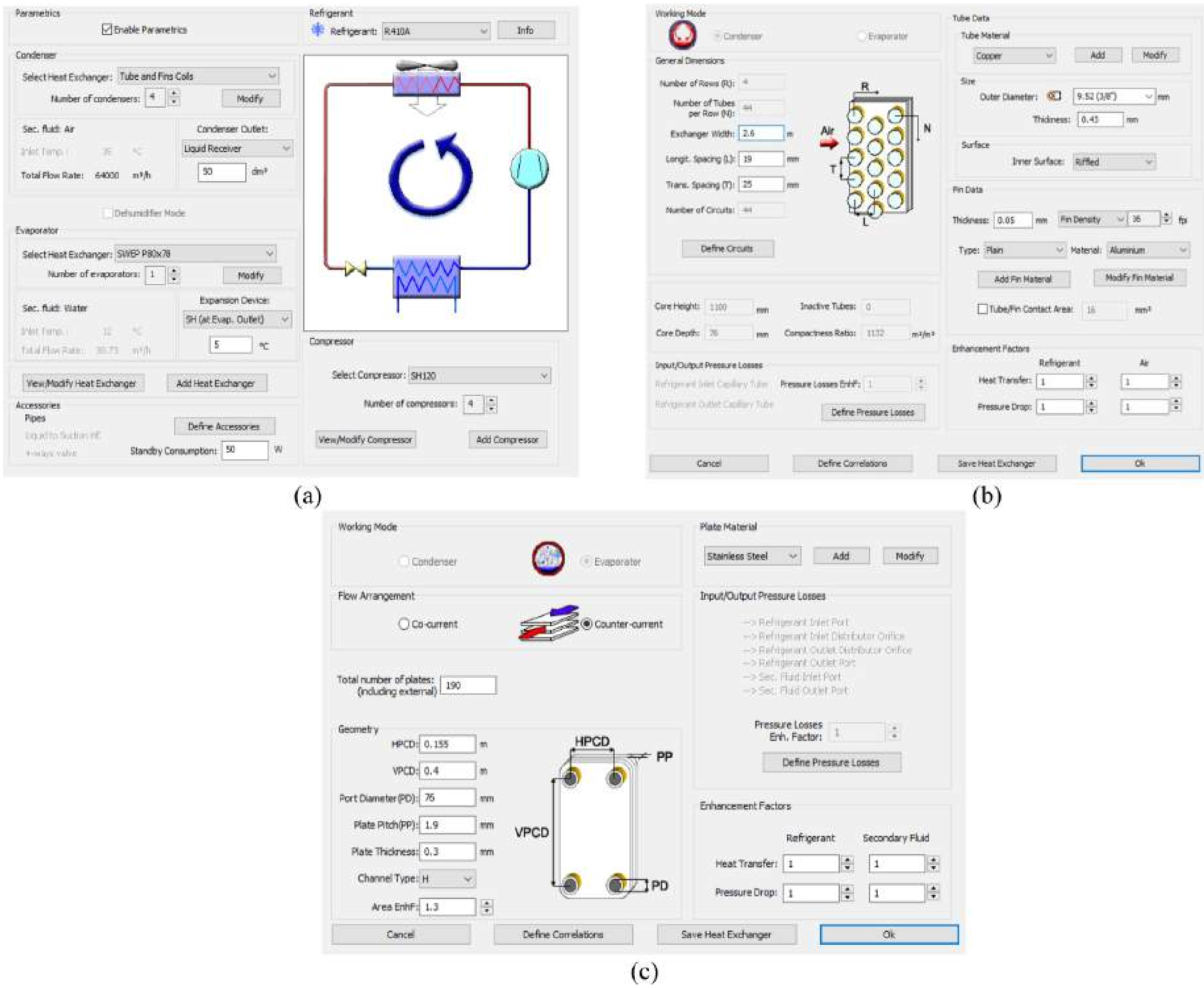

Fig. 8. Reversible heat pump developed in IMST-ART v4.0: (a) component selections, (b) condenser modeling, (c) evaporator modeling.

$$COP_{,t} = \frac{HC_{,t}}{P_{m,H,t}} \ [-] \quad (9)$$

$$SCOP_{,T} = \frac{\int_0^T HC_{,t}\,dt}{\int_0^T P_{m,H,t}\,dt} \ [-] \quad (10)$$

Similar equations were used to calculate the instantaneous Energy Efficiency Ratio ($EER_{,t}$) and the Seasonal Energy Efficiency Ratio ($SEER_{,T}$).

$$EER_{,t} = \frac{CC_{,t}}{P_{m,C,t}} \ [-] \quad (11)$$

$$SEER_{,T} = \frac{\int_0^T CC_{,t}\,dt}{\int_0^T P_{m,C,t}\,dt} \ [-] \quad (12)$$

Following model validation, the resulting Eqs. 1-12 were implemented in TRNSYS by TYPE Equation Editor.

The model validation was carried out by systematically comparing numerical results obtained with IMST-Art v. 4.0 using input data from the Magellano AERMEC catalog [79]. Magellano is a proprietary engineering software developed by AERMEC for the selection and performance evaluation of HVAC equipment, with particular focus on HPs, chillers, and ACs. It is widely used in the literature as a manufacturer-based tool for generating certified performance data according to standardised procedures (e.g., EN 14511). The software relies on semi-empirical performance maps derived from experimental testing, which describe system behaviour across a range of operating conditions, including temperature variations and part-load operation. Performance indicators such as capacity, power input, *COP* and *EER* are represented through tabulated or regression-based formulations, enabling fast interpolation while preserving consistency with validated manufacturer data. Consequently, Magellano is primarily suited for rapid sizing, comparative analysis, and integration of HVAC systems within broader energy modelling frameworks, where computational efficiency and adherence to certified performance data are required.

Figs. 9-a.b illustrate the validation of the *CC* and *EER* of the constant-speed HP under varying operating conditions. These conditions account for different *ODT* and water flow rates through the evaporator, with the return water temperature maintained between 9 °C and 14 °C. The comparison indicates a close agreement between simulation results and the manufacturer's catalog data, confirming the reliability of the model. The percentage error for *CC* remains below 4%, whereas for *EER* it exceeds 10% in only one case, which corresponds to 9°C and 20°C as $T_{wr,EVP}$ and *ODT*, respectively. However, this operating condition is not typically encountered during summer operation.

Fig. 9. Comparison between IMST-Art simulations and Magellano catalog data: (a) CC, (b) EER, and percentage errors.

A similar analysis was conducted for the *HC* and the *COP* under varying *ODT* and condenser water flow rates, with the return water temperature ranging from 30 °C to 50 °C (Figs. 10-a.b). In this case as well, the comparison indicates good agreement between the simulation results and the manufacturer's catalogue data. The percentage error for HC exceeds 10% only under the most critical operating condition, corresponding to $T_{wr,CND}$= 50°C and *ODT* = 5°C. Such a condition is characterized by a high temperature lift across the HP and represents an extreme operating point for air-to-water systems. However, within the Mediterranean climatic conditions of Palermo, outdoor air temperatures close to 5°C occur only for limited periods during the heating season and mainly during night-time hours. Since the proposed control strategy switches off the HP during the night and limits its operation approximately between 07:00 and 18:00, the system rarely operates under such severe conditions. Therefore, the influence of this deviation on the overall seasonal performance is expected to be negligible. Regarding the COP, percentage errors higher than 10% was observed for $T_{wr,CND}$= 45°C with *ODT* = 10°C. This condition is associated with daytime operation under relatively mild outdoor temperatures. Despite the TES setpoint temperature being equal to 50°C, the HP predominantly operates within the 45 – 50 °C return temperature range. Consequently, the observed deviations are deemed acceptable for the intended application of the model, since the HP is expected to operate predominantly within conditions for which a satisfactory agreement between the simulated and reference data is achieved, whereas only a limited number of hours are expected to fall within this operating point.

Summarising, some features of the HP and TES are detailed in Table 4. The TES volume equal to 4 m^3 was chosen according to the approach presented in [80] (approximately 0.01 m^3/kW of HP's rated capacity). In all simulations, the heat pump is pre-activated from 07:00 to 08:00 to ensure acceptable comfort conditions at the start of occupancy.

2.4. Photovoltaic-battery modeling

The PV module was simulated using TYPE 194, a validated model based on a five-parameter equivalent circuit (I_L, I_0, R_s, R_{sh}, and temperature-dependent α), whose accuracy was previously assessed against experimental data for photovoltaic technologies from the US National Institute of Standards and Technology [81]. The model reproduces the current-voltage characteristics of a PV cell or array [82]. A power conversion system was implemented using TYPE 48c for the inverter, which manages the DC/AC conversion of the electricity generated by the PV array. Instead, the battery energy storage system was simulated using TYPE 47 (Fig. 11). The global efficiency value equal to η_{glob} of 78.4% was adopted to account for the cumulative losses occurring along the entire PV-B energy conversion chain [83]. More specifically, it was estimated as the product of the efficiencies of the main system components, including the inverter, charge controller, and battery round-trip efficiency:

$$\eta_{glob} = \eta_{inv} \bullet \eta_{cc} \bullet \eta_{bat} \tag{13}$$

Where: η_{inv} is the inverter efficiency, assumed to be 95% (reflecting standard commercial bidirectional inverters); η_{cc} is the charge controller efficiency, assumed to be 96% (typical for high-efficiency maximum power point tracking units); η_{bat} is the battery round-trip efficiency, assumed to be 86%. The obtained value is consistent with the overall

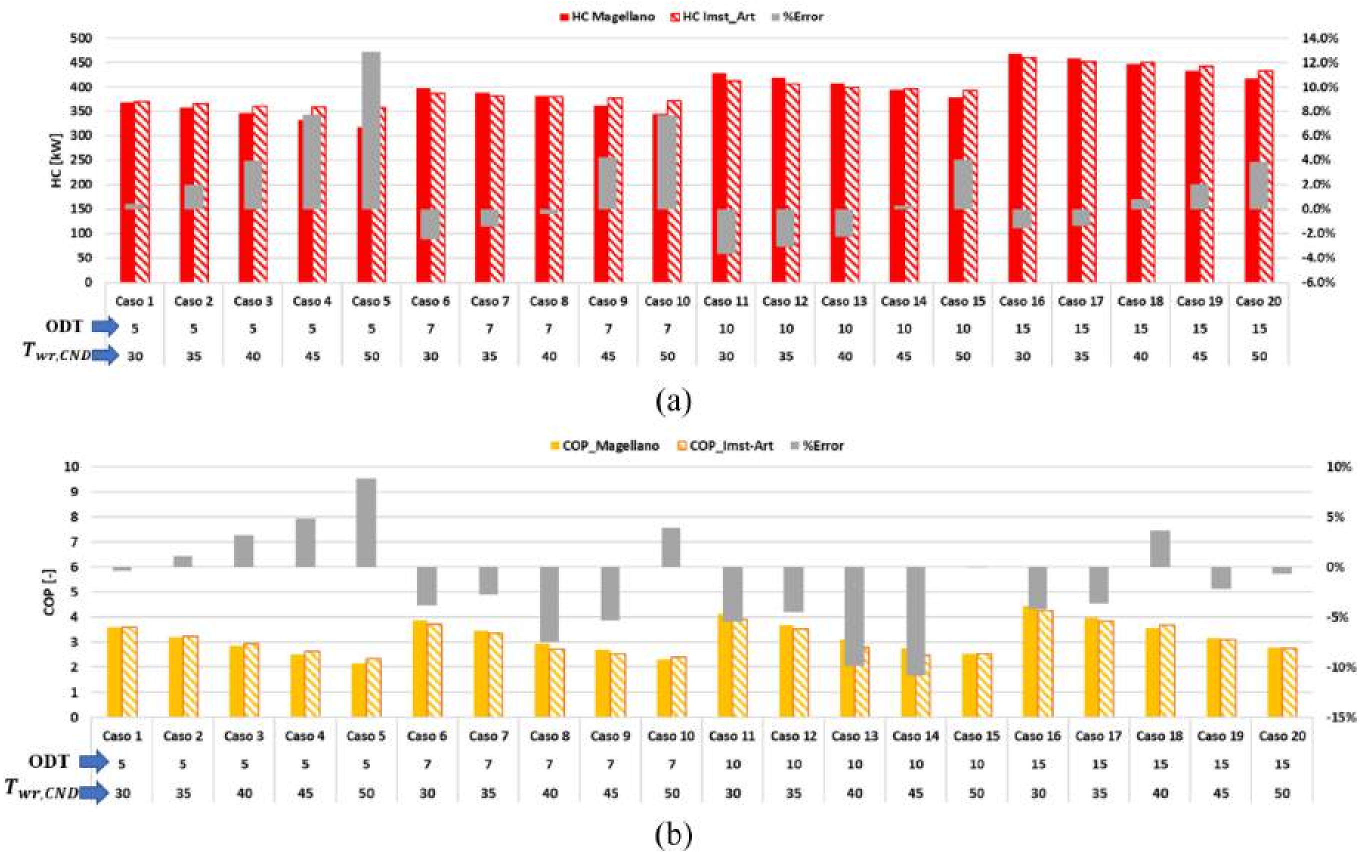

Fig. 10. Comparison between IMST-Art simulations and Magellano catalog data: (a) HC, (b) COP, and percentage errors.

Table 4
Heat pump and thermal energy storage: rating parameters and schedules.

HP	TES	Daily schedule	Seasonal schedule
Rated HC = 380 kW Rated $P_{m,H}$ = 140.74 kW COP = 2.7 (at $T_{wr,CND}$ = 40°C, ODT = 7°C) Rated CC = 323 kW Rated $P_{m,C}$ = 150.93 kW EER = 2.14 (at $T_{wr,EVP}$ = 12°C, ODT = 35°C)	Volume = 4 m^3 Height = 3 m	Weekly: 07:00 – 18:00 (ON) 18:00 – 07:00 (OFF) Saturday: 07:00 – 18:00 (ON) 18:00 – 07:00 (OFF) Sunday: 00:00 – 24:00 (OFF)	Winter: Dec 8 – Mar 23 (ON) Summer: Jun 1 – Sep 30 (ON) Intermediate: Mar 24 – May 31 (OFF) Oct 1 - Dec 8 (OFF)

system efficiencies commonly reported in the literature for integrated PV-B systems [84], where additional conversion and auxiliary losses are considered beyond the nominal battery round-trip efficiency [85]. The battery was operated within a State of Charge (SoC) range of 5-95%. The battery operating range was restricted to 5-95% SoC, rather than the full 0-100% range, to prevent deep-discharge and full-charge conditions, which are known to accelerate lithium-ion battery degradation and shorten cycle life [86]. Therefore, the adopted SoC operating window was selected as a realistic compromise between usable storage capacity and battery lifetime preservation. Once the upper SoC threshold was reached, any excess electrical energy generated by the PV-B system was injected into the grid.

Parameters for the photovoltaic [87] and the battery system [88] was taken from the manufacturer's data under standard test conditions (Table 5).

The PV-B system was sized based on the annual electricity demand from the building under the No DR scenario, which totals 408193.6 kWh/year. This value accounts for the electrical loads associated with lighting and equipment in the thermal zones, as well as the electricity required to operate the reversible heat pump. The installed capacity of the photovoltaic system was determined using an annual energy balance method. Assuming a specific energy yield of 1600 kWh/kW_p [89], representative of climatic conditions in Southern Italy, the required nominal PV capacity was estimated at approximately 258 kW_p. According to the manufacturer's technical specifications, the PV field was configured with 22 modules connected in series and 29 parallel strings, resulting in a total of 638 modules and an active PV surface equal to 1276 m^2. Even with a 20% allowance for spacing and shading losses, the required PV area remains well within the available rooftop surface of approximately 1660 m^2. This confirms that the PV system is fully compatible with the available installation area.The battery sizing was carried out using an adapted methodology developed in [90], which defines the storage capacity as a function of the average daily energy demand, the overall system efficiency, and the selected autonomy period. In the proposed configuration, the building's mean daily electricity consumption was about 1118.34 kWh/day, while a daily-cycling operational strategy in which the battery is fully charged and discharged once per day was defined. Based on the manufacturer's performance parameters, the resulting nominal storage capacity was estimated to be approximately 500 kWh. The performance of the designed PV-B system was investigated through annual dynamic simulations. Fig. 12-a.b illustrates the system behaviour on a representative summer day in August, highlighting a significant temporal overlap between the building's electricity demand and photovoltaic power generation. In fact, the maximum electricity consumption of the building (dashed black line, Fig. 12b) is largely coincident with the peak producibility of the PV system (solid red line, Fig. 12b). The electrical load profile exhibits

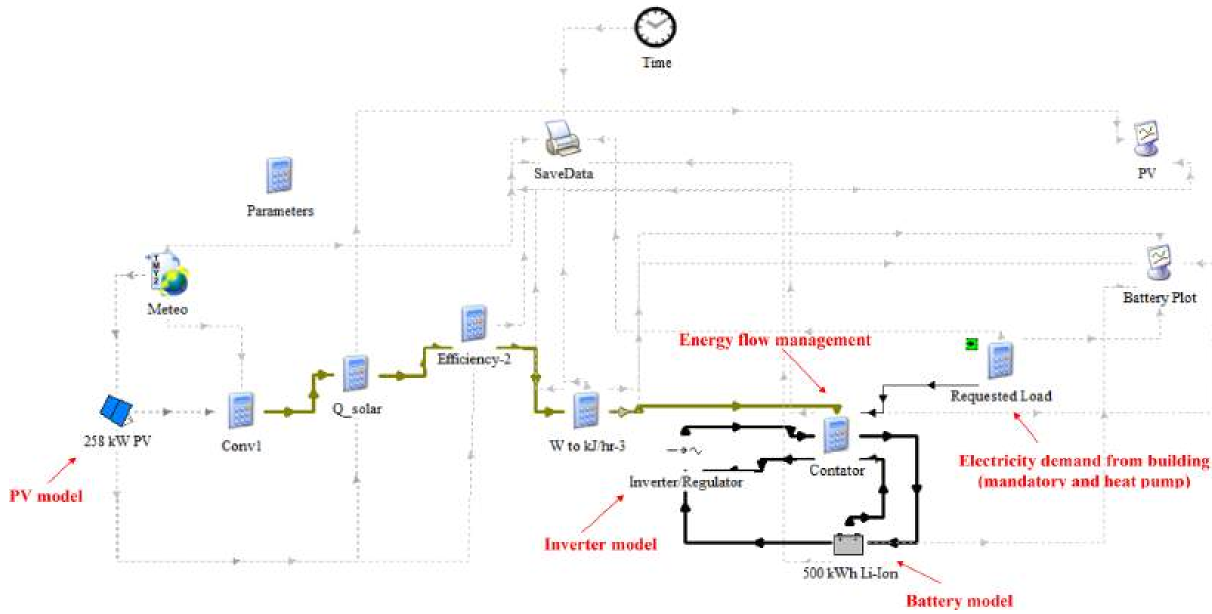

Fig. 11. PV-Battery system modelled in TRNSYS.

Table 5
PV-Battery system: rating parameters and schedules.

		SCHEDULE
PV[87]	- Data single PV module = 405 W – 2 m^2	Jan 1 – Dec 31 (ON)
BATTERY [88]	- Data single cell (lithium battery) = 16.7 Ah, 2.8 V	Jan 1 – Dec 31 (ON)

pronounced demand peaks during the early morning, around midday, and in the early afternoon hours (Fig. 12a). At the same time, PV electricity production follows the typical diurnal pattern of solar irradiance, reaching its highest values around midday (Fig. 12b). This favourable temporal alignment between demand and generation mitigates reliance on the electrical grid; nevertheless, the battery energy storage system remains essential for storing excess photovoltaic electricity produced during periods of high solar availability and supplying it during later time intervals, particularly in the early evening [91]. As a result, the level of on-site consumption of renewable electricity is further enhanced. The operational control strategy of the PV-B system was defined through a priority-based logic. When the instantaneous electrical demand of the building, including both thermal zones (solid green line, Fig. 12a) and HP (solid red line, Fig. 12a) is lower than the photovoltaic array, the demand is fully met by local renewable generation, while any surplus is exported to the grid (dashed light blue line, Fig. 12b) and the battery (dashed gold line, Fig. 12b). Conversely, when the electricity demand exceeds the available contribution from the PV system and the battery (solid purple line, Fig. 12b), the remaining load is supplied by the power grid (solid green line, Fig. 12b).

3. Demand response strategies

In this study, two demand-side flexibility strategies were investigated and compared against a reference scenario without DR. Both strategies were implemented by modulating the temperature setpoints of the thermal zones and the thermal energy storage system. The analysis encompasses a price-based approach, defined according to PUN, as well as a PV-driven strategy aimed at increasing the effective integration of variable renewable energy sources. The price-based approach dynamically modulates setpoint values in response to the PUN, whereas the PV-driven strategy relies on static setpoint adjustments applied at predefined time slots.

3.1. Price-based approach

The price-based strategy relies on the temporal variation of the PUN as an external control signal. Wholesale electricity prices in Italy reflect both the marginal cost of electricity generation from the available mix of technologies, including renewable and conventional sources, and the overall system demand. Low prices typically occur during periods of abundant renewable generation or low demand, while high prices indicate stressed grid conditions, which often require dispatching less efficient plants. By responding to these price signals, building loads can shift consumption to periods of lower cost, thereby supporting the grid and reducing operating expense. The PUN is calculated hourly by balancing national electricity supply and demand, considering generation efficiency, costs, and transmission capacity [92]. As illustrated in Fig. 7, the annual PUN profile for 2023 is reported with hourly resolution. Instead, Fig. 13 displays the PUN for two typical days: January 16th (solid blue line) and July 26th (solid orange line), with the average values indicated by $\overline{PUN}$ with the dashed red and purple lines, respectively. Those profiles are representative of the typical daily variation of PUN during the heating and cooling season. In particular, reduced PUN values are typically recorded between 11:00 and 13:00, coinciding with periods of abundant solar power generation. Conversely, increased PUN values are observed from 08:00 to 10:00 and from 15:00 to 17:00 in winter, and from 06:00 to 08:00 and from 19:00 to 21:00 in summer.

It is worth noting that the same electricity price signal (the 2023 PUN profile) was used consistently across all DR simulations. No forecasting or look-ahead control was considered, and the price signal was applied as a deterministic input.

Assuming "x" is a measure of the "*required degree of flexibility*", expressed as a percentage value, DR no. 1 and no. 2 were introduced by dynamically varying the setpoints of the thermal zones ($T_{set\text{-}th.zone}$) with the parameter ΔT_{sp} in response to the PUN profile, following the approach described below. The "x" value was set to 0.1, which means that flexibility was applied only for PUN values within ±10% of the daily average $\overline{PUN}$ (for example, in Fig. 13, the red band for January 16th and the light blue band for July 26th).

- **DR no. 1**: in this scenario, Eqs. (14) and (15) govern the adjustment of ΔT_{sp} during heating and cooling seasons, respectively. When PUN

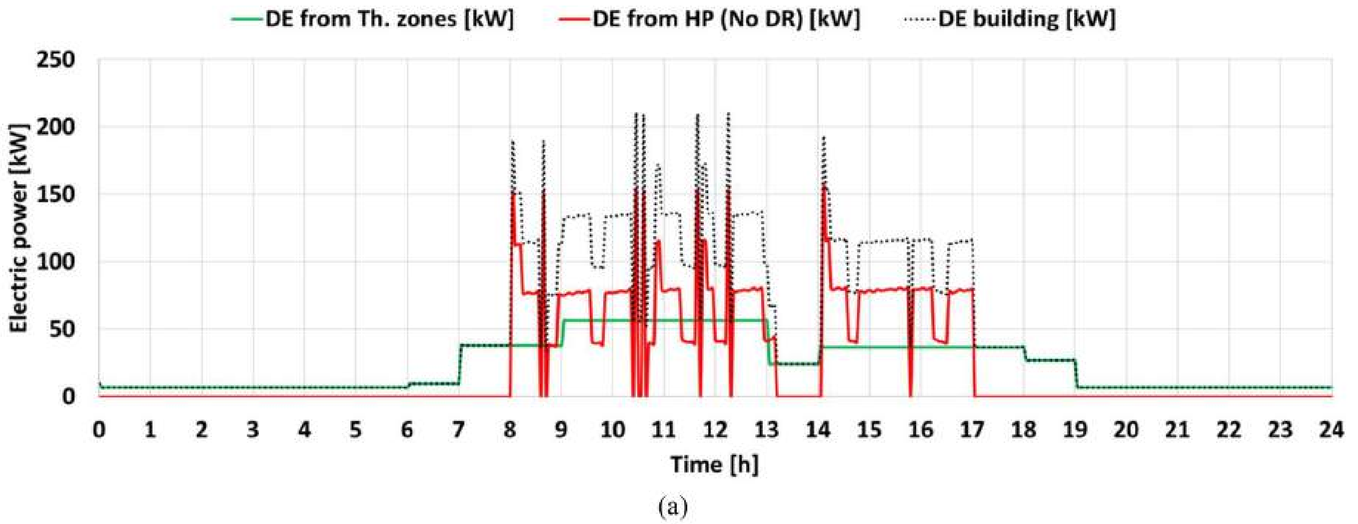

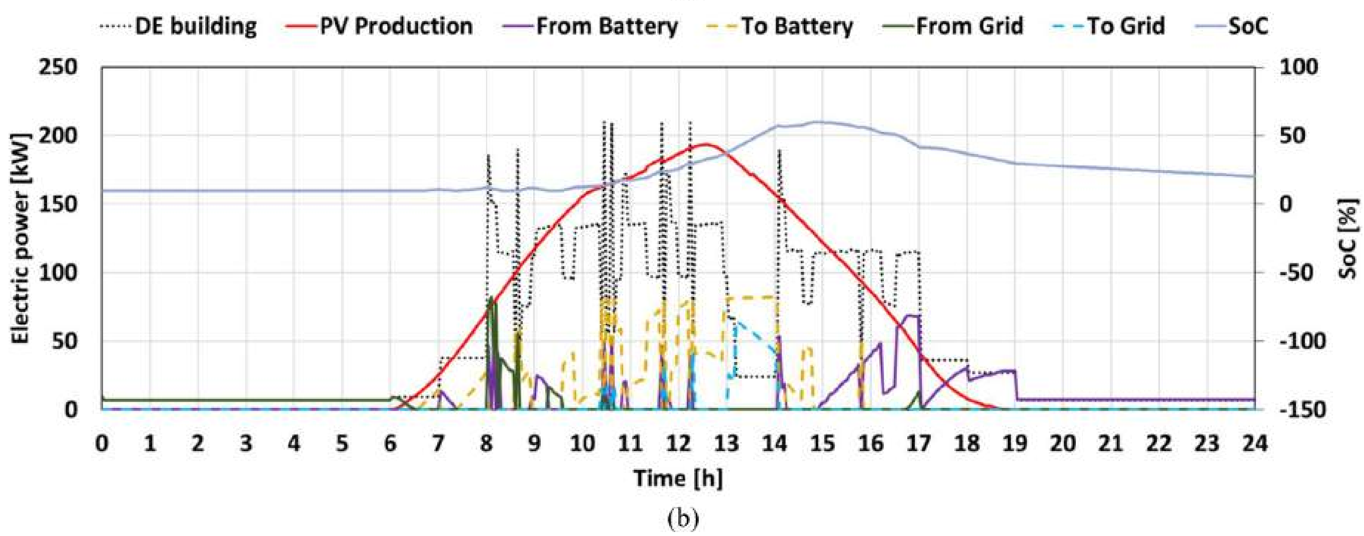

Fig. 12. PV-Battery system operation during a representative summer day in August: (a) electric demand from the office building (thermal zone and HP), (b) electric power exchanged between the PV-B system, the building and the grid.

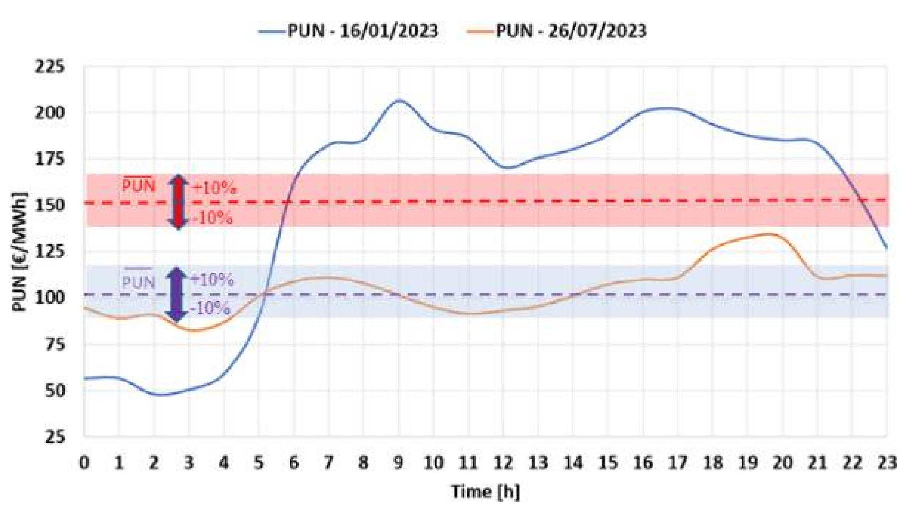

Fig. 13. PUN profile for January 16th and July 26th in 2023.

exceeds $\overline{PUN}(1 + x)$, maximum flexibility is applied (ΔT_{sp}= -2 °C in winter, +2 °C in summer). If PUN is below $\overline{PUN}(1 + x)$, ΔT_{sp} remains at 0, with no flexibility. For intermediate PUN values, ΔT_{sp} changes linearly: decreasing from 0 to -2 °C in winter and increasing from 0 to +2 °C in summer.

$$\mathbf{DR\,no.}\,1\,(\mathbf{winter})\,\Delta T_{sp\_winter}(^{\circ}C) = \begin{cases} -2 & \mathit{if}\ PUN > \overline{PUN}(1+x) \\ -\left(\dfrac{PUN - \overline{PUN}(1-x)}{\overline{PUN}x}\right) & \text{if}\ \overline{PUN}(1-x) \leq PUN \leq \overline{PUN}(1+x) \\ 0 & \mathit{if}\ PUN < \overline{PUN}(1-x) \end{cases} \tag{14}$$

$$\mathbf{DR\,no.}\,1\,(\mathbf{summer})\,\Delta T_{sp\_summer}(^{\circ}C) = \begin{cases} 2 & \mathit{if}\ PUN > \overline{PUN}(1+x) \\ \dfrac{PUN - \overline{PUN}(1-x)}{\overline{PUN}x} & \text{if}\ \overline{PUN}(1-x) \leq PUN \leq \overline{PUN}(1+x) \\ 0 & \mathit{if}\ PUN < \overline{PUN}(1-x) \end{cases} \tag{15}$$

- **DR no. 2:** in this scenario, Eqs. (16) and (17) define, during heating and cooling seasons, respectively, the adjustment of ΔT_{sp} for both high and low PUN conditions, enabling flexibility when electricity from renewables is abundant. When PUN exceeds $\overline{PUN}(1 + x)$, maximum flexibility is applied (ΔT_{sp} = -2 °C in winter, +2 °C in summer). When PUN falls below $\overline{PUN}(1 - x)$, ΔT_{sp} is reversed (+2 °C in winter, -2 °C in summer) to increase HP consumption. For intermediate PUN values, ΔT_{sp} varies linearly from +2 °C to -2 °C in winter and from -2 °C to +2 °C in summer.

$$\mathbf{DR\,no.}\,2\,(\mathbf{winter})\,\Delta T_{sp\_winter}(^{\circ}C) = \begin{cases} -2 & \mathit{if}\ PUN > \overline{PUN}(1+x) \\ 2 - \dfrac{2(PUN - \overline{PUN}(1-x))}{\overline{PUN}x} & \text{if}\ \overline{PUN}(1-x) \leq PUN \leq \overline{PUN}(1+x) \\ 2 & \mathit{if}\ PUN < \overline{PUN}(1-x) \end{cases} \tag{16}$$

$$\mathbf{DR\,no.}\,2\,(\mathbf{summer})\,\Delta T_{sp\_summer}(^{\circ}C) = \begin{cases} 2 & \mathit{if}\ PUN > \overline{PUN}(1+x) \\ -2 + \dfrac{2(PUN - \overline{PUN}(1-x))}{\overline{PUN}x} & \text{if}\ \overline{PUN}(1-x) \leq PUN \leq \overline{PUN}(1+x) \\ -2 & \mathit{if}\ PUN < \overline{PUN}(1-x) \end{cases} \tag{17}$$

The intuitive rationale behind the two DR schemes is to dynamically link the building's thermal demand to electricity price signals through a controlled, physically meaningful mechanism. DR no. 1 operates exclusively on a cost-avoidance logic, responding solely when electricity prices are elevated, specifically within and above the upper threshold of a ±10% band centred around the daily average PUN. Under these conditions, the indoor thermal setpoint is relaxed (i.e., decreased during the heating season and increased during the cooling season). This modification curtails HP operation, thereby limiting electricity consumption during peak-price periods. Conversely, when prices fall below the band, no control action is taken, allowing the system to operate under standard comfort configurations. For intermediate price ranges, the control response scales proportionally, ensuring a smooth transition between baseline operation and maximum demand flexibility. Consequently, DR no. 1 constitutes a unidirectional strategy optimized to mitigate peak-period expenditures without actively exploiting low-price intervals. In contrast, DR no. 2 integrates both cost-avoidance and load-shifting functionalities. While DR no. 2 mirrors the peak-shaving behaviour of DR no. 1 during high-price periods, it actively responds to low-price signals falling below the lower bound of the price band. Under low-cost conditions, the control logic is inverted: the thermal setpoint is shifted aggressively (i.e., increased in winter and decreased in summer). This adjustment drives higher HP electricity consumption, deliberately overheating or overcooling the building structure to store thermal energy. For intermediate price variations, the setpoint modulates continuously between these two operational extremes. DR no. 2 thus represents a bidirectional strategy that concurrently mitigates demand during expensive periods and intensifies it during economically favourable windows, effectively shifting the energy load over time. Ultimately, while DR no. 1 prioritizes operational simplicity by curtailing demand exclusively during unfavourable price conditions, DR no. 2 delivers an advanced form of flexibility. By actively redistributing power consumption across the entire spectrum of price volatility, DR no. 2 provides superior grid-balancing capabilities and enhances the integration of fluctuating renewable energy sources.

3.2. Photovoltaic-driven approach

As highlighted in Fig. 12, daily simulations for a representative summer day show a significant temporal overlap between the building's peak electricity demand and the PV-B production. In the PV-driven approach, the temperature setpoints of the thermal zones and the thermal energy storage were adjusted statically in a defined time slot using two control strategies, referred to as DR no. 3 and DR no. 4. In DR no. 3, during 11:00-13:00, the $T_{set\text{-}th.zone}$ was increased with the parameter ΔT_{sp}= +2 °C in winter and decreased at -2 °C in summer, by forcing the heat pump to consume more electrical energy precisely when the PV-B system production was available. This was followed by a complete shutdown of the HP from 15:00 to 17:00. In DR no. 4, during 11:00-13:00, analogous set-point adjustments with the parameter ΔT_{sp} was applied to $T_{set\text{-}TES}$ rather than the thermal zone set-point, with the heat pump similarly deactivated from 15:00 to 17:00. The selected activation periods were identified through a combined analysis of national electricity demand patterns, electricity market dynamics and renewable energy generation profiles. As discussed in the manuscript, the PUN is determined by the balance between electricity supply and demand. Consequently, intervals with peak PV generation typically align with favourable electricity price valleys, reflecting the high penetration of renewable sources. Consequently, the adopted control logic simultaneously maximizes PV self-consumption, increases the utilization of locally generated renewable electricity, and shifts electrical consumption away from periods characterized by less favourable market conditions.

Initially, the impact of DR on the HP's electricity consumption was quantified. Subsequently, the analysis was extended to the whole-building level. It should be noted that the assessment of the impact associated with the PV-B system under DR no. 3 and 4 necessitate an analysis at the whole-building level, encompassing the total electrical energy demand. As highlighted in Fig.12a, this demand is defined as the sum of the electrical loads associated with the thermal zones (i.e., lighting and equipment) and those attributable to the HP. In the absence of dedicated sub-metering systems capable of disaggregating end-use electricity consumption, it is not technically feasible in real applications to reliably determine the fraction of PV-B generated electricity allocated to lighting and equipment as opposed to that consumed by the heat pump. Accordingly, the impact assessment must be conducted on the aggregate electrical consumption of the entire building. As an initial step, the present study numerically quantified the impact of the four proposed strategies on the HP's electrical demand. Then, the analysis was extended to the overall building electricity consumption to assess the DR no. 3 and 4, the resulting reduction in electrical demand when the HP is combined with a PV-B system.

3.2.1. Photovoltaic-driven strategy implemented in a well-insulated building

The impact of a well-insulated building combined with the HP and PV-B system was also studied. The developed model notably incorporates night-time natural ventilation as a passive cooling strategy to mitigate the risk of overheating [93], a common challenge in well-insulated buildings during the summer months [94]. The well-insulated building exhibits faster indoor temperature rises during heat pump shutdowns due to reduced heat dissipation, leading to internal heat accumulation and an increased overheating risk [95]. Integrating night ventilation into the building's energy management system enables effective heat removal during cooler night-time hours without additional energy use [96], thereby reducing daytime cooling demand and improving occupant comfort [97]. This additional case study, referred to as DR no. 4 (INS), was provided only for Strategy no. 4. It highlights the crucial role of combining high insulation, HPs with TES, PV-battery systems, and night ventilation control using 5 ACH to achieve both energy efficiency and thermal comfort [98]. The analysis focused exclusively on DR no. 4, because in a future scenario characterized by the widespread adoption of highly insulated buildings equipped with HPs and combined RESs, the Distribution System Operator (DSO) would be able to achieve more effective operational control over plants integrated within buildings: power modulation through TES setpoint adjustment or heat pump ON-OFF switching appears easy to address. Conversely, direct intervention on the thermal zone setpoints is more complex. It would likely require incentive mechanisms to encourage end users to adjust thermal zone setpoint levels in response to grid needs.

3.3. Summary on model assumptions & limitations

Fig. 14 summarises the connected types and DR strategies implemented in TRNSYS, while Fig. 15 provides an overview of the corresponding modelling architecture, operational constraints, control logic, and key assumptions adopted throughout the simulations. The latter also summarizes the adopted boundary conditions, global simulation settings, key system parameters, and the main limitations of the proposed framework. These graphical representations provide a clearer and more intuitive visualization of the interaction between the physical system components, control strategies, and operational constraints governing the DR implementation.

Despite the comprehensive modelling approach adopted, some limitations of the present study should be acknowledged: (i) the analysis relies entirely on dynamic simulations, and no direct experimental validation of the specific case study was performed, although the reliability of the HP model is supported by a validation approach (see Section 2.3); (ii) the proposed framework relies on deterministic schedules for occupancy, internal gains, and weather conditions. In addition, the electrical grid is represented through simplified import/export interactions without detailed network constraints; (iii) the study is limited to a single building typology (an office building) and a specific location (Palermo), which may limit the generalizability of the results to other building categories and climate zones outside the Mediterranean region; (iv) economic aspects and regulatory constraints were not explicitly addressed, as the focus of the work is on the technical assessment of energy flexibility and thermal comfort.

3.4. Key performance indicators

The impact of the DR programs was assessed using the following Key Performance Indicators (*KPIs*).

3.4.1. Key performance indicators for human comfort evaluation

The effect of DR strategies on thermal comfort was assessed through the *mean PMV* and *PPD values* ($PMV^{DR}_{t\_mean}$ and $PPD^{DR}_{t\_mean}$), calculated from the corresponding instantaneous values at each time step t (PMV^{DR}_{t} and PPD^{DR}_{t}) over the daytime period comprising N time steps. The resulting averages were then compared with those obtained for the No

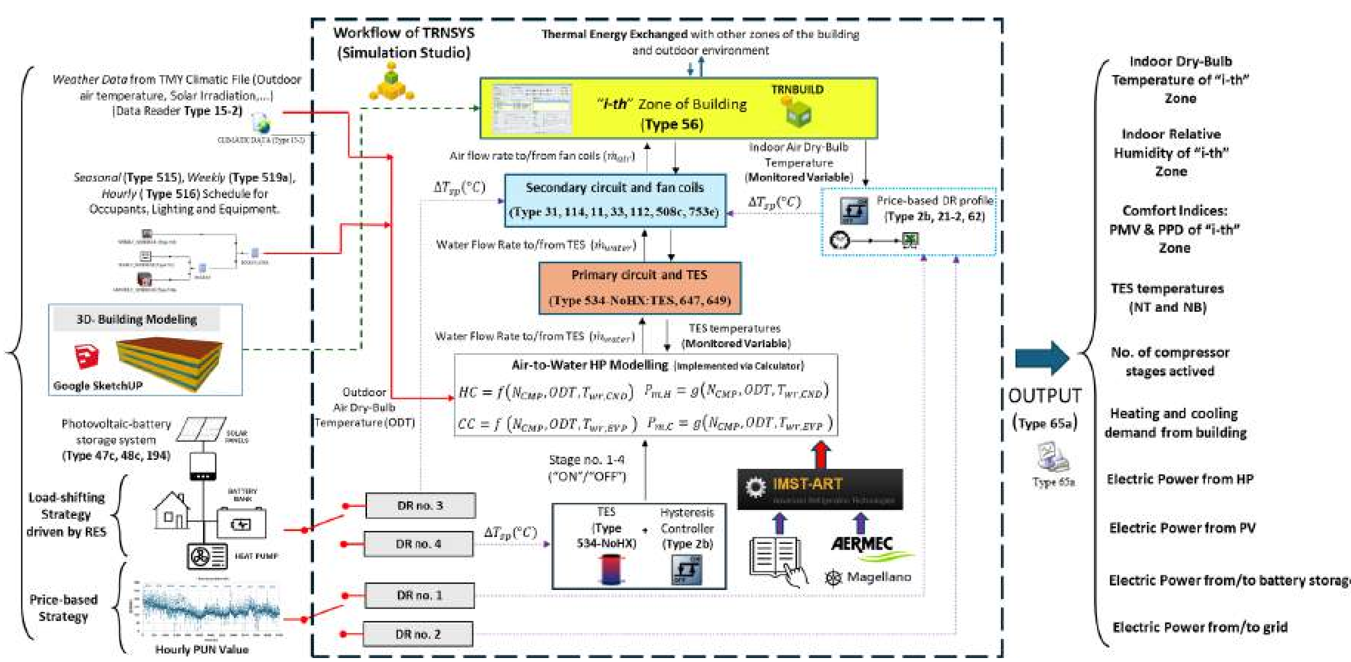

Fig. 14. Workflow project implemented in TRNSYS.

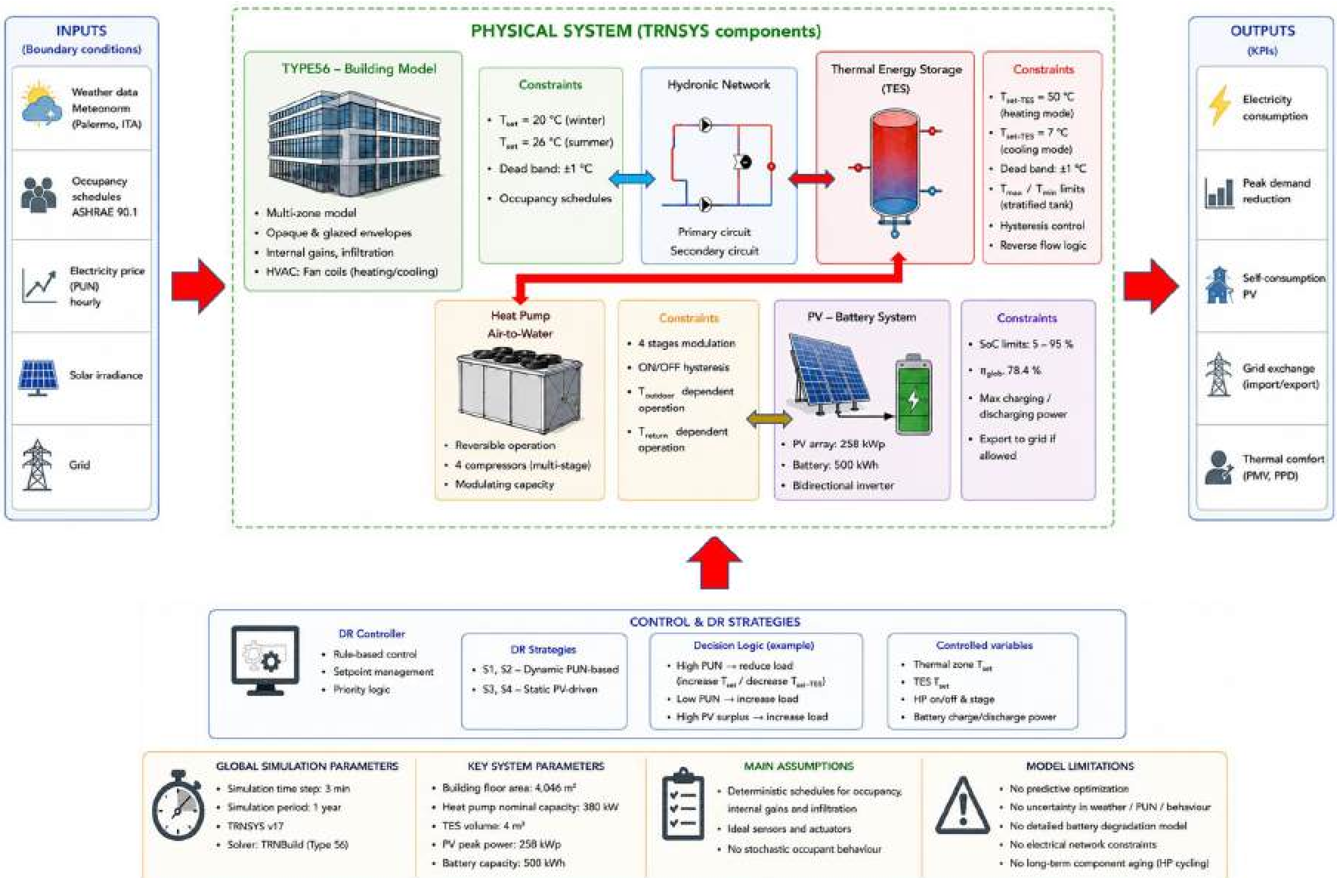

Fig. 15. Integrated simulation framework & operational constraints.

DR scenario ($PMV_{t\_mean}^{NO\,DR}$ and $PPD_{t\_mean}^{NO\,DR}$).

$$PMV_{t\_mean}^{DR} = \frac{1}{N}\sum_{t=1}^{N} PMV_t^{DR}\ [-] \tag{18}$$

$$PPD_{t\_mean}^{DR} = \frac{1}{N}\sum_{t=1}^{N} PPD_t^{DR}\ [\%] \tag{19}$$

To compute the DR impact on an annual basis, the *Comfort Compliance Ratio* (*CCR*), was introduced. It quantifies the ratio of the cumulative number of time steps *t* during which the human comfort satisfies the criterion $PPD_t \leq 10\%$ (δ_t) to the total analysed period T over the same time span. It provides a synthetic measure of annual thermal comfort performance.

$$CCR = \frac{\sum_{t=1}^{T}\delta_t}{\sum_{t=1}^{T} t}\ [\%]\ with\ \delta_t = \begin{cases} t\ if\ PPD_t \leq 10\% \\ 0\ if\ PPD_t > 10\% \end{cases} \tag{20}$$

3.4.2. Key performance indicators for energy flexibility evaluation

To assess the effect of DR measures on HP energy consumption relative to No DR, the following KPIs were evaluated:

- the *time shifting* (Δt_s) or the *variance percentage of time shifting* ($Var\Delta t_s$). They can be evaluated on a daily or annual basis, and quantify the number of hours during which energy use can be either delayed or anticipated. Δt_s can be evaluated graphically by comparing the energy cumulative curves with and without DR (i.e., the horizontal distance between the curves) [99]. Numerically, the delay can be determined by comparing the latest hour in electricity load duration curves (t_{S_last}), when DR is applied and not. A positive value of Δt_s indicates that the demand is delayed compared to the No DR. Otherwise, it is anticipated.

$$\Delta t_{s\_last} = t_{s\_last}^{DR} - t_{s\_last}^{NODR}\ [\mathrm{h}] \tag{21}$$

$$Var\Delta t_{s\_last} = \frac{t_{s\_last}^{DR} - t_{s\_last}^{NODR}}{t_{s\_last}^{NODR}}\ [\%] \tag{22}$$

- the *peak load shifting potential* ($VarP_t$) and the *cumulative load shifting potential* ($VarE_t^{DR}$). The peak load shifting potential, based on daily o annual basis, was computed as the percentage variation in the maximum power consumption when the DR is in place ($P_{t\_max}^{DR}$) compared to No DR scenario ($P_{t\_max}^{NO\,DR}$) [100]. It can also be used to evaluate the rebound effect resulting from the DR events.

$$VarP_{t\_max} = \frac{P_{t\_max}^{DR} - P_{t\_max}^{NODR}}{P_{t\_max}^{NODR}}\ [\%] \tag{23}$$

In Eq. 23, P_t^{DR} and $P_t^{NO\,DR}$ represent the power consumption at the time step *t* when the DR is in place or not, respectively.

The cumulative load shifting potential parameter, based on daily o annual basis, was computed in terms of percentage variation of energy consumption when the DR programs is in place (E_t^{DR}) compared to No DR scenario (E_t^{NODR}) in the same time span T.

$$VarE_t^{DR} = \frac{E_t^{DR} - E_t^{NODR}}{E_t^{NODR}} = \frac{\int_0^T P_t^{DR}dt - \int_0^T P_t^{NODR}dt}{\int_0^T P_t^{NODR}dt}\ [\%] \tag{24}$$

3.4.3. Normalized key performance indicators

To provide a comprehensive overview, a synthetic indicator (KPI_{NORM}) and a radar chart were used to summarize the annual KPI results for all investigated DR strategies. Starting from the previously KPIs, the KPI_{NORM} was normalized to a [1] scale based on the *best*- and *worst*-performing scenarios. Specifically, a min-max normalization approach was adopted. For KPIs where higher values indicate better performance (e.g., *CCR*), Eq. (25a) was applied. Conversely, for KPIs where lower values indicate better performance (e.g., $VarP_{t\_max}$, $VarP_{t\_max}$ and $Var\Delta t_{s\_last}$), Eq. (25b) was used. Consequently, normalized values closer to 1 consistently represent superior performance across all evaluation criteria.

$$KPI_{NORM} = \begin{cases} \dfrac{KPI - KPI_{min}}{KPI_{MAX} - KPI_{min}} & (25a) \\ 1 - \dfrac{KPI - KPI_{min}}{KPI_{MAX} - KPI_{min}} & (25b) \end{cases} \quad [-]$$

This approach accounts for the full observed data range, enabling a more robust comparison across heterogeneous indicators. As a result, the KPIs are consistently mapped while preserving the relative information of the original values.

4. Results and discussion

Dynamic simulations covering the entire year were performed for all DR scenarios and compared with the reference case using the defined KPIs. To assess the potential and impact of the proposed demand response strategies on electricity consumption and occupant comfort, two representative days for Palermo were identified: January 16th (winter) and July 26th (summer) in 2023.

For the sake of brevity, only the most significant strategies are presented here, namely DR no. 2 and DR no. 3 for the poorly insulated building, and DR no. 4 (INS). The human comfort analysis, heat pump electricity consumption, and the corresponding annual cumulative energy for DR no. 1 and DR no. 4, evaluated over the two representative days, are provided in the Supplementary Material.

4.1. Human comfort and energy performance evaluation

The results are shown for two representative thermal zones of the building: the Core Top Zone (CTZ), the top floor of the building characterized by high internal gains, and the Perimeter Top Zone (PTZ) defined by a high glazed surface (65.28 m^2, corresponding to a WWR of 47.68% for this thermal zone) and a south-facing orientation, typically associated with the highest solar radiation levels in Mediterranean climates.

4.1.1. Demand response no. 2 scenario

Human comfort and energy analyses for DR no. 2 are presented.

4.1.1.1. Human comfort analysis for demand response no. 2. Fig. 16-a.d compares the daily profiles of the Indoor Dry Bulb Temperature (IDBT) and Indoor Relative Humidity (IRH) on January 16th and July 26th for CTZ and PTZ under the No DR (dashed blue line) and DR no. 2 (solid grey line) scenarios.

In winter, flexibility is required between 08:00 and 17:00, based on the PUN and the occupancy schedule. During this time slot, the PUN value exceeds the threshold defined by $\overline{PUN}(1 + x)$, and ΔT_{sp}, is dynamically set to -2 °C (Figs. 16-a.b). In this configuration, the CTZ provides flexibility throughout the entire working day (Fig. 16a), while the PTZ contributes only from 08:00 to 10:00 (Fig. 14b).

In summer, DR no. 2 (Figs. 16-c.d) involves a more dynamic setpoint profile for CTZ and PTZ: it slightly increases around 27.03°C between 08:00 and 10:00, and then drops to 24°C from 10:00 to 12:00. This reduction increases the HP's power consumption during midday hours, thereby supporting the integration of RES into the power grid. Subsequently, the setpoint rises progressively from 24 °C to 27.06 °C between 12:00 and 17:00. The DR no. 2 strategy (solid red line) does not result in unacceptable variations in IRH when compared to the No DR scenario (dashed green line).

Fig. 17a.d illustrates the PMV (dashed blue and solid grey lines) and

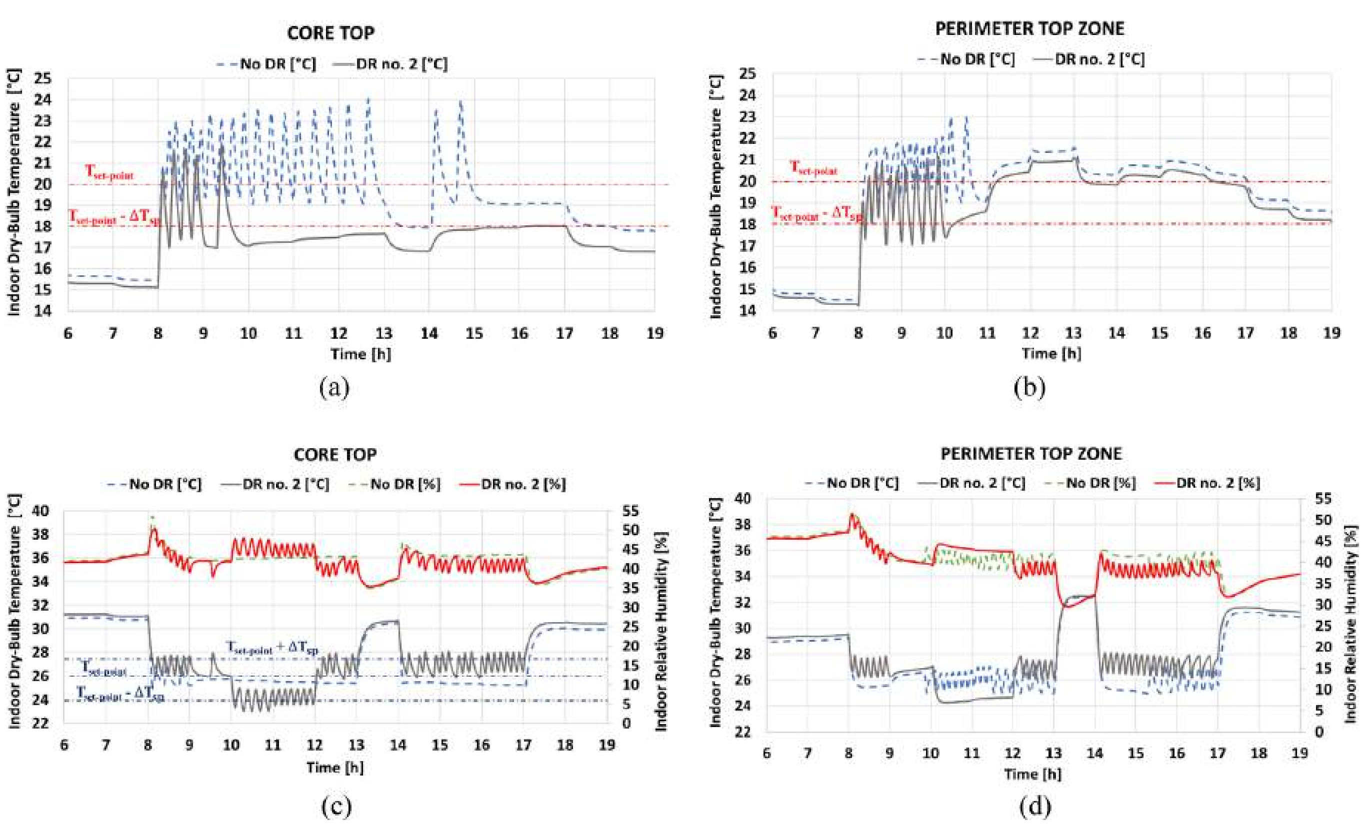

Fig. 16. IDBT and relative IRH profiles in DR no. 2 on January 16th and July 26th for CTZ and PTZ: (a,b) in winter, (c,d) in summer.

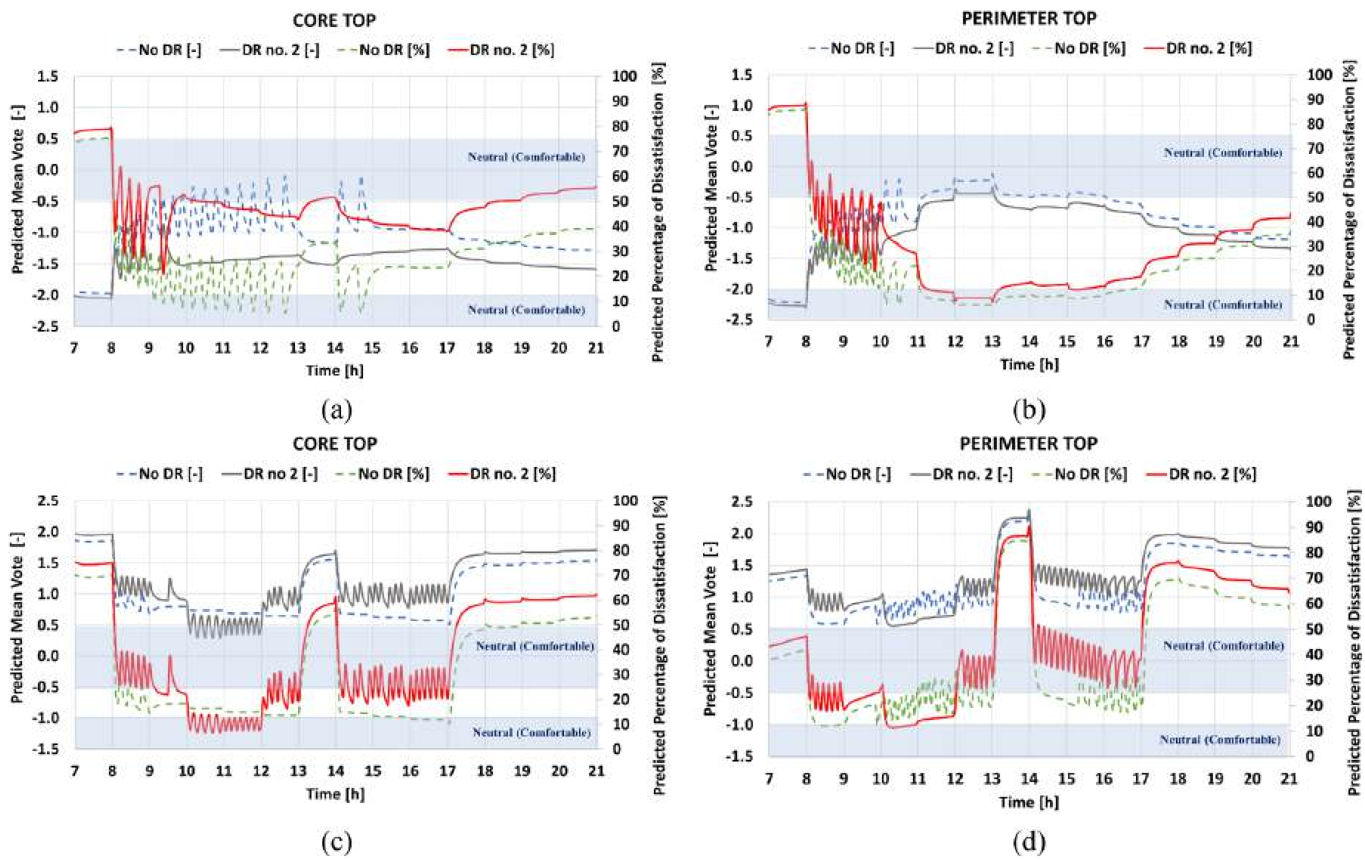

Fig. 17. PMV and PPD in DR no. 2 on January 16th and July 26th for CTZ and PTZ: (a,b) in winter, (c,d) in summer..

PPD (dashed green and solid red lines) indices for the two thermal zones analyzed. It is worth noting that, during most working hours of the two representative days considered, the comfort parameters fall outside the neutral zone (indicated by the blue band in Fig. 17), primarily due to extreme outdoor conditions, high internal gains, and the poor thermal performance of the building envelope. The results indicate that a reduction in setpoint temperature during winter and an increase during summer leads to a deterioration of these comfort indices compared to the reference case.

In detail, considering the defined thermal comfort KPIs during the analysed daytime period, in winter, PMV decreases from -0.78 to -1.43 between 08:00 and 13:00 for the CTZ, accompanied by an increase in PPD from +19.73% to +47.10%, corresponding to a deterioration of thermal comfort from Category IV to conditions outside the acceptable comfort range (PMV ≤ -1.0). During the 14:00-17:00 period, the PMV drops from -0.86 to -1.43, while the PPD rises from +21.30% to +41.30%, again indicating a transition from Category IV to out-of-category conditions (Fig. 17a). For the PTZ, between 08:00 and 13:00, the PMV decreases from -0.66 to -0.97, and the PPD increases from +17.36% to +27.92%, corresponding to a deterioration from Category III to Category IV. From 14:00 to 17:00, the PMV decreases from -0.50 to -0.65, with PPD increasing from +10.33% to +14.56%, indicating a transition from Category II to Category III (Fig. 17b).

In summer, for the CTZ, the PMV increases from +0.76 to +0.81 during the 08:00-13:00 interval, resulting in an increase in PPD from +17.55% to +20.60%, while thermal comfort remains within Category IV. In the subsequent 14:00-17:00 period, the PMV also increases from +0.65 to +0.99, accompanied by PPD from +14.33% to +26.08%, corresponding to a variation from Category III to Category IV (Fig. 17c). For PTZ, between 08:00 and 13:00, the PMV slightly increases from +0.84 to +0.87, leading to a PPD increase from +20.44% to +21.99%. At the same time, thermal comfort remains within Category IV. In the 14:00-17:00 time slot, the PMV rises from +1.00 to +1.31, with a corresponding increase in PPD from +26.78% to +40.66%, indicating a deterioration from Category IV to conditions outside the acceptable comfort range (Fig. 17d).

4.1.1.2. Energy performance evaluation for demand response no. 2. Heating and cooling demands (Figs. 18-a.b) and the power consumption of the HP (Figs. 18-c.d) during the DR no. 2 (solid grey line) event were quantified and compared to No DR (dashed blue line) for the two representative days, using the defined energy KPIs.

In winter, the peak thermal load is significantly reduced to 280.44 kW (-44.77%) (Fig. 18a), whereas in summer, a slight increase is observed, reaching 464.85 kW (+0.62%) (Fig. 18b). Correspondingly, the electrical power consumption of the HP decreases to 105.33 kW (-22.38%) in winter (Fig. 18c), and slightly drops to 149.47 kW (-0.86%) in summer (Fig. 18d). Peak shaving is observed throughout the winter working day. For instance, the power demand drops from 78 kW to 42 kW (-46.15%) around 08:30-09:30 and 10:00 time slots, and from 40 kW to zero around 10:30 and 14:30-15:00 intervals (Fig. 18c). Notably, no rebound effects are detected in winter. In summer (Fig. 18d), although the peak is reduced from 78 kW to 38 kW (-51.28%) around 08:30 and 09:30 and in the afternoon, a pronounced high load emerges at 11:00 with power demand peaking equal to 150 kW (+92.30%). The pronounced increase in HP electrical power (Figs. 18-c.d, blue and red asterisks) is directly linked to the activation of the third and fourth compressor stages (Figs. 18-e.f, solid green and purple lines, respectively). During this period, the reduced cooling setpoint imposed by DR no. 2 increases the cooling demand, prompting the controller to activate additional compressors to satisfy the thermal load. This behaviour is accompanied by a significant increase in HP power consumption (+41.02%), which is required to compensate for the reduced indoor temperature setpoint of 24 °C during the 10:00-12:00 time slot.

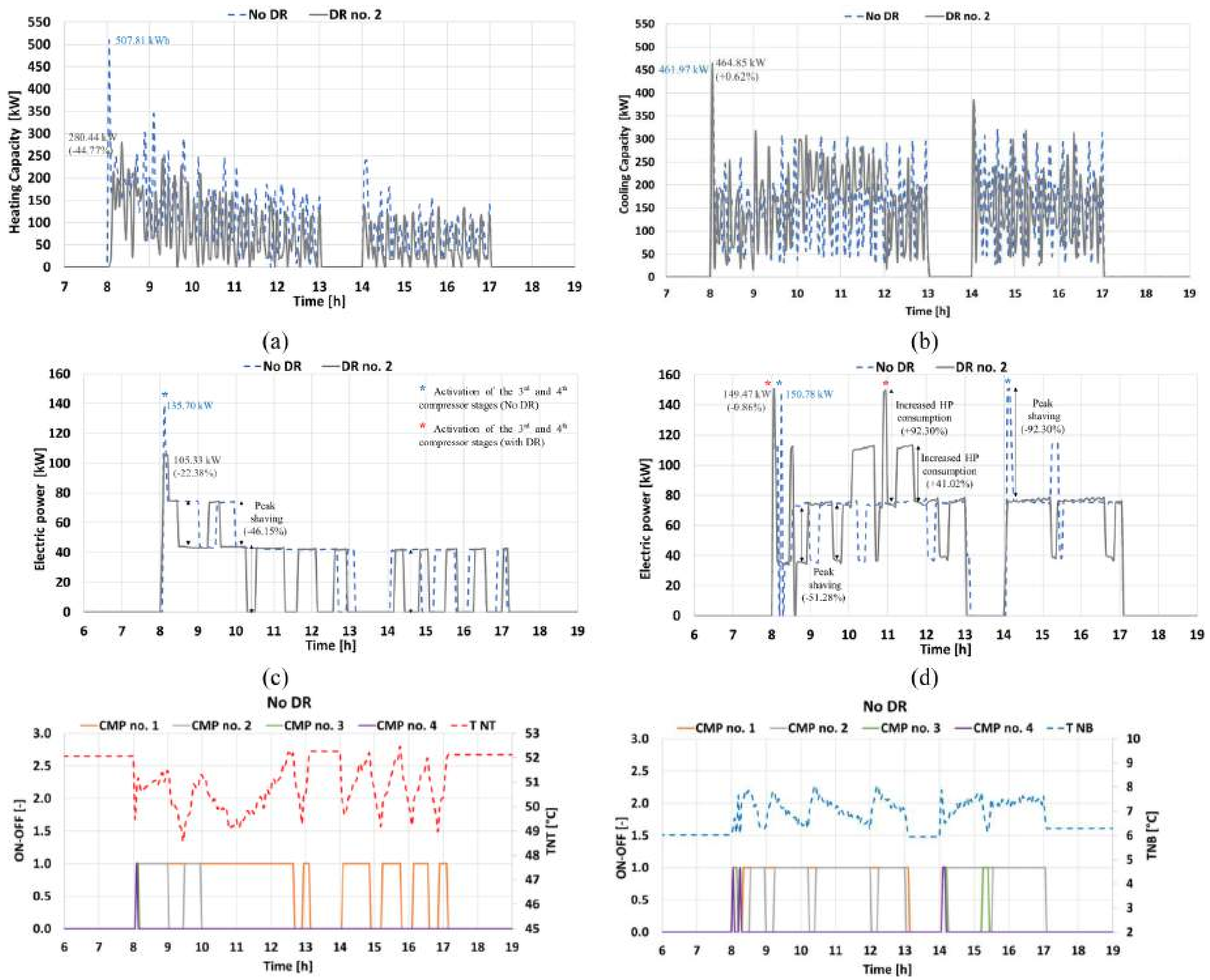

Fig. 18. Energy analysis in DR no. 2 on January 16th and July 26th: (a) heating demand (b) cooling demand, (c) electricity demand in winter (d) electricity demand in summer, (e) TES temperature (NT) and number of compressor stages actived in winter, (f) TES temperature (NB) and number of compressor stages actived in summer, (g) daily cumulative energy curve in winter, (h) daily cumulative energy curve in summer.

In detail, Figs. 18-e.f show the variation in TES temperature and the activation of compressor stages during winter (dashed red line) and summer (dashed blue line). As highlighted, the HP can meet both heating and cooling demands by shifting from part-load to full-load operation, activating additional compressor stages as needed to maintain the TES setpoint temperature. It is worth noting that in the summer scenario (Fig. 18f), compressor stages 3 and 4 are activated in a 10:00-12:00 interval, coinciding with a high RES availability.

Finally, the total energy consumption decreases to 244.82 kWh (-28.17%) in winter (solid grey line) (Fig. 18g), while it slightly increases to 595.02 kWh (+0.89%) in summer (Fig. 18h), when compared to No DR (dashed blue line).

4.1.2. Demand response no. 3 scenario

Human comfort and energy analyses for DR no. 3 are highlighted.

4.1.2.1. Human comfort analysis for demand response no. 3. Figs. 19-a.d compare the daily profiles of the IDBT and IRH on January 16th and July 26th for CTZ and PTZ, under the No DR (dashed blue line) and DR no. 3 (solid purple line) scenarios.

During winter, flexibility is required between 11:00 and 13:00, with the setpoint temperature ΔT_{sp} statically increased by +2 °C, followed by a complete HP shutdown from 15:00 to 17:00. According to high internal gains, the indoor temperature increases up to 25°C for both CTZ and PTZ in the 11:00-13:00 time slot. After 15:00, no significant deviation in indoor temperature is observed with respect to the No DR scenario (Fig. 19-a.b).

In the summer period, the setpoint temperature is reduced by -2 °C between 11:00 and 13:00, thereby providing flexibility for both CTZ and PTZ. After 15:00, the DR strategy delivers enhanced flexibility, which is accompanied by a measurable deviation in indoor thermal conditions attributable to elevated internal gains. In particular, for CTZ, the presence of the TES maintains compliance with the thermal zone setpoint until 15:30, whereas in PTZ, solar gains through the glazed surfaces and internal loads result in high deviations starting from 15:00 (Fig. 19-c.d). Regarding IRH (solid black line), this strategy causes a deviation from the No DR scenario (dashed green line) starting at 15:30 for CTZ and at 15:00 for PTZ.

Figs. 20-a.d illustrate the PMV (dashed blue and solid purple lines) and PPD (dashed green and solid black blue) indices for the two thermal

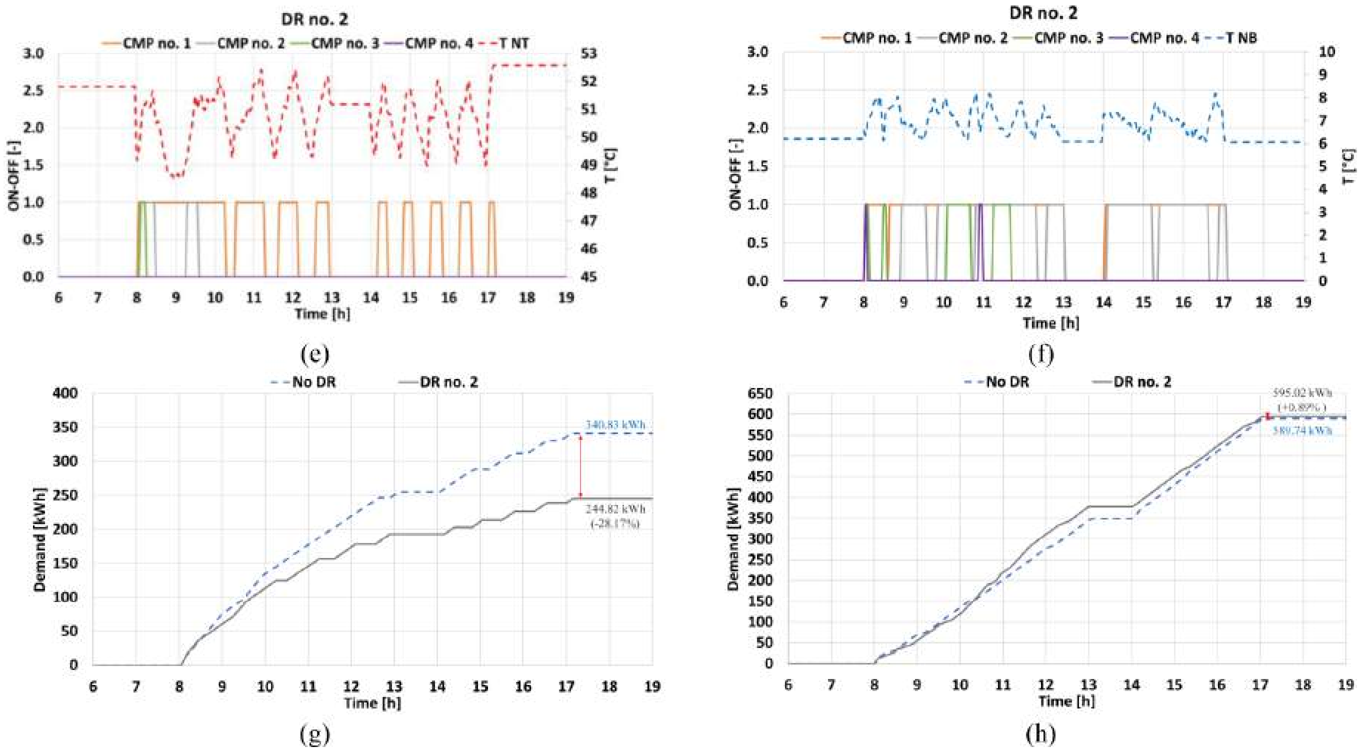

Fig. 18. (*continued*).

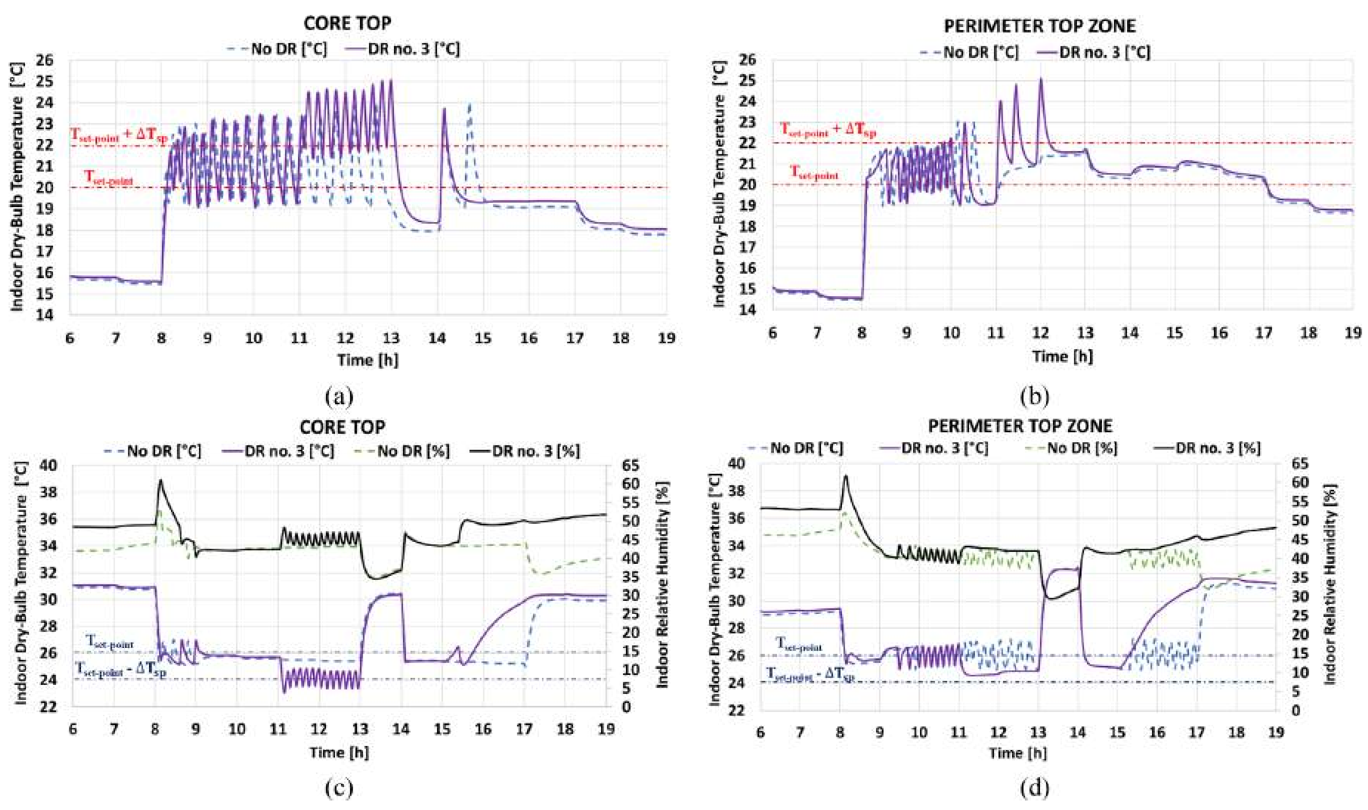

Fig. 19. IDBT and relative IRH profiles in DR no. 3 on January 16th and July 26th for CTZ and PTZ: (a,b) in winter, (c,d) in summer.

zones under investigation. The results indicate that increasing the thermal zone setpoint temperature in winter and decreasing it in summer slightly improve the mean values of the thermal comfort indices compared to the reference case, except for the 14:00-17:00 period during summer.

In winter, PMV increases from -0.78 to -0.65 between 08:00 and 13:00 for the CTZ, accompanied by a decrease in PPD from +19.73% to +17.51%, corresponding to an improvement from Category IV to

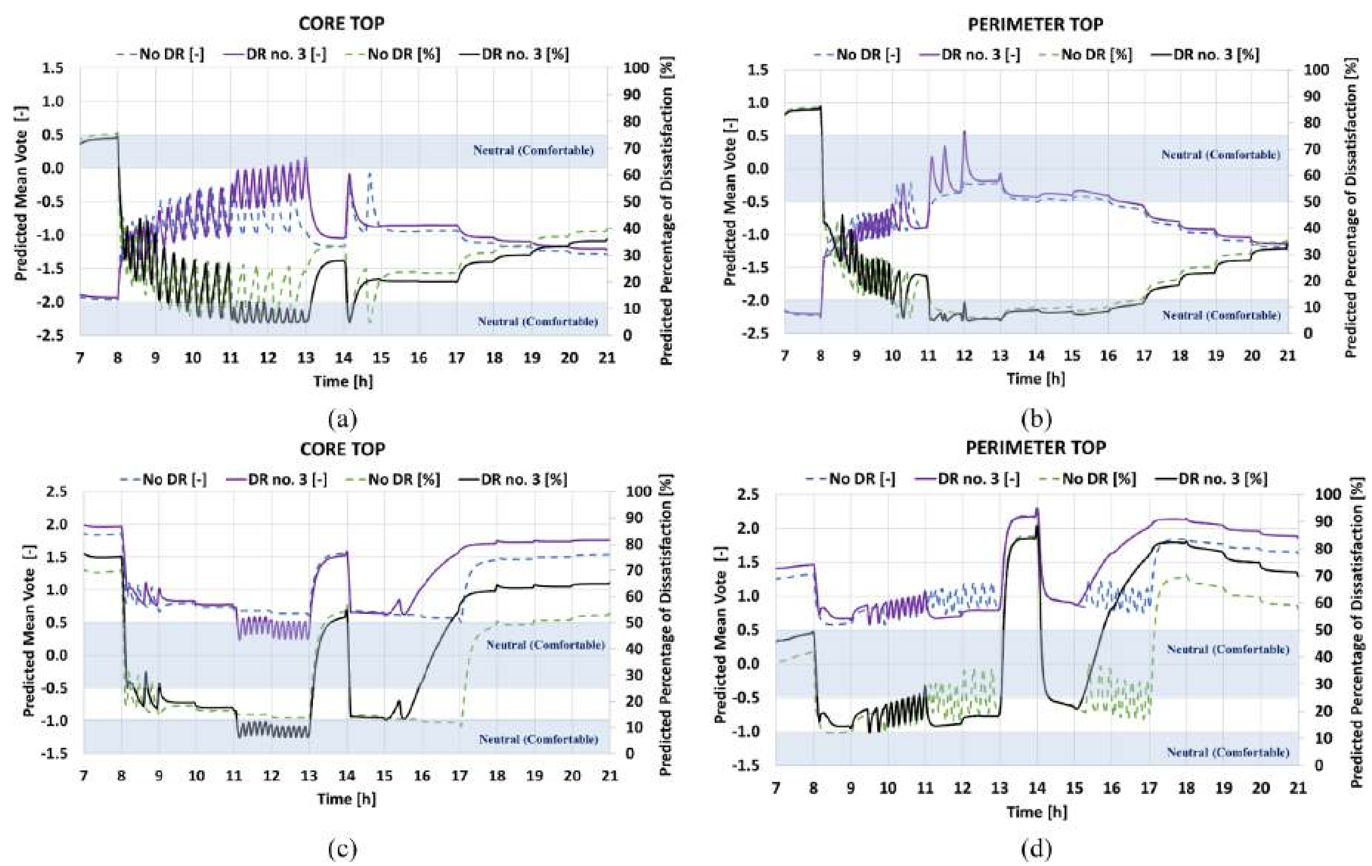

Fig. 20. PMV and PPD in DR no. 3 on January 16th and July 26th for CTZ and PTZ: (a,b) in winter, (c,d) in summer.

Category III. During the 14:00-17:00 period, the PMV grows from -0.86 to -0.82, while the PPD drops from +21.30% to +19.51%, indicating that thermal comfort remains within Category IV (Fig. 20a). For the PTZ, between 08:00 and 13:00, the PMV slightly increases from -0.66 to -0.63, and the PPD slightly grows from +17.36% to +18.36%, indicating stable conditions within Category III. From 14:00 to 17:00, the PMV increases from -0.50 to -0.42, with PPD decreasing from +10.33% to +8.80%. This suggests that the comfort remains within Category II (Fig. 20b).

In summer, PMV decreases from +0.76 to +0.70 between 08:00 and 13:00 for the CTZ, with a corresponding PPD drop from +17.55% to +16.92%, indicating an improvement from Category IV to Category III (Fig. 20c). Between 14:00 and 17:00, PMV increases from +0.65 to +0.95, and PPD from +14.33% to +26.03%, corresponding to a deterioration from Category III to Category IV (Fig. 20c). For the PTZ, during the 08:00-13:00 time slot, PMV decreases from +0.84 to +0.79, and PPD from +20.44% to +18.46%, indicating stable conditions within Category IV. In the 14:00-17:00 period, the PMV increases significantly from +1.00 to +1.39, while PPD rises from +26.78% to +46.15%, leading to a deterioration from Category IV to out-of-category conditions (Fig. 20d).

4.1.2.2. Energy performance evaluation for demand response no. 3. Heating and cooling demands (Figs. 21-a.b) and the power consumption of the HP (Figs. 21-c.d) during the DR no. 3 (solid purple line) event were quantified and compared to No DR (dashed blue line) for the two representative days.

The peak heating and cooling loads decrease under DR no. 3: from 507.81 kW to 362.37 kW in winter (-28.64%) (Fig. 21a), and from 461.97 kW to 375.36 kW in summer (-18.75%) (Fig. 21b). Similar to previous strategy, the power consumption of the HP shows only minor variations: it slightly decreases in winter from 135.70 kW to 135.23 kW (-0.34%) (Fig. 21c) and increases in summer from 150.78 kW to 151.17 kW (+0.26%) (Fig. 21d). In winter, the load is increased from 41.86 kW to 72.82 kW (+73.97%) around 11:30 and 12:30 (Fig. 21c). A clear peak shaving effect is observed from 15:00 to 17:00 (-100%) when the HP is tuned off. In summer, peak demand increases from 73.82 kW to 148.43 kW (+101.08%) around 09:30 and 12:00, followed by a peak shaving effect from 15:00 to 17:00 (-100%) (Fig. 21d). It is worth noting that, due to the shutdown of the HP during the 15:00-17:00 interval, rebound effects are observed in both winter and summer (+100%) at 07:00, when the heat pump is turned on.

Figs. 21-e.f show the variation in TES temperature and the activation of compressor stages during winter (dashed red line) and summer (dashed blue line). As shown, the HP shutdown at 15:00 leads to a pronounced temperature decrease in the thermal energy storage during winter, whereas in summer it causes a substantial temperature rise. This necessitates the activation of all 4 compressors at 07:00 the following morning to reestablish the target setpoint. Also, in the summer scenario (Fig. 21f), compressor stages 3 (solid green line) and 4 (solid purple line) are activated when high RES production occurs.

Finally, Figs. 21-g.h illustrate the daily cumulative energy curves. Under DR no. 3 (solid purple line), the total energy use in winter increases at 378.20 kWh (+10.96%) (Fig. 21g). In summer, it decreases at 540.08 kWh (-8.42%) (Fig. 21h).

4.1.3. Demand response no. 4 scenario – insulated building

Human comfort and energy analyses for DR no. 4 (INS) are presented.

4.1.3.1. Human comfort analysis for demand response no. 4 (INS). Figs. 22-a.d compare the daily profiles of the IDBT and IRH on January 16th and July 26th for CTZ and PTZ, under the No DR (dashed blue line) and DR No. 4 (INS) (solid back line) scenarios. In DR no. 4 (INS),

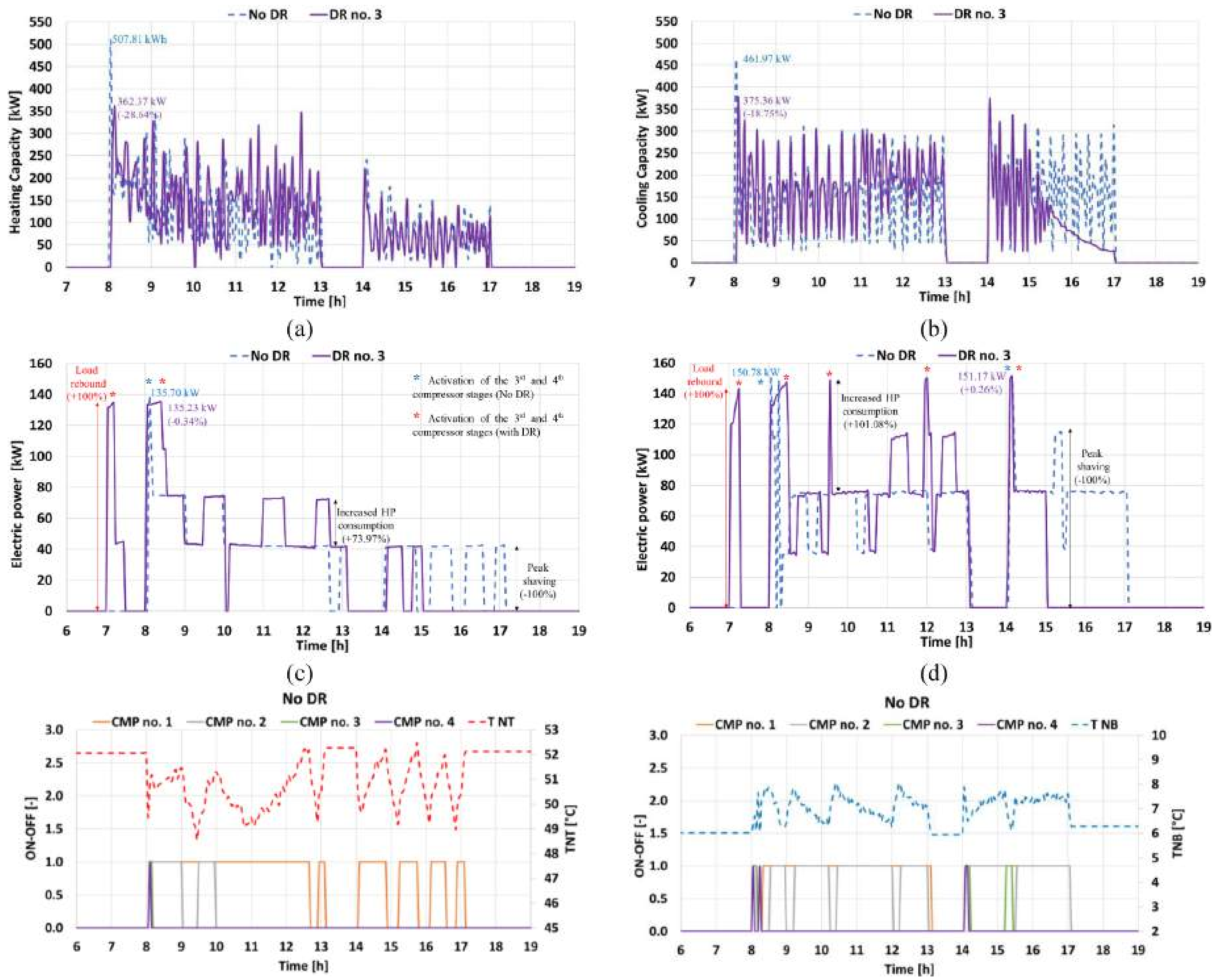

Fig. 21. Energy analysis in DR no. 3 on January 16th and July 26th: (a) heating demand (b) cooling demand, (c) electricity demand in winter (d) electricity demand in summer, (e) TES temperature (NT) and number of compressor stages actived in winter, (f) TES temperature (NB) and number of compressor stages actived in summer, (g) daily cumulative energy curve in winter, (h) daily cumulative energy curve in summer.

between 11:00 and 13:00, static set-point adjustments using the parameter ΔT_{sp} is applied to the TES (+2°C in winter and -2°C in summer), while the thermal zone set-point remains unchanged. The HP is deactivated from 15:00 to 17:00.

During the winter period, the well-insulated building exhibits the following behavior: (a) an indoor temperature of approximately 19°C, higher than in the No DR scenario (about 15-16°C), prior to HP activation for both CTZ and PTZ; and (b) a gradual variation in indoor temperature (Fig. 22-a.b), attributable to the higher thermal inertia of the envelope, which dampens temperature fluctuations and delays the indoor thermal response to control actions.

In summer, night-time ventilation maintains the indoor temperature at approximately 25°C, which is lower than in the No DR scenario (e.g., about 31°C for CTZ), and close to the thermal zone setpoint before HP activation for both CTZ and PTZ. As a result, the HP experiences a reduced energy consumption during start-up (Fig. 22-c.d). Conversely, for IRH (solid light blue line), this strategy leads to an increase compared to the No DR scenario (dashed green line).

Figs. 23-a.d illustrate the PMV (dashed blue and solid black lines) and PPD (dashed green and solid light blue lines) values for the two thermal zones under investigation. Similar to DR no. 3, and excluding the 14:00-17:00 period during summer, the results indicate that adjusting the TES setpoint, by increasing it during winter and decreasing it during summer, leads to a slight improvement in the mean values of the thermal comfort indices compared to the No DR and other DR strategies. This improvement is also attributable to the enhanced thermal insulation.

In winter, PMV increases from -0.78 to -0.76 between 08:00 and 13:00 for the CTZ, accompanied by a decrease in PPD from +19.73% to +17.67%, indicating that thermal comfort remains within Category IV. During the 14:00-17:00 period, the PMV grows from -0.86 to -0.51, while the PPD decreases from +21.30% to +10.58%, corresponding to an improvement from Category IV to close Category II (Fig. 23a). For the PTZ, between 08:00 and 13:00, the PMV increases from -0.66 to -0.36, and the PPD decreases from +17.36% to +13.63%, indicating a transition from Category III to Category II. From 14:00 to 17:00, the PMV increases from -0.50 to -0.06, and PPD decreases from +10.33% to +5.13%, corresponding to an improvement from Category II to Category I (Fig. 21b).

In summer, PMV decreases from +0.76 to +0.29 between 08:00 and

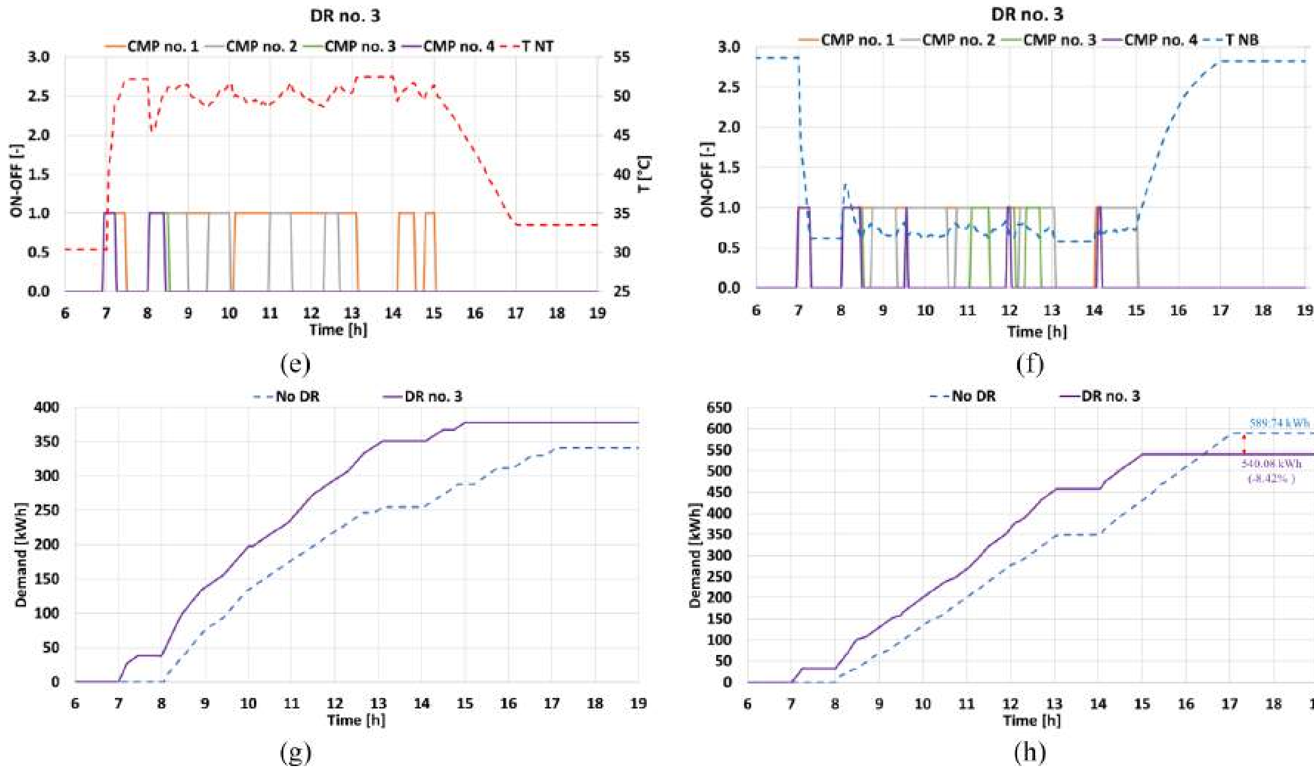

Fig. 21. (*continued*).

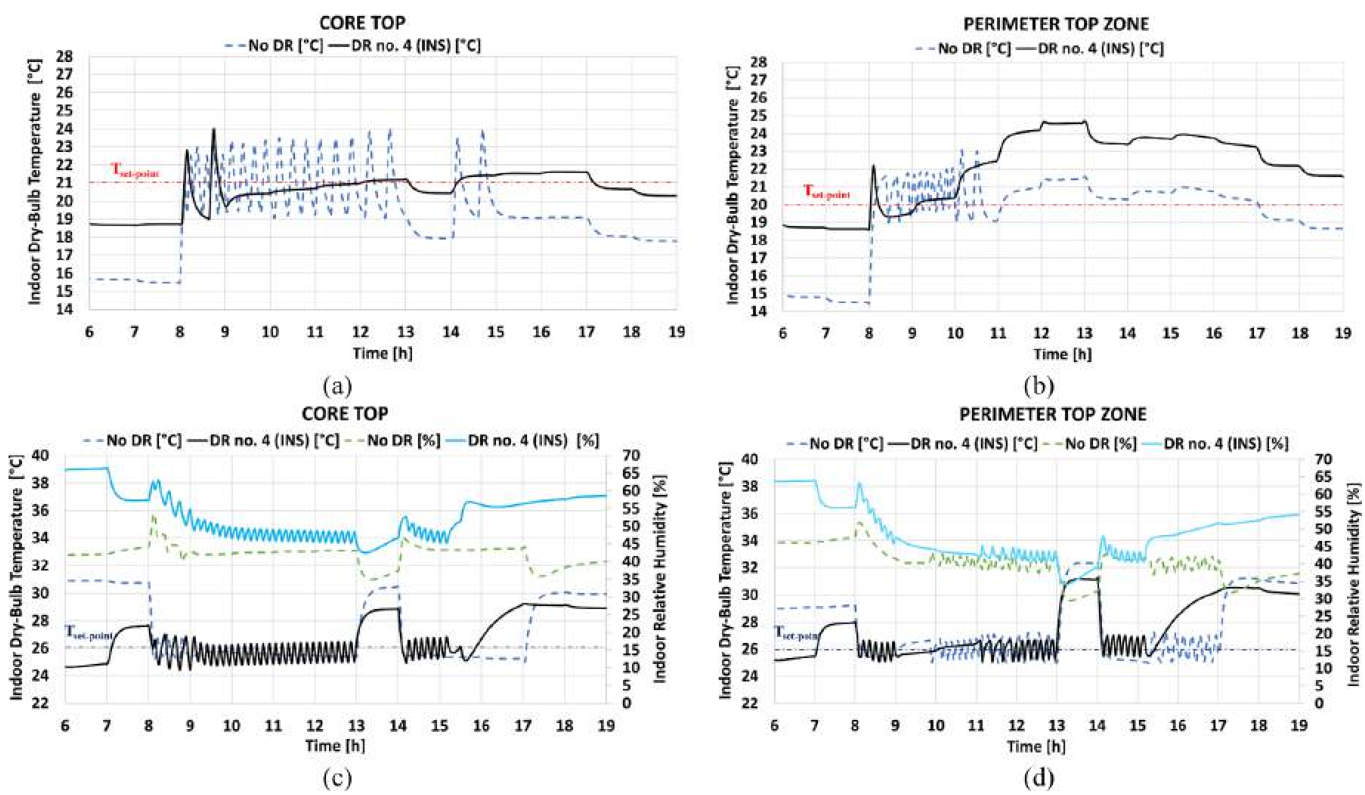

Fig. 22. IDBT and relative IRH profiles in DR no. 4 (INS) on January 16th and July 26th for CTZ and PTZ: (a,b) in winter, (c,d) in summer.

13:00 for the CTZ, with a corresponding PPD drop from +17.55% to +7.21%, indicating a significant improvement from Category IV to Category II (Fig. 23c). Between 14:00 and 17:00, PMV slowly decreases from +0.65 to +0.61, and PPD increases from +14.33% to +14.75%, indicating stable conditions within Category III. For the PTZ, during the 08:00-13:00 time slot, PMV decreases from +0.84 to +0.56, with PPD dropping from +20.44% to +12.09%, indicating an improvement from Category IV to Category III. In the 14:00-17:00 period, the PMV

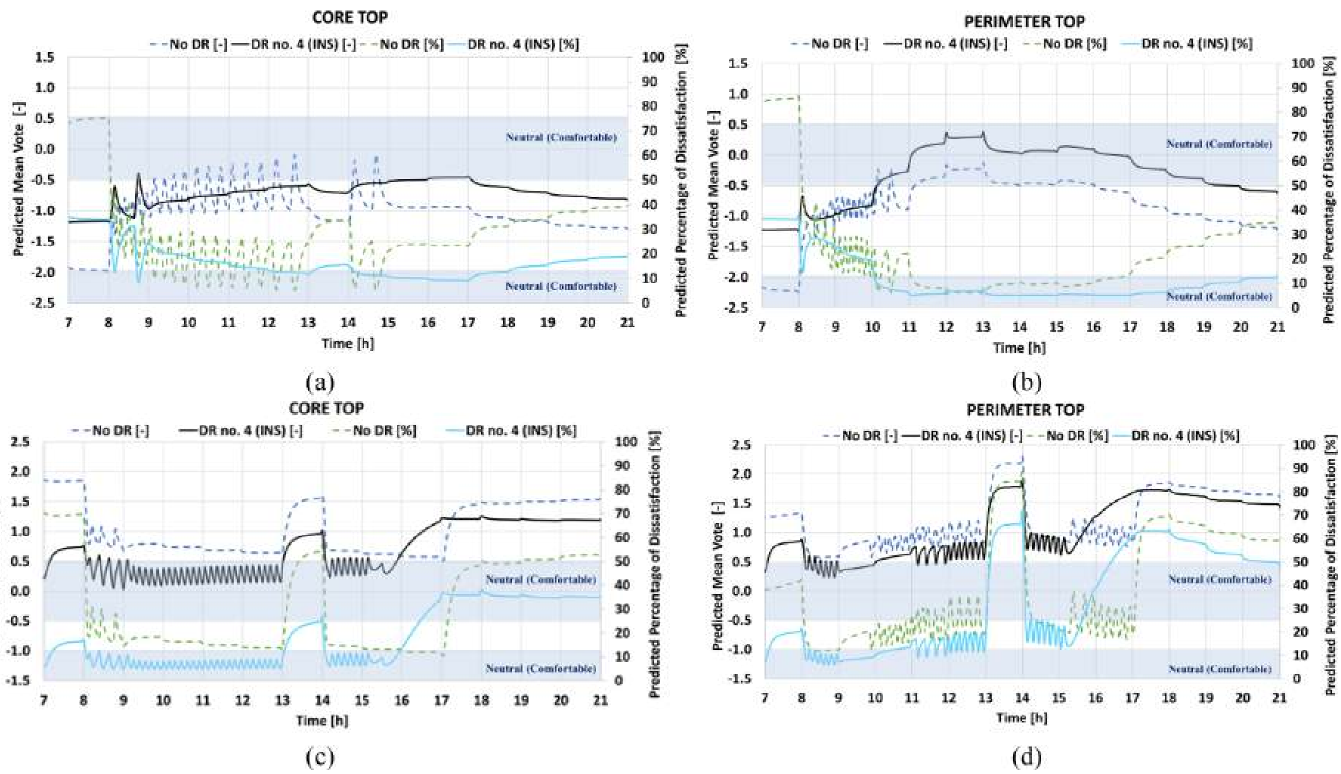

Fig. 23. PMV and PPD in DR no. 4 (INS) on January 16th and July 26th for CTZ and PTZ: (a,b) in winter, (c,d) in summer.

increases from +1.00 to +1.12, while PPD rises from +26.78% to +33.12%, corresponding to a deterioration from the boundary of Category IV to conditions outside the acceptable comfort limits (Fig. 23d).

The results highlight that DR no. 4 (INS) significantly enhances occupant comfort between 08:00 and 13:00 during both summer and winter seasons. However, a slight reduction in comfort indices is observed between 14:00 and 17:00 compared to the baseline scenario, occurring exclusively in summer and primarily affecting the PTZ zone, which receives increased solar radiation through the windows. This decrease is mainly attributed to the HP being deactivated between 15:00 and 17:00.

4.1.3.2. Energy performance evaluation for demand response no. 4 (INS). Heating and cooling demands (Figs. 24-a.b) and the power consumption of the HP (Figs. 24-c.d) during the DR no. 4 (INS) (solid black line) event were quantified and compared to No DR (dashed blue line) for the two representative days.

The peak heating and cooling loads decrease under DR no. 4 (INS): from 507.81 kW to 350.79 kW in winter (-30.92%) (Fig. 24a), and from 461.97 kW to 452.90 kW in summer (-2.15%) (Fig. 24b). Only minor changes are observed in the HP power consumption: it slightly increases in winter from 135.70 kW to 136.00 kW (+0.23%) (Fig. 24c) and in summer from 150.78 kW to 154.28 kW (+2.32%) (Fig. 24d). During winter, peak shaving is observed throughout the entire working day, with reductions ranging from -22.42% to 100% around at 08:00 and 11:00, respectively. In summer, peak demand increases to +95.98% around 11:00, followed by a peak shaving effect from 15:00 to 17:00 (-100%) (Fig. 24d). Similarly to DR no. 3, due to the shutdown of the HP during the 15:00-17:00 interval, rebound effects are observed in both winter and summer (+100%) at 07:00, when the HP is turned on.

Figs. 24-e.f show the variation in TES temperature and the activation of compressor stages during winter (dashed red line) and summer (dashed blue line). Similar considerations to DR no. 3 can be done. However, during winter, since the building demands less thermal energy from the indoor spaces, the TES temperature remains close to the set-point for most of the day. In the summer scenario (Fig. 24f), compressor stages 3 (solid green line) and 4 (solid purple line) are activated during periods of high PV production.

Finally, Figs. 24-g.h illustrate the daily cumulative energy curves. Under DR no. 4 (INS) (solid black line), the total energy use in winter decreases to 93.13 kWh (-72.68%) (Fig. 24g). In summer, it drops to 515.27 kWh (-12.62%) (Fig. 24h). These correspond to the lowest power consumption values observed among all the evaluated strategies.

4.1.4. Impact of demand response strategies on the heat pump performance

Supplementary daily and annual dynamic analyses revealed that the TES significantly stabilised HP operation under the No DR scenario, ensuring quasi-steady behaviour with SCOP and SEER values of approximately 3.83 and 2.14, respectively. Conversely, the implementation of DR strategies induced severe transient effects, including TES thermal depletion/saturation, aggressive compressor over-staging, and large heating/cooling capacity overshoots. More specifically, DR strategies do not merely reduce the average seasonal efficiency indicators but also induce a substantial loss of operational continuity and thermodynamic stability. While aggressive DR strategies are highly effective for building-side flexibility, peak-shaving, and grid-stress mitigation, they simultaneously penalize the HP via intensified compressor cycling and large electrical power fluctuations, which must be carefully evaluated when designing advanced smart-grid control architectures.

Additional results concerning the variations in heating capacity, cooling capacity, electrical power consumption, seasonal performance indicators (SCOP/SEER), and instantaneous COP/EER as functions of the condenser return temperature (winter operation), evaporator return temperature (summer operation), number of activated compressors and outdoor air temperature under the investigated DR strategies were included in Section 3 of the Supplementary Material.

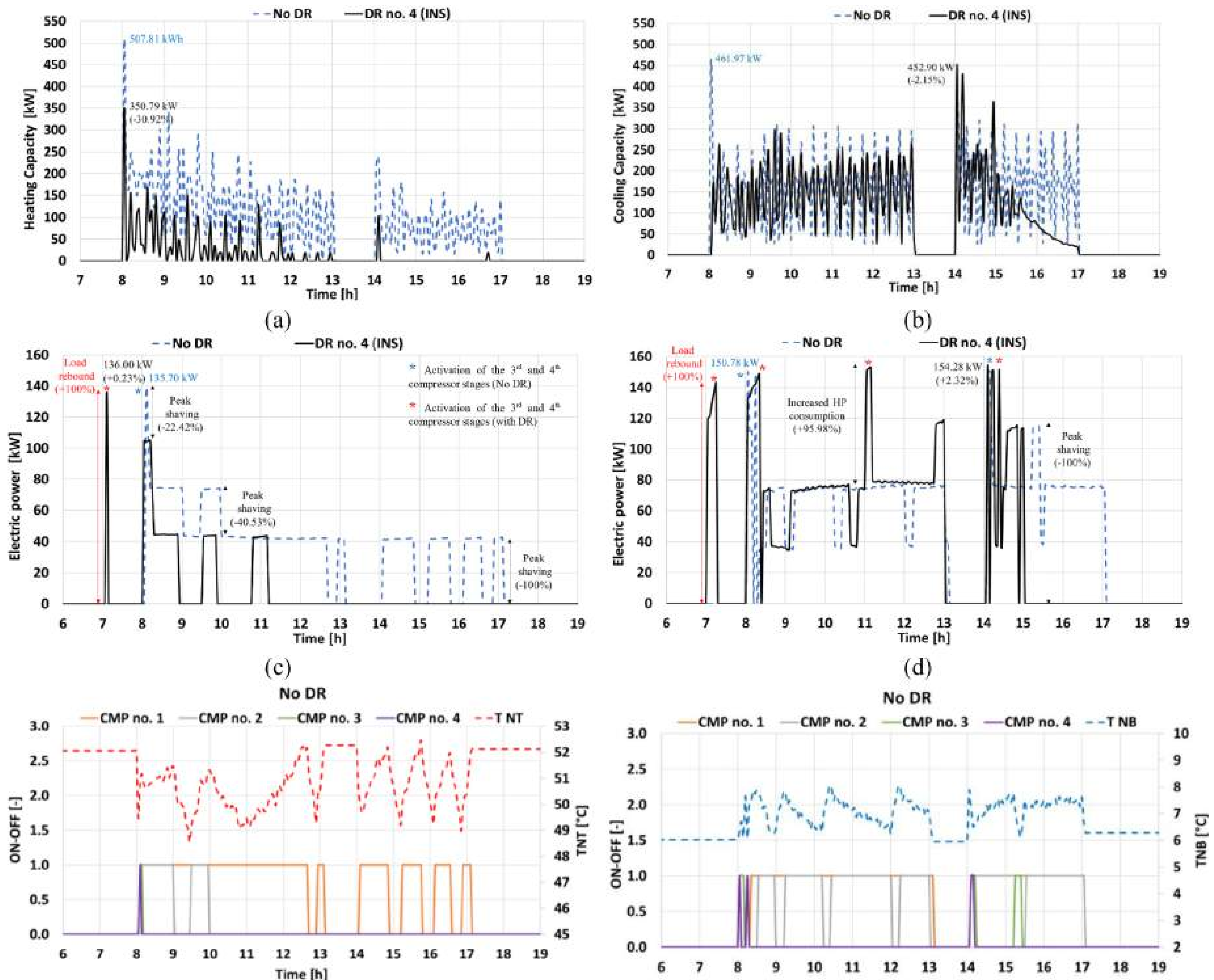

Fig. 24. Energy analysis in DR no. 4 (INS) on January 16th and July 26th: (a) heating demand (b) cooling demand, (c) electricity demand in winter (d) electricity demand in summer, (e) TES temperature (NT) and number of compressor stages actived in winter, (f) TES temperature (NB) and number of compressor stages actived in summer, (g) daily cumulative energy curve in winter, (h) daily cumulative energy curve in summer.

4.2. Yearly results

Annual results for human comfort, heat pump and overall building electricity consumption across all DR strategies are presented.

4.2.1. Annual human comfort analysis

The analysis of the representative winter and summer DR events reveals distinct differences among the investigated control strategies. The PV-driven approaches based on static setpoint adjustments during predefined time slots (DR no. 3 and DR no. 4) generally exhibit a lower temporary impact on occupant thermal comfort during the specific short-term events analysed compared to the dynamic price-based strategies (DR no. 1 and DR no. 2). In particular, the combination of TES setpoint modulation, improved envelope insulation, and night-time ventilation as a passive cooling strategy (DR no. 4 (INS)) provides the most favourable comfort conditions among all investigated cases. Compared with the No DR scenario, DR no. 4 (INS) reduces energy consumption while maintaining, and in some cases improving, the mean thermal comfort indices. When assessed according to the comfort categories reported in Table 3, this configuration clearly represents the best-performing solution. It is the only strategy capable of achieving Category II and, in some periods, Category I conditions during winter, while maintaining the CTZ zone within Categories II-III during summer operation. A remaining limitation is observed in the afternoon period within the PTZ zone during summer, where the combination of solar gains and temporary heat pump deactivation leads to PMV values exceeding the upper acceptability threshold (PMV $> +1.0$). Nevertheless, its overall thermal comfort performance during the representative DR events remains superior to that of the other investigated strategies. It should be noted that the conclusions above refer specifically to the analysed representative days and therefore describe the short-term impact of the different demand response actions on indoor environmental conditions. A broader assessment can be obtained by extending the analysis to the entire year through the CCR, which quantifies the fraction of annual operating hours during which the indoor environment satisfies the criterion PPD $\leq$ 10%. The CCR was evaluated only for the CTZ thermal zone, as it is characterized by a higher occupancy density (53 occupants) than the PTZ (11 occupants). The reference scenario achieved a value of 34.71%, indicating that highly comfortable indoor conditions were maintained for approximately one-third of the analysed

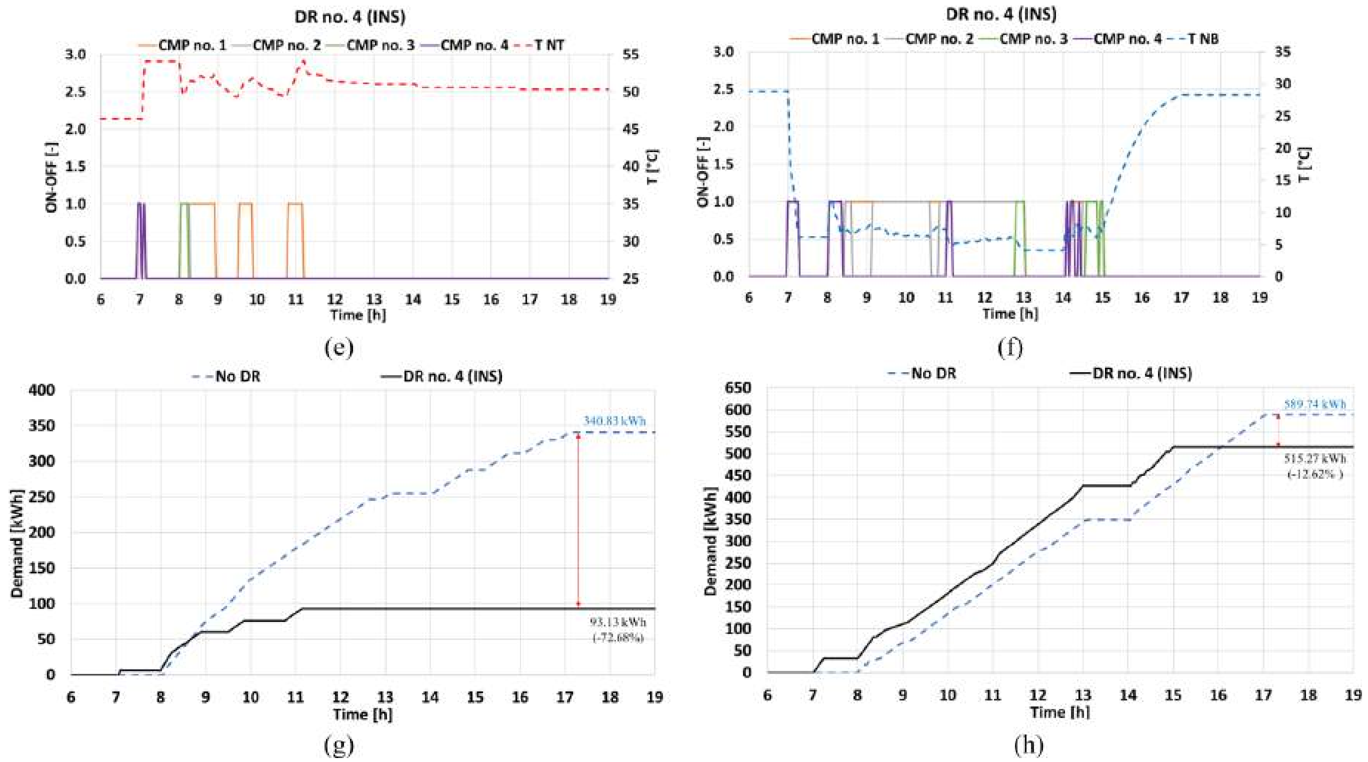

Fig. 24. (*continued*).

period. Similarly, DR no. 2 achieved 36.14%, slightly outperforming the reference case and demonstrating that demand response flexibility can be provided without reducing the annual availability of acceptable comfort conditions. DR no. 3 yielded 31.18%, indicating a moderate reduction in annual comfort availability. In contrast, DR no. 1 and the uninsulated DR no. 4 exhibited the lowest values, both close to 24%, suggesting a significant decrease in the fraction of time during which the PPD remained below 10%.The most remarkable result was obtained for DR no. 4 (INS), which achieved 81.22%, more than doubling the value observed for the reference scenario. This finding confirms that the combination of envelope improvements, passive cooling through night ventilation, and TES management substantially enhances the long-term availability of comfortable indoor conditions, marking a fundamental difference from its uninsulated counterpart (DR no. 4). Overall, the annual analysis reveals that the mean thermal comfort performance observed during representative DR events does not necessarily translate directly into annual comfort availability. While some strategies may successfully mitigate discomfort during specific events, their long-term effectiveness can differ considerably when evaluated over the entire year. These results therefore highlight the importance of complementing event-based PMV/PPD analyses with annual comfort indicators such as CCR, allowing a more comprehensive assessment of the trade-offs between energy flexibility and occupant comfort.

4.2.2. Annual electricity consumption of the heat pump

Fig. 25 shows the electricity load duration curve and the annual cumulative energy consumption of the HP under all investigated DR strategies. Moving from the reference case (dashed blue line), the load duration curve (Fig. 25a) indicates that the annual peak electric power demand in the No DR (156.82 kW) is only marginally affected by the implementation of DR strategies. Specifically, the peak reduction moves from -0.56% for DR no. 3 (155.94 kW) to +1.79% for DR no. 4 (INS) (159.63 kW). The time-shifting analysis indicates that DR no. 4 (INS) enables the heat pump to operate for the fewest annual hours (-45.67%).

The cumulative energy curve (Fig. 25b) reveals a substantial reduction in annual electricity consumption with all DR strategies. DR no. 1 achieves the greatest energy savings when the building is non-insulated, reducing the total consumption by -9.42% (49598.31 kWh) compared to the reference case (54754.11 kWh). DR no. 3 results in a more modest reduction of -3.84%, corresponding to 52654.17 kWh. Instead, the maximum annual reduction is obtained for DR no. 4 (INS) by -28.22% (39304.41 kWh). The findings demonstrate that, even without integrating renewable energy systems with the heat pump, demand response strategies can deliver significant economic benefits through reduced electricity consumption, particularly in well-insulated buildings. It is worth noting that the annual heat pump electricity consumption can be further reduced by increasing the night-time ventilation rate during the summer season. An additional simulation performed with a ventilation rate of 10 ACH resulted in a reduction of annual HP electricity consumption of up to 37.54%, highlighting the significant potential of enhanced night-time free cooling to decrease cooling loads and improve overall system performance.

The radar chart (Fig. 26) provides a comprehensive comparison of the investigated DR strategies by simultaneously considering peak reduction, time-shifting capability, energy reduction, and comfort compliance. The results highlight the existence of a trade-off between energy flexibility and occupant comfort. While DR no. 1-3 are primarily effective in reducing peak demand, DR no. 4 (INS) emerges as the most balanced solution, achieving the highest performance in terms of energy reduction, load shifting, and annual thermal comfort availability.

4.2.3. Impact of the required flexibility level on heat pump electricity consumption and thermal comfort

A sensitivity analysis was carried out only for DR no. 2 to investigate the effect of the *required flexibility level* "*x*" on yearly energy consumption of the HP and comfort compliance ratio. As illustrated in Fig. 27, the energy consumption and the annual human comfort decrease with the level of flexibility. Overall, the results highlight a clear trade-off between energy savings and thermal comfort degradation: higher flexibility improves energy performance but simultaneously increases the risk of occupant discomfort.

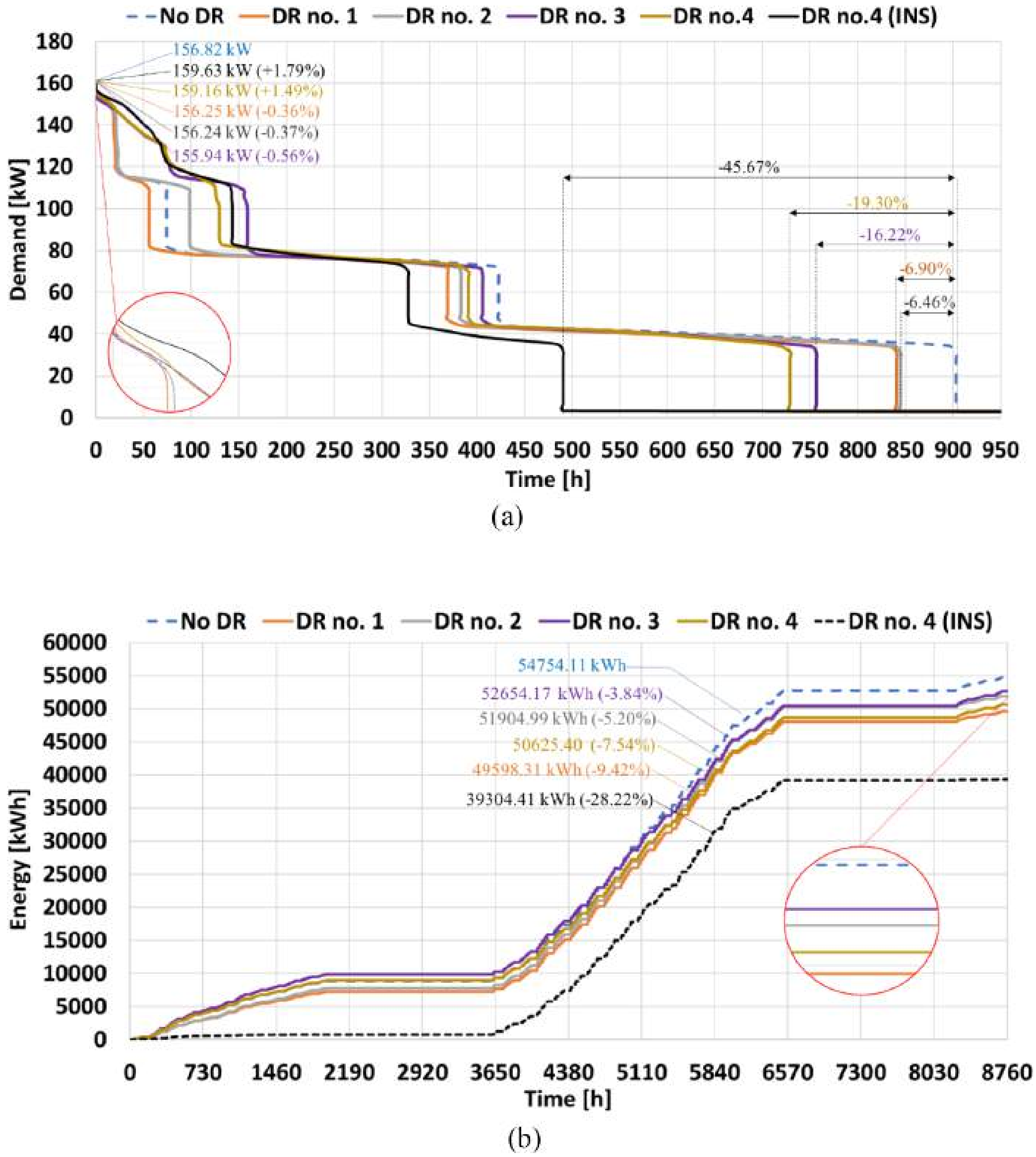

Fig. 25. Energy consumption of the HP: (a) electricity load duration curve, (b) annual cumulative energy curve.

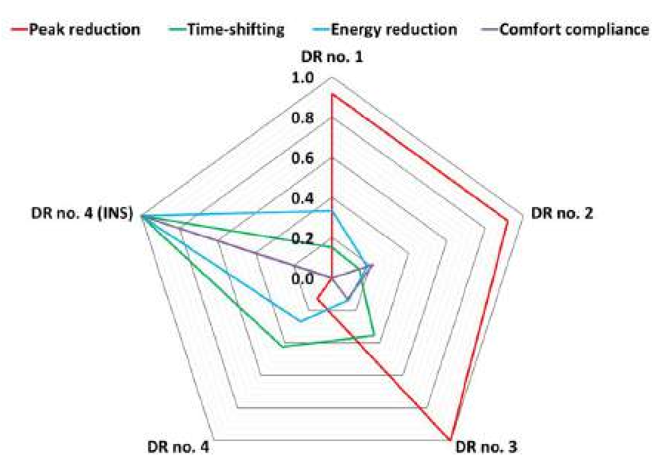

Fig. 26. Radar chart for the main KPIs.

4.2.4. Annual energy consumption of the building with a heat pump and a photovoltaic-battery system

Fig. 28 presents the electricity load duration curve and the annual cumulative energy consumption of the building under different DR strategies. Strategies from DR no. 1 to DR no. 4, characterized by poor insulation, as well as DR no. 4 (INS), were evaluated without the PV-battery system (w/o PV). Additionally, Strategies 3 and 4 were analyzed with the heat pump coupled to a PV-battery system (w PV), with Strategy 4 also performed in combination with insulation (INS w PV). To the No DR (w/o PV) scenario, the results show that: (i) the maximum annual peak reduction (-14.62%) is obtained under DR no. 3 (w PV), instead is increased in DR no. 4 (w/o PV) by +1.40%, and it is slowly reduced when the building is insulated (+1.37%) (Fig. 28a); (ii) the annual electricity consumption is decreased from -0.51% for DR no. 3 (w/o PV) to -59.89% for DR no. 4 (INS w PV) (Fig. 28b).

5. Conclusions

This study investigated the implementation of DR strategies in a tertiary office building located in Palermo, representative of a cooling-dominated Mediterranean climate. A dynamic building model,

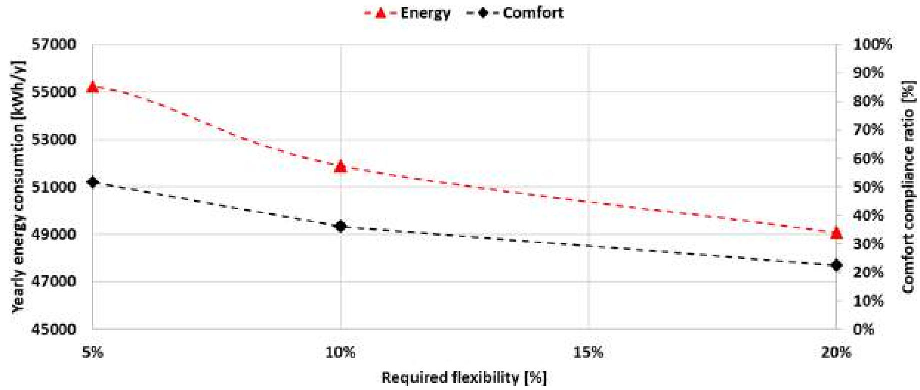

Fig. 27. Sensitivity analysis of annual energy consumption and comfort compliance ratio with respect to the required flexibility level.

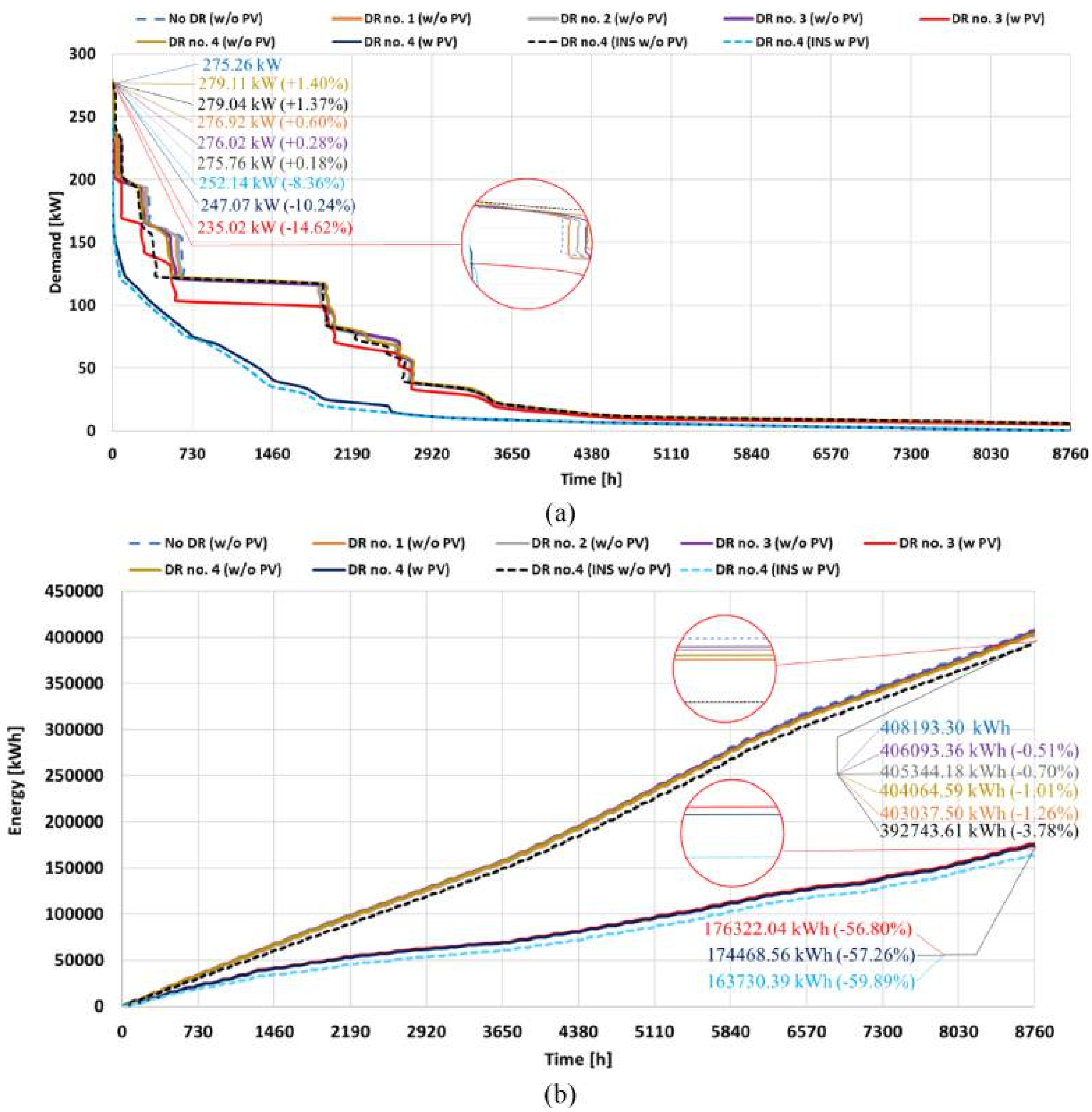

Fig. 28. Energy consumption of the building: (a) electricity load duration curve, (b) annual cumulative energy curve.

featuring varying insulation levels, was developed in TRNSYS and coupled with a reversible air-to-water HP, a TES, and a hydronic distribution network comprising circulation pumps and fan coils, a PV-B system and associated control strategies. The reversible heat pump was modeled in detail using IMST-ART v4.0, incorporating one-dimensional thermo-hydraulic simulations of the condenser and evaporator, with compressor performance characterized via manufacturer-validated maps. Starting from a baseline scenario without DR, the study evaluated both price-based and photovoltaic-driven DR strategies through dynamic and static adjustments of the thermal zone and TES temperature setpoints. The price-based strategy was defined according to the Italian wholesale market's PUN, while the PV-driven program aimed to maximize integration of VRE sources. Their impacts on energy consumption and occupant comfort were analyzed on daily and annual timescales. Furthermore, the influence of building envelope insulation was incorporated into the assessment to provide a comprehensive evaluation. The developed model notably included night-time natural ventilation as a passive cooling strategy to mitigate the risk of overheating during summer months.

The annual analysis highlights that the dynamic price-based strategy DR no. 1 severely degrades indoor environmental quality, causing the CCR to collapse to 23.82% (compared to the 34.71% baseline) while providing a modest energy saving of 3.42%. Conversely, DR no. 2 successfully shifts loads, slightly improving annual comfort availability to 36.14% and reducing annual electricity consumption by 2.14%. The static photovoltaic-driven strategy DR no. 3 exhibits an intermediate behaviour, reducing the CCR to 31.18% but achieving a substantial electricity consumption reduction of 14.73%. In contrast, the uninsulated DR no. 4 triggers a severe performance mismatch: it fails to maintain acceptable indoor conditions, dragging the CCR down to 24.11%, while its annual energy savings are limited to 4.31%.The most remarkable outcome is achieved by introducing structural modifications to the photovoltaic-driven control through DR no. 4 (INS). The synergy of envelope insulation, night-time ventilation, and TES management elevates the annual CCR to 81.22%, more than doubling the baseline. From an energy perspective, this insulated configuration achieves an annual electricity consumption reduction of up to 28.22% compared to the reference case. This benefit is further enhanced by the integration of the PV-B system, which exploits the favourable temporal overlap between solar generation and building demand to increase grid electricity savings by up to 59.89%.

As the main implications in the field, the present work suggests that well-insulated buildings utilizing night-time ventilation and equipped with HPs combined to a PV-B system could provide support to power grid operators in cooling-dominated zones, with low sensible effects on occupants' comfort according to the imposed level of setpoint variation. In addition, the adopted detailed modelling approach allows capturing the dynamic interaction between multizone buildings, heat pump operation, and control strategies. Although no direct comparison with simplified models is performed in this study, such level of detail is expected to improve the reliability of flexibility assessments, particularly in representing transient responses and control-induced effects. It is crucial in flexibility studies, as it reveals how control responses can both constrain energy savings and mitigate occupant discomfort.

Although HPs combined with advanced digital technologies (e.g., smart thermostats and home energy management systems, smart meters with real-time communication capabilities, advanced control algorithms, and predictive analytics) offer significant potential for enhancing flexibility and facilitating the integration of RES into power systems, their high additional costs continue to hinder large-scale deployment [101]. To overcome these barriers, governments could support initial investments in enabling infrastructure such as smart meters, while regulatory frameworks may allow utilities to recover the costs of digitalization and grid modernization through network tariffs. In this regard, incentivizing end-users to participate in DR programs through financial compensation mechanisms can further enhance the economic viability of these technologies while promoting active consumer engagement in energy system flexibility [102].

Market barriers, regulatory frameworks, and government support are not directly supported by the results of the present study and are intended as a broader contextual perspective rather than a finding derived from the analysis. These aspects fall beyond the scope of the current work and will be systematically investigated in future research, with particular attention to the role of market mechanisms and policy incentives in supporting the large-scale adoption of DR-enabled technologies.

CRediT authorship contribution statement

Maurizio La Villetta: Writing – review & editing, Writing – original draft, Visualization, Validation, Supervision, Software, Resources, Project administration, Methodology, Investigation, Funding acquisition, Formal analysis, Data curation, Conceptualization. **Pietro Catrini:** Writing – review & editing, Writing – original draft, Visualization, Validation, Supervision, Software, Resources, Project administration, Methodology, Investigation, Funding acquisition, Formal analysis, Data curation, Conceptualization. **Antonio Piacentino:** Writing – review & editing, Writing – original draft, Visualization, Validation, Supervision, Software, Resources, Project administration, Methodology, Investigation, Funding acquisition, Formal analysis, Data curation, Conceptualization.

Declaration of competing interest

The authors declare that they have no known competing financial interests or personal relationships that could have appeared to influence the work reported in this paper.

Acknowledgment

This study was developed in the framework of the research activities carried out within:

- the Project "*Partenariato Esteso "Made in Italy Circolare e Sostenibile - MICS*", tematica "*11. Circular and sustainable Made-in-Italy*", Project code PE00000004, CUP: B73C22001270006.
- the Project "*Network 4 Energy Sustainable Transition - NEST*", Spoke 7: Smart Sector Integration, Project code PE0000021, CUP: B73C22001280006, funded under the National Recovery and Resilience Plan (NRRP), Mission 4, Component 2, Investment 1.3 - Call for tender No. 1561 of 11.10.2022 of Ministero dell'Università e della Ricerca (MUR); funded by the European Union - NextGenerationEU.

Appendix A

Table A.1 integrates the literature review presented in Section 1.1 ("*Literature Review*"). The contents are organised by year, building/plant type, geographic location, demand response strategies, constraints, and main results.

Table A.1
Literature review on DR programs according to strategies and building type.

Year	Building/Plant	Location	Strategy/Constraints	Main results	Ref.
2010	Office building&ASHP	California(USA)	Pre-cooling strategies.	The results showed that the pre-cooling with exponential temperature setup and pre-cooling with step temperature setup strategies proved to be more effective than the pre-cooling with linear temperature setup in terms of demand response effectiveness. Across all test buildings, peak-period electrical demand was reduced by 15-30% on auto-DR event days.	[30]
2015	Office building&HVAC	University of Girona (Spain)	Short-term load forecasting strategy for non-residential buildings using machine learning models (MLR, MLP, SVR) combined with feature selection and wireless sensor network data. The main strategy relies on selecting the most relevant inputs, especially outdoor temperature and occupancy, through genetic search and correlation-based filtering to reduce redundancy and improve prediction efficiency.	Results show that the SVR model performs best, achieving extremely high accuracy (0.06% MAPE) using only temperature and occupancy data, with occupancy proving more informative than calendar or indoor environmental variables. Overall, the approach demonstrates that accurate load forecasting can be achieved with minimal, well-selected data while reducing computational complexity.	[64]
2016	Commercial building&HVAC	Pacific Northwest National Laboratory campus(USA)	Transactive control strategy using a double-auction market mechanism to coordinate multiple HVAC subsystems as interacting agents for DR.	Simulation results show effective peak shaving, load shifting, and strategic energy conservation while maintaining occupant comfort and providing reliable DR to the grid.	[46]
2016	Nearly zero energy buildings&HPs + TES + PVs + Solar thermal systems + CHP units	Mediterranean region	DR strategies considering the integration of HPs + TES + PVs + Solar thermal systems + CHP units and advanced building energy management Systems. Demand response is mainly enabled through load shifting, storage management, and smart control of HVAC systems in response to grid signals, weather, and occupancy conditions.	Results highlight that the flexibility potential of buildings significantly increases when thermal loads are electrified and coupled with TES and advanced information and communication technology infrastructure, allowing buildings to improve grid stability, increase renewable energy utilisation, and maintain thermal comfort while supporting the transition toward smart, decarbonised energy systems.	[65]
2017	Service sector buildings&HPs + TES	Lucerne(Switzerland)	Modular tariff-driven load shifting framework for service sector buildings that uses simplified building energy models to optimize HVAC operation for demand response under time-of-use pricing.	By shifting heating demand toward low-tariff periods while respecting comfort and storage constraints, the framework achieves up to 34-37% cost savings and around 20% energy reduction, with results strongly dependent on tariff differentiation and the presence of adequate thermal storage. Its flexible architecture allows integration with existing building management systems and different optimizers, enabling effective peak shaving and load valley filling without requiring major infrastructure changes.	[47]
2018	Plus-energy dwelling&HP connected to a DHCN + PV-B	Wüstenrot(Germany)	Dynamic pricing-based DR strategies using adaptive price and temperature thresholds to shift operation from peak to off-peak periods by exploiting building thermal mass in the District Heating and Cooling Network (DHCN).	Results showed cost savings of up to 25%, significant peak demand reduction with near-zero heat pump operation during peak hours, and increased PV self-consumption while maintaining thermal comfort conditions.	[44]
2018	Residential building&GSHP + TES	Finland	Four rule-based DR strategies (momentary, blocking, sliding, and moving average algorithms) aiming to shift electricity use from high-price to low-price periods while preserving thermal comfort.	Results showed that the sliding-maximum subarray algorithm performed best, achieving up to 10% heating energy savings and 15% cost reduction for GSHP systems (and up to 8% cost reduction for electric heating systems), while all strategies successfully maintained indoor comfort conditions.	[45]
2019	Controllable environmental chamber with test rooms&ASHP	China	Chiller-side DR strategies based on on-off control and chilled water temperature control.	Exploiting the air-conditioning system's thermal inertia, the on-off control reduces peak electricity demand by 16.74%, while chilled water temperature control adds a further 1.93%, contributing respectively 18.73% and 10.60% to the total reduction.	[29]

(*continued on next page*)

Table A.1 (*continued*)

2019	Residential buildings&HPs	United Kingdom	Building-to-grid DR flexibility of aggregated residential HPs based on novel metrics.	Load curtailment strategies produced power and energy paybacks between 0% and 50%, with high-thermal-inertia dwellings showing smaller but more prolonged rebound effects, and hybrid heating systems limiting both to below 20%.	[25]
2019	Residential buildings&HPs	Island of Bornholm (Denmark)	Direct load control of residential heat pumps through temporary throttling/ shutdown during peak demand periods, combined with a rebound damping strategy to mitigate post-event power peaks.	Achieved load reductions of 40-65% of the aggregate load from more than 300 residential buildings with heat pumps.	[24]
2019	Single-family houses&HPs and TES	Braunschweig(Germany)	Heuristic control strategies for minimising heating costs and the surplus energy from PV within a residential area using DR with modulating heat pumps.	Reduce heating costs and surplus energy in residential applications.	[23]
2020	Residential buildings&ASHP and TES	Dusseldorf(German)	Demand-side management strategy focused on optimal day-ahead scheduling of heat pumps to reduce peak loads in the electrical distribution grid.	Heat pump control reduces peak electricity demand in residential districts (100 houses) by shifting operation toward off-peak hours, with results varying according to season and user behaviour, while hot water storage increases system flexibility at the expense of a modest rise in daily start-up cycles.	[27]
2020	Controllable environmental chamber with test rooms&HP	China	Pre-cooling, temperature resetting and passive cooling storage from furniture, building envelope and an active water storage tank.	Thermal mass thickness dictates DR suitability: thin masses (desks, files) release 28-93% of stored cooling for short-term DR, while thick walls release only 5-35% for long-term DR. Optimal passive thermal mass weight is ~120 kg/m^2. Pre-cooling enabled chiller shutdown for >90 minutes. A 200 L chilled water storage tank (9°C) independently met cooling demand for 2 hours over 32 m^2. Combining active storage with passive mass yielded 532 W average load reduction over 3 hours.	[33]
2020	Commercial (small/medium/large office, primary/secondary school, retail store, supermarket, small/large hotel) and residential (single-family homes) buildings&HVAC	15 ASHRAE climate zones across the US and California(USA)	Ventilation-based DR by temporarily curtailing or modulating building ventilation systems to reduce peak electricity demand while maintaining acceptable indoor air quality using equivalent ventilation and exposure metrics.	Results show that commercial buildings can achieve peak reductions up to 40% (0-2 W/ft^2) with safe curtailment durations of 1.5-8 hours, depending on building type, while residential buildings reach up to 30% peak demand reduction (~ 0.2 W/ft^2) and about 10% energy savings, with the highest flexibility observed in tight, energy-efficient homes and humid climates.	[63]
2021	Terminal room&ASHP and TES	Chang'a University(China)	Thermal energy storage for peak shaving and load shifting.	ASHP ON/OFF cycles decreased in summer and in winter. The system improves HVAC stability and peak shaving capability.	[22]
2021	Office building&HP	Beijing(Northern China)	The control strategy defines energy flexibility as two modulations: upward (lower set-point during off-peak to store cooling in thermal mass) and downward (higher set-point during on-peak to release stored cooling for peak shaving).	The proposed rule-based strategy maximises off-peak storage and minimises on-peak energy use. The rule-based strategy enabled valley-filling and peak-shaving: upward modulation stored 67.7 Wh/m^2, downward modulation curtailed 53.9 Wh/m^2. Peak power dropped 55.6% and peak energy 54.0%. High thermal mass boosts flexibility but plateaus beyond 242 kJ/(m^2·K). Internal heat gains and terminal inertia improve flexibility; wall insulation has little effect.	[35]
2022	Commercial building&Rooftop unit	Purdue Herrick Laboratory (USA)	Hierarchical model predictive control strategy was implemented for HVAC load shifting through precooling in small and medium-sized commercial buildings, exploiting the building thermal mass as a virtual battery to reduce electricity demand during peak time-of-use tariff periods.	The proposed approach achieved demand cost savings exceeding 30%, with on-peak demand cost reductions above 40%, while maintaining effective load reduction for approximately 4-5 h thanks to the building thermal inertia. However, energy cost savings remained below 10%, mainly due to the poor building envelope and the limited efficiency of thermal energy storage and release.	[37]
2022	Commercial building&HVAC	Eight university campus buildings in Michigan and North Carolina (USA)	A Grid-Triggered Adjustment (GTA) strategy was applied to commercial building HVAC systems for load-shifting	GTA-based DR reduces renewable energy curtailment while maintaining indoor temperature and humidity within	[36]

(continued on next page)

Table A.1 (*continued*)

			DR, modulating HVAC operation to mitigate grid ramp rates caused by high renewable energy penetration.	occupant comfort limits, with the additional building energy consumption remaining significantly lower than the renewable energy otherwise curtailed.	
2022	Shopping center&HVAC	Catania(Italy)	HVAC-based DR through temperature setpoint adjustments, power cutting during morning and evening peak periods, without pre-heating or pre-cooling strategies.	Results show that setpoint control delivers moderate flexibility (over 60 kW in summer and >50 kW in winter) with energy savings up to 160 kWh and generally acceptable comfort, especially in winter, while power cutting achieves higher peak reductions (up to 77 kW) but significantly degrades indoor conditions in summer, leading to about 40% occupant dissatisfaction. Overall, winter operation maintains comfort with limited trade-offs, whereas summer flexibility is strongly constrained by thermal comfort requirements despite higher economic potential (€9.8-24 per DR event).	[55]
2022	Detached houses&AC Unit	Adelaide, Brisbane, Melbourne, Sydney (Australia)	Residential pre-cooling strategies for air-conditioning load shifting using building thermal mass as a storage medium to shift cooling demand from peak (02:00-20:00) to off-peak periods (22:00-07:00) through optimized HVAC scheduling.	Results show that pre-cooling can deliver seasonal cost savings up to $261 in higher-efficiency (6-star) lightweight buildings, with greater percentage savings and peak demand reductions observed in higher-rated and heavier constructions, while also improving thermal comfort even in cases where direct cost savings are limited or negative, particularly when AC systems are undersized.	[50]
2022	Urban district energy systems, rather than specific building types&HPs + TES + Electric boiler + Wind power + PVs + CHP units	Zagreb, Osijek, Velika Gorica, Slavonski Brod, Karlovac, Sisak, Split, Rijeka, Zadar(Croatia)	DR strategies based on DHCN coupled with renewable electricity generation, using power-to-heat technologies such as heat pumps, electric boilers, CHP units, and thermal storage to absorb excess wind and PV electricity.	Results show that advanced DHCN can substantially improve renewable integration, reducing critical excess electricity production from 96% to 36%, while enabling wind and PV systems to cover up to 73% of annual electricity demand with only 5% excess generation.	[59]
2022	Classrooms, laboratories, offices, library and residential buildings&HVAC	University campus in Palermo, Lampedusa and Favignana(Italy)	Blockchain-based DR platform using smart contracts to coordinate user participation in DR and vehicle-to-grid services under a simplified single-actor energy market. The strategy focuses on peak shaving and load shifting to reduce diesel consumption, improve generator efficiency, and avoid grid overloads and infrastructure expansion, particularly in high-demand summer periods such as in Lampedusa.	Results show that DR can significantly improve system operation by flattening demand peaks, reducing fuel use of inefficient diesel units, lowering CO_2 emissions, and enhancing grid stability while deferring network and generation investments. User participation is financially rewarded through smart contracts that link remuneration directly to measurable fuel savings and system efficiency gains, making DR economically viable in isolated island energy systems.	[63]
2023	Classrooms, laboratories, offices, and library&Nuclear and coal-fired generators + PV + wind turbines + gas power generators	University campusIn Hong Kong	Multi-agent system for coordinated optimal load scheduling in building clusters, using distributed optimization (alternating direction method of multipliers) to enable DR based on both dynamic electricity prices and MEFs.	Three strategies are compared, price-based, MEF-based, and hybrid optimization, showing that while single-objective approaches can lead to trade-offs (e.g., cost reduction at the expense of higher emissions or vice versa), the hybrid strategy effectively balances both objectives, achieving up to 5.54% peak load reduction without increasing either costs or emissions under adverse conditions.	[48]
2023	Terminal room&ASHP and TES	Chang'a University(China)	Global temperature adjustment, active energy storage strategy, and on-off ASHP strategy of a central HVAC system.	Integrating a buffer tank reduced heat pump cycling from 46 to just 6 cycles. Thermal inertia enabled DR participation for 40-50 minutes, achieving a power reduction of 8.9-12.6%. Active storage extended DR participation to 120 minutes, reduced peak power by 23.4%, and lowered operating costs by 21.7%.	[31]
2023	Residential buildings&ASHPs + PV-B	Barnsley (United Kingdom)	Automated DR strategies using turn-down and turn-up interventions to respectively reduce evening peak demand and absorb excess midday electricity.	Results showed a 67% reduction in grid electricity import during turn-down events and a 645% increase during turn-up periods, while network-level power variations reached -21% and +307%, respectively, with minimal impacts on occupant comfort and daily routines.	[43]
2023	North Khorasan province&HP + wind + PV-B	Khorasan(Iran)	Business-as-usual, power plant optimization, and DR scenarios	Results show that the wind-based DR scenario provides the best long-term	[58]

(continued on next page)

Table A.1 (*continued*)

			combined with wind or solar generation to optimize energy supply, CO_2 emissions, and system costs.	performance, reducing CO_2 emissions by up to 227.78 kt/year and saving up to €156 million annually by 2030 compared to business as usual, while supporting future electrification through heat pumps and renewable-based district heating.	
2023	Office building&HP	Aristotle University of Thessaloniki's Faculty of Engineering(Greek)	Rule-based DR controls driven by hourly electricity prices and CO_2 intensity signals, exploiting the building thermal mass for load shifting.	Results show that price-based control can reduce heating costs and CO_2 emissions by about 3.6% and 3.3%, respectively, while carbon-based control achieves emission reductions up to 3.5%. However, in less thermally efficient buildings, the increased energy consumption caused by load shifting can offset the economic and environmental benefits.	[58]
2023	Office/classroom buildings&HVAC	University campus in Northern California(USA)	DR potential through controlled HVAC cooling setpoint adjustments, increasing indoor temperature setpoints from 74°F to 76°F and using statistical stress testing methods to characterize building flexibility.	Field tests across six Northern California buildings showed cooling load reductions of 13-28% in office buildings and 3-4% in laboratories, while indoor temperatures increased by less than 1.5°F, demonstrating significant flexibility potential with limited impacts on occupant comfort.	[64]
2024	Building (N/A)&SAHPD	Kunming, Yunnan, (China)	Optimal scheduling strategy for SAHP drying systems to participate in both price-based and incentive-based DR programs, exploiting virtual energy storage based on the thermal inertia of the drying chamber.	Results showed electricity cost reductions of up to 13.81%, while incentive-based demand response enabled load reductions of 71.92% for up to 4 h, demonstrating the high flexibility potential of SAHP drying systems for grid support.	[42]
2024	Office building&HP + TES + PV	Guangdong(China)	Dynamic temperature set-point control-based photovoltaic direct-driven air-conditioning system	DR reduced peak power by 45.2% and raised self-sufficiency/consumption ratios to 0.83/0.91. Adding short-term storage cut peak power by another 23.4% and reduced supply-demand mismatch.	[34]
2024	Office building&ASHP	Beijing(China)	Optimal water temperature scheduling method optimizes supply water temperature schedules in response to time-of-use tariffs, utilizing building thermal mass for passive energy storage rather than just adjusting indoor temperature setpoints	Field testing demonstrated a significant improvement in DR capability, with the flexibility factor increasing from 0.134 to 0.728, while reducing operating costs by 20.8-43.0% compared to benchmark methods and maintaining indoor temperatures within the 24 ± 1 °C comfort range.	[39]
2024	Residential buildings (district)&HPs	Karlsruhe(Germany)	The study proposed EPSC+, a rule-based strategy for coordinating modulating heat pumps in building clusters to provide DR and peak shaving based on electricity price signals.	Compared to conventional hysteresis control, EPSC+ achieved a 38.8% reduction in median peak load and a 15% decrease in electricity costs, while maintaining performance close to hierarchical MPC approaches with significantly lower computational complexity.	[41]
2024	Residential buildings (district)&HPs + Electric resistance	Montreal, Quebec (Canada)	Reinforcement learning-based DR incorporating occupant thermostat preferences and override behaviours into automated setpoint management during peak periods.	The strategy reduces heating setpoints by about 2°C during demand response events while adapting to occupant types and minimizing overrides. Results show that the most realistic scenario (including overrides) achieves 12% cost savings and 17% energy reduction, with strong thermal comfort retention (less than 5% of time with >1°C deviation), while also revealing that simplified models without occupant interaction can overestimate savings by about 5%.	[52]
2025	Office building&GSHP	Hangzhou(China)	Operational control strategy based on system energy efficiency, ground-temperature conditions, and the load-imbalance rate between the ground source and the end user.	Improved efficiency and limited ground thermal imbalance.	[21]
2025	University building&SAHP with PCM	University of Nottingham's Park Campus(United Kingdom)	Controllable phase change material storage to shift demand from peak hours to periods of high solar availability.	The system shifts electricity demand for space heating from peak to off-peak periods, employs a control methodology for managing charging and discharging, and achieves a weekly coefficient of performance of 3.56 through load shifting.	[26]

(*continued on next page*)

Table A.1 (*continued*)

2025	Residential buildings&HPs	Brussels(Belgium)	Frequency-control DR strategy based on day-ahead scheduling of a baseline load and a flexibility band, activated in real time via grid signals. Heat pumps are controlled indirectly through thermostat setpoints within a predictive control framework	Piecewise-affine model improves prediction accuracy over a linear one, while both achieve similar control performance (about 57-59% flexibility and 12-14% tracking error). Battery storage and aggregation further enhance performance, with tracking errors decreasing exponentially as storage size and aggregation increase.	[28]
2025	Hypermarket-sized grocery store&HP	Southern Finland	DR potential in grocery stores responding to electricity spot-price variations in the Nord Pool Finnish market	Spot-price-based demand response achieved annual energy cost savings of 5-13%, increasing up to 20% with larger buffer tanks. The strategy increased winter electricity consumption by 8-21% while reducing district heating demand by 7-40%, mainly through dynamic air-handling unit temperature control and optimized buffer tank charging.	[38]
2025	Residential and small-business end-users (district)&HPs	Capriasca(Canton Ticino, CH)	Optimal scheduling strategy for district-level heat pumps to provide both IDR and DDR services through quadratic programming optimization.	Results demonstrated effective peak shaving and valley filling under IDR, with reductions of up to 13% in peak consumption and 34% in peak-to-dip gap, while also showing that flexibility services can be provided without additional costs for end users. Under DDR, upward flexibility reduced peak and average consumption by up to 20% and 35%, respectively, although secondary rebound effects caused peak increases outside the flexibility window of up to 50%, together with moderate increases in total energy costs.	[20]
2025	Residential buildings&ASHP, GSHP + TES + PV-B	Leoben(Austria)	The study adopted a multi-objective optimization strategy combining market-oriented and grid-oriented DR approaches, using day-ahead electricity prices as control signals for heat pump operation. Flexibility was enhanced through load shifting and the integration of thermal and battery energy storage systems, enabling heat pumps to shift electrical demand toward periods with favorable grid or price conditions.	The study demonstrated that day-ahead energy prices can effectively reduce price volatility, limit grid peak loads, and increase energy self-sufficiency through optimized heat pump operation. Results showed that thermal storage combined with heat pumps achieved high self-sufficiency more cost-effectively than hybrid electrical-thermal storage systems, while heat pumps proved highly flexible controllable loads capable of shifting 33-100% of electrical demand according to grid requirements.	[40]
2025	4 smart communities&1000 HPs	China	DR strategy based on a hierarchical control architecture that combines an improved PSO optimization for load allocation with a state-queueing scheduling algorithm guided by a PMV-PPD thermal comfort model.	By explicitly incorporating user discomfort into the dispatch process, the method achieves both accurate power tracking and substantial comfort improvements, reducing average dissatisfaction from 26.41% (baseline) to 6.29%, while keeping most PPD values within the 5-10% range.	[49]
2025	Commercial building&RTU	Palermo(Italy)	DR strategies responding to electricity spot-price variations in the Italian market by comparing partial RTUs deactivation and thermostat setpoint adjustments to assess trade-offs between peak shaving, energy use, and comfort.	Results show that partial RTUs deactivation is the most effective strategy, achieving up to 50% peak shaving and 22.72% seasonal energy reduction with acceptable comfort limits (up to 4°C deviation), while increasing setpoints yields additional 5.2% energy savings but significantly worsens comfort (13% more discomfort hours), and decreasing setpoints leads to adverse effects, including a threefold increase in peak demand and a 43.6% rise in seasonal energy consumption.	[53]
2025	Residential buildings&Mixed-mode ventilation system (natural ventilation and split-unit air conditioning)	Telemly(Algeria)	Adaptive thermal comfort strategies by comparing three comfort models (ISSO 74, ASHRAE 55, and EN 16798-1) under present and future climate scenarios, while evaluating passive and mixed-mode ventilation measures to mitigate overheating.	Results indicate that thermal discomfort already exceeds 33% of annual hours and may rise above 40% by 2100, with summer discomfort becoming dominant, while ISSO 74 showed better adaptation to temperature variations and EN 16798-1 better accounted for high humidity conditions. The study recommends passive and mixed-mode ventilation strategies, such as shading, operable windows, and ceiling fans, to improve	[61]

(*continued on next page*)

Table A.1 (*continued*)

				resilience and reduce cooling energy demand.	
2025	Residential buildings&HVAC	Palermo, Caserta, Genoa, and Milan(Italy)	Passive energy flexibility strategies by comparing traditional brick masonry and ICF systems, focusing on the role of thermal mass and insulation through hourly dynamic simulations.	Results show that ICF walls significantly reduce peak heating demand and heating energy consumption during winter, achieving savings up to 56-58% compared to brick walls, while also providing greater thermal lag during summer. However, their cooling performance is more limited due to the internal insulation layer that thermally decouples the concrete core, leading to only moderate cooling peak reductions and higher decrement factors than brick walls, which better exploit exposed thermal mass for summer heat attenuation.	[56]
2026	Residential buildings&PCMs + solar chimney + reflective roofing + mechanical ventilation	Tabarka, Sousse,Tozeur (Tunisia)	Passive and hybrid ventilation-based DR strategies.	Optimized natural ventilation reduces annual energy consumption by 38.4-42.6% and lowers CO_2 emissions by 6-10.8%, depending on the region. In contrast, the hybrid ventilation system increases energy use by 14-16% but significantly improves thermal comfort, raising comfortable occupied hours to nearly 76% and enhancing PMV and PPD indices.	[60]

Appendix B. Supplementary data

Supplementary data to this article can be found online at https://doi.org/10.1016/j.enconman.2026.121856.

Data availability

Data will be made available on request.

References

[1] Santamouris M, Vasilakopoulou K. Present and Future Energy Consumption of Buildings: Challenges and Opportunities towards Decarbonisation. E-Prime 2021: 100002. 10.1016/j.prime.2021.100002.

[2] International Energy Agency (IEA). Energy Efficiency 2024 2024. https://iea.blob.core.windows.net/assets/f304f2ba-e9a2-4e6d-b529-fb67cd13f646/EnergyEfficiency2024.pdf (accessed January 5, 2025).

[3] Hu W, Scholz Y, Yeligeti M, Deng Y, Jochem P. Future electricity demand for Europe: Unraveling the dynamics of the Temperature Response Function. Appl Energy 2024;368:123387. https://doi.org/10.1016/j.apenergy.2024.123387.

[4] Peplinski M, Dilkina B, Chen M, Silva SJ, Ban-Weiss GA, Sanders KT. A machine learning framework to estimate residential electricity demand based on smart meter electricity, climate, building characteristics, and socioeconomic datasets. Appl Energy 2024;357:122413. https://doi.org/10.1016/j.apenergy.2023.122413.

[5] Sikow C. Towards a sustainable and integrated Europe. Report of the Commission Expert Group on electricity interconnection targets. 2017.

[6] Leobner I, Smolek P, Heinzl B, Raich P, Schirrer A, Kozek M, et al. Simulation-based Strategies for Smart Demand Response. Journal of Sustainable Development of Energy, Water and Environment Systems 2017;6:33–46. 10.13044/j.sdewes.d5.0168.

[7] Pietro C, Testasecca T, La Villetta M, Morale M, Piacentino A. Thermodynamic-based method for supporting design and operation of thermal grids in presence of distributed energy producers. Journal of Sustainable Development of Energy, Water and Environment Systems 2023;11:1–23. 10.13044/j.sdewes.d11.0459.

[8] Alqurashi A. The State of the Art in Model Predictive Control Application for Demand Response. Journal of Sustainable Development of Energy, Water and Environment Systems 2022;10:1–21. 10.13044/j.sdewes.d9.0401.

[9] Beyza J, Yusta JM. The effects of the high penetration of renewable energies on the reliability and vulnerability of interconnected electric power systems. Reliab Eng Syst Saf 2021;215:107881. https://doi.org/10.1016/j.ress.2021.107881.

[10] Walker IS, Less BD, Casquero-Modrego N. Carbon and energy cost impacts of electrification of space heating with heat pumps in the US. Energy Build 2022;259:111910. https://doi.org/10.1016/j.enbuild.2022.111910.

[11] Bakare MS, Abdulkarim A, Zeeshan M, Shuaibu AN. A comprehensive overview on demand side energy management towards smart grids: challenges, solutions, and future direction. Energy Informatics 2023;6:4. https://doi.org/10.1186/s42162-023-00262-7.

[12] International Energy Agency (IEA). Using Digitalisation in Emerging Markets and Developing Economies to Enable Demand Response in Buildings 2023. https://www.iea.org/reports/using-digitalisation-in-emerging-markets-and-developing-economies-to-enable-demand-response-in-buildings (accessed April 7, 2025).

[13] Arteconi A, Polonara F. Assessing the Demand Side Management Potential and the Energy Flexibility of Heat Pumps in Buildings. Energies (Basel) 2018;11:1846. https://doi.org/10.3390/en11071846.

[14] Mugnini A, Ramallo-González AP, Parreño A, Molina-Garcia A, Skarmeta AF, Arteconi A. Dynamic building thermal mass clustering for energy flexibility assessment: An application to demand response events. Energy Build 2024;308:114011. https://doi.org/10.1016/j.enbuild.2024.114011.

[15] Mugnini A, Polonara F, Arteconi A. Quantification of the energy flexibility of residential building clusters: Impact of long-term refurbishment strategies of the italian building stock. Energy Build 2023;296:113416. https://doi.org/10.1016/j.enbuild.2023.113416.

[16] Lind J, Möllerström E, Averfalk H, Ottermo F. Energy flexibility using the thermal mass of residential buildings. Energy Build 2023;301:113698. https://doi.org/10.1016/j.enbuild.2023.113698.

[17] Wang H, Wang S. A hierarchical optimal control strategy for continuous demand response of building HVAC systems to provide frequency regulation service to smart power grids. Energy 2021;230:120741. https://doi.org/10.1016/j.energy.2021.120741.

[18] Yadav MK, Verma A, Panigrahi BK, Rakshit D. Real-time optimal hierarchy control of HVAC system with maximized ancillary service support in smart buildings: An experimental approach. Energy Build 2024;324:114844. https://doi.org/10.1016/j.enbuild.2024.114844.

[19] Naderi S, Pignatta G, Heslop S, MacGill I, Chen D. Demand response via pre-cooling and solar pre-cooling: A review. Energy Build 2022;272:112340. https://doi.org/10.1016/j.enbuild.2022.112340.

[20] Rocca R, Leonori S, Aznar GF, Toffanin R, Luengo-Baranguan L. Optimal scheduling of district heat pumps conceived for implementation in Energy Management Systems to participate in demand response. Energy Convers Manage: X 2025;27:101074. https://doi.org/10.1016/j.ecmx.2025.101074.

[21] Zhao Y, Gao J, Wu F, Sun Y, Liu A, Yu Z, et al. Study on the thermal imbalance characteristics and optimal operation strategy of ground source heat pump system in hot summer and cold winter areas. Energy Convers Manag 2025;343:120184. https://doi.org/10.1016/j.enconman.2025.120184.

[22] Meng Q, Ren X, Wang W, Xiong C, Li Y, Xi Y, et al. Reduction in on-off operations of an air source heat pump with active thermal storage and demand response: An experimental case study. J Energy Storage 2021;36:102401. https://doi.org/10.1016/j.est.2021.102401.

[23] Dengiz T, Jochem P, Fichtner W. Demand response with heuristic control strategies for modulating heat pumps. Appl Energy 2019;238:1346–60. https://doi.org/10.1016/j.apenergy.2018.12.008.

[24] Müller FL, Jansen B. Large-scale demonstration of precise demand response provided by residential heat pumps. Appl Energy 2019;239:836–45. https://doi.org/10.1016/j.apenergy.2019.01.202.

[25] Zhang L, Good N, Mancarella P. Building-to-grid flexibility: Modelling and assessment metrics for residential demand response from heat pump aggregations. Appl Energy 2019;233–234:709–23. https://doi.org/10.1016/j.apenergy.2018.10.058.

[26] Kutlu C, Erdinc MT, Dik A, Chen Z, Lyu Q, Su Y, et al. A study on the combination of crystallization-controllable phase change materials and solar-assisted heat pump for electricity demand shifting in space heating. Energy Convers Manag 2025;324:119260. https://doi.org/10.1016/j.enconman.2024.119260.

[27] Vivian J, Prataviera E, Cunsolo F, Pau M. Demand Side Management of a pool of air source heat pumps for space heating and domestic hot water production in a residential district. Energy Convers Manag 2020;225:113457. https://doi.org/10.1016/j.enconman.2020.113457.

[28] Koch M, Sawant P, Eismann R, Jones CN. A commissioning-oriented approach to data-driven modeling of buildings with heat pumps for predictive demand response. Journal of Building Engineering 2025;111:113016. https://doi.org/10.1016/j.jobe.2025.113016.

[29] Li W, Yang L, Ji Y, Xu P. Estimating demand response potential under coupled thermal inertia of building and air-conditioning system. Energy Build 2019;182:19–29. https://doi.org/10.1016/j.enbuild.2018.10.022.

[30] Yin R, Xu P, Piette MA, Kiliccote S. Study on Auto-DR and pre-cooling of commercial buildings with thermal mass in California. Energy Build 2010;42:967–75. https://doi.org/10.1016/j.enbuild.2010.01.008.

[31] Meng Q, Gao T, Zhang X, Zhao F, Wang L, Lei Y, et al. Load rebound suppression strategy and demand response potential of thermal storage HVAC systems: An experimental and simulation study. J Energy Storage 2023;73:108872. https://doi.org/10.1016/j.est.2023.108872.

[32] Klein MJDSA, Beckman WA, Mitchell JW, Duffie JA, Duffie NA, Freeman TL, et al. Trnsys17. 2009.

[33] Chen Y, Xu P, Chen Z, Wang H, Sha H, Ji Y, et al. Experimental investigation of demand response potential of buildings: Combined passive thermal mass and active storage. Appl Energy 2020;280:115956. https://doi.org/10.1016/j.apenergy.2020.115956.

[34] Ye A, Zhao Z, Liu S, Liu X, Zhang T, Liu X, et al. Flexible energy utilization potential of demand response oriented photovoltaic direct-driven air-conditioning system with energy storage. Energy Build 2024;323:114818. https://doi.org/10.1016/j.enbuild.2024.114818.

[35] Lu F, Yu Z, Zou Y, Yang X. Cooling system energy flexibility of a nearly zero-energy office building using building thermal mass: Potential evaluation and parametric analysis. Energy Build 2021;236:110763. https://doi.org/10.1016/J.ENBUILD.2021.110763.

[36] Keskar A, Lei S, Webb T, Nagy S, Hiskens IA, Mathieu JL, et al. Assessing the performance of global thermostat adjustment in commercial buildings for load shifting demand response. Environ Res: Infrastruct Sustainability 2022;2:015003. https://doi.org/10.1088/2634-4505/ac51c5.

[37] Kim D, Braun JE. MPC solution for optimal load shifting for buildings with ON/OFF staged packaged units: Experimental demonstration, and lessons learned. Energy Build 2022;266:112118. https://doi.org/10.1016/j.enbuild.2022.112118.

[38] Söderholm N, Niemelä T, Jokisalo J, Kosonen R. Demand response potential of a grocery store refrigeration and heat pump system for heat recovery by using real time electricity pricing. Energy Build 2025;344:115977. https://doi.org/10.1016/j.enbuild.2025.115977.

[39] Li X, Sun Y, Wang W, Wei W. Enhancing demand response and heating performance of air source heat pump through optimal water temperature scheduling: Method and application. Energy Build 2024;323:114839. https://doi.org/10.1016/j.enbuild.2024.114839.

[40] Gradwohl C, Maxim DC, Islam S, Kienberger T. Unlocking heat pump flexibility: A multi-objective optimisation approach for self sufficiency and energy costs. Energy Convers Manag 2025;334:119822. https://doi.org/10.1016/j.enconman.2025.119822.

[41] Langner F, Kovačević J, Zwickel P, Dengiz T, Frahm M, Waczowicz S, et al. Coordinated price-based control of modulating heat pumps for practical demand response and peak shaving in building clusters. Energy Build 2024;324:114940. https://doi.org/10.1016/j.enbuild.2024.114940.

[42] Chen X, Tao S, Sun Y, Wang H, Wang Y, Xing J, et al. Research on optimal scheduling method of solar assisted heat pump drying system based on demand response. Appl Therm Eng 2024;243:122414. https://doi.org/10.1016/j.applthermaleng.2024.122414.

[43] Gupta R, Morey J. Evaluation of residential demand response trials with smart heat pumps and batteries and their effect at the substation feeder. J Clean Prod 2023;403:136760. https://doi.org/10.1016/j.jclepro.2023.136760.

[44] Romero Rodríguez L, Sánchez Ramos J, Álvarez Domínguez S, Eicker U. Contributions of heat pumps to demand response: A case study of a plus-energy dwelling. Appl Energy 2018;214:191–204. https://doi.org/10.1016/j.apenergy.2018.01.086.

[45] Alimohammadisagvand B, Jokisalo J, Sirén K. Comparison of four rule-based demand response control algorithms in an electrically and heat pump-heated residential building. Appl Energy 2018;209:167–79. https://doi.org/10.1016/j.apenergy.2017.10.088.

[46] Hao H, Corbin CD, Kalsi K, Pratt RG. Transactive Control of Commercial Buildings for Demand Response. IEEE Trans Power Syst 2017;32:774–83. https://doi.org/10.1109/TPWRS.2016.2559485.

[47] Birrer E, Picard C, Huber P, Bolliger D, Klapproth A. Demand response optimized heat pump control for service sector buildings. Comput Sci Res Dev 2017;32:25–34. https://doi.org/10.1007/s00450-016-0320-9.

[48] Zhang H, Xiao F, Zhang C, Li R. A multi-agent system based coordinated multi-objective optimal load scheduling strategy using marginal emission factors for building cluster demand response. Energy Build 2023;281:112765. https://doi.org/10.1016/j.enbuild.2022.112765.

[49] Xiaozhi G, Pengyu C, Qiyang Z, Hsiung-Cheng L, Huiqin S, Shiwei X, et al. Operational optimization for electric heat pump clusters based on demand response considering user comfort. Energy Build 2025;347:116272. https://doi.org/10.1016/j.enbuild.2025.116272.

[50] Naderi S, Heslop S, Chen D, MacGill I, Pignatta G. Consumer cost savings, improved thermal comfort, and reduced peak air conditioning demand through pre-cooling in Australian housing. Energy Build 2022;271:112172. https://doi.org/10.1016/j.enbuild.2022.112172.

[51] Kaspar K, Nweye K, Buscemi G, Capozzoli A, Nagy Z, Pinto G, et al. Effects of occupant thermostat preferences and override behavior on residential demand response in CityLearn. Energy Build 2024;324:114830. https://doi.org/10.1016/j.enbuild.2024.114830.

[52] Haizea Analytics, King Abdullah University of Science and Technology. Köppen Climate Explorer 2026. https://koppen.earth/ (accessed May 11, 2026).

[53] Catrini P, La VM, Piacentino A. Energy flexibility assessment of commercial buildings in cooling season based on advanced modeling of rooftop units. Appl Therm Eng 2025;279:127511. https://doi.org/10.1016/j.applthermaleng.2025.127511.

[54] Di Silvestre ML, Gallo P, Restifo GL, Sanseverino ER, Sciume G, Zizzo G. A blockchain platform for Demand Response in Mediterranean islands: a smart contract for remuneration. In: IECON 2022–48th Annual Conference of the IEEE Industrial Electronics Society; 2022. p. 1–6. https://doi.org/10.1109/IECON49645.2022.9969002.

[55] Tina GM, Aneli S, Gagliano A. Technical and economic analysis of the provision of ancillary services through the flexibility of HVAC system in shopping centers. Energy 2022;258:124860. https://doi.org/10.1016/j.energy.2022.124860.

[56] Morrone B, De Santis M, Rubino L, Djellal H. Evaluating the role of thermal mass in energy flexibility: A comparative study of insulated concrete forms and conventional building materials. J Phys Conf Ser 2025;3143:012051. https://doi.org/10.1088/1742-6596/3143/1/012051.

[57] Massana J, Pous C, Burgas L, Melendez J, Colomer J. Short-term load forecasting in a non-residential building contrasting models and attributes. Energy Build 2015;92:322–30. https://doi.org/10.1016/j.enbuild.2015.02.007.

[58] Chantzis G, Giama E, Papadopoulos AM. Building Energy Flexibility Assessment in Mediterranean Climatic Conditions: The Case of a Greek Office Building. Appl Sci 2023;13:7246. https://doi.org/10.3390/app13127246.

[59] Novosel T, Feijoo F, Duić N, Domac J. Impact of district heating and cooling on the potential for the integration of variable renewable energy sources in mild and Mediterranean climates. Energy Convers Manag 2022;272:116374. https://doi.org/10.1016/j.enconman.2022.116374.

[60] Hadded MH, Dardouri S, Arıcı M, Sghaier J. Towards sustainable housing in Tunisia: Optimizing passive and hybrid ventilation strategies across various climatic zones. Energy Rep 2026;15:108922. https://doi.org/10.1016/j.egyr.2025.108922.

[61] Tellache A, Lazri Y, Laafer A, Attia S. Adaptive Thermal Comfort Assessment in Residential Buildings Under Current and Future Mediterranean Climate Scenarios. Buildings 2025;15:3171. https://doi.org/10.3390/buildings15173171.

[62] Noorollahi Y, Rezaei M, Mirzaei M. Energy systems modeling for maximizing renewable energy share in fossil fuel dominated Mediterranean climate. Environ Prog Sustain. Energy 2023;42. https://doi.org/10.1002/ep.14255.

[63] Young M, Less BD, Dutton SM, Walker IS, Sherman MH, Clark JD. Assessment of peak power demand reduction available via modulation of building ventilation systems. Energy Build 2020;214:109867. https://doi.org/10.1016/j.enbuild.2020.109867.

[64] de Chalendar JA, McMahon C, Fuentes Valenzuela L, Glynn PW, Benson SM. Unlocking demand response in commercial buildings: Empirical response of commercial buildings to daily cooling set point adjustments. Energy Build 2023;278:112599. https://doi.org/10.1016/j.enbuild.2022.112599.

[65] New OS. Challenges in Covering Buildings' Thermal Load. Energy Performance of Buildings. Cham: Springer International Publishing; 2016. p. 271–90.

[66] Mugnini A, Polonara F, Arteconi A. Energy flexibility in residential buildings clusters. E3S Web of Conferences 2020;197:03002. https://doi.org/10.1051/e3sconf/202019703002.

[67] Bagheri A, Genikomsakis KN, Ioakimidis CS. Implementation of System Identification Techniques and Optimal Control for RC Model Selection by Means of TRNSYS Simulation Results and Experimental Data. Buildings 2022;12:1625. https://doi.org/10.3390/buildings12101625.

[68] Deru M, Field K, Studer D, Benne K, Griffith B, Torcellini P, et al. U.S. Department of Energy Commercial Reference Building Models of the National Building Stock. 2011.

[69] Ente Nazionale Italiano di Unificazione (UNI). UNI/TR 11552:2014, Opaque envelope components of buildings - Thermo-physical parameters 2014. https://store.uni.com/en/uni-tr-11552-2014 (accessed December 20, 2024).

[70] Congedo PM, Baglivo C, D'Agostino D, Albanese PM. Overview of EU building envelope energy requirement for climate neutrality. Renew Sustain Energy Rev 2024;202:114712. https://doi.org/10.1016/j.rser.2024.114712.

[71] Ente Nazionale Italiano di Unificazione (UNI). UNI EN ISO 7730, Ergonomics of the thermal environment - Analytical determination and interpretation of thermal

comfort using calculation of the PMV and PPD indices and local thermal comfort criteria 2006. https://store.uni.com/en/uni-en-iso-7730-2006 (accessed December 20, 2024).
[72] Dong Z, Boyi Q, Pengfei L, Zhoujian A. Comprehensive evaluation and optimization of rural space heating modes in cold areas based on PMV-PPD. Energy Build 2021;246:111120. https://doi.org/10.1016/j.enbuild.2021.111120.
[73] Lenzuni P. Compliance with limits of acceptability for thermal comfort, and implications for long-term comfort. Build Environ 2021;204:108067. https://doi.org/10.1016/j.buildenv.2021.108067.
[74] IMST-Group Instituto de Ingeniería Energética Universidad Politécnica de Valencia VS. IMST_ART v4.10, Advanced Refrigeration Technologies n.d. https://www.imst-art.com/?page_id=128 (accessed January 9, 2025).
[75] Llopis-Mengual B, Navarro-Peris E. Modeling the performance of electronic expansion valves in heat pumps under soft faults. Results Eng 2024;23:102832. https://doi.org/10.1016/j.rineng.2024.102832.
[76] Hassan AH, Corberán JM, Ramirez M, Trebilcock-Kelly F, Payá J. A high-temperature heat pump for compressed heat energy storage applications: Design, modeling, and performance. Energy Rep 2022;8:10833–48. https://doi.org/10.1016/j.egyr.2022.08.201.
[77] Corberan JM, Finn DP, Montagud CM, Murphy FT, Edwards KC. A quasi-steady state mathematical model of an integrated ground source heat pump for building space control. Energy Build 2011;43:82–92. https://doi.org/10.1016/j.enbuild.2010.08.017.
[78] Jafargholi H, Catrini P, Munith Kumar D, La Villetta M, Panno D. Mapping the performance of reversible air-to-water heat pump for improving energy savings estimation in energy flexibility scenarios. Energy Convers Manag 2024;315:118762. https://doi.org/10.1016/j.enconman.2024.118762.
[79] AERMEC. Magellano 2025. https://magellano.aermec.com/LogMe.aspx (accessed May 5, 2025).
[80] Michele Vio, Diego Danieli. Le centrali frigorifere. Milan, Italy: Editoriale Delfino; 2007.
[81] De Soto W, Klein SA, Beckman WA. Improvement and validation of a model for photovoltaic array performance. Sol Energy 2006;80:78–88. https://doi.org/10.1016/j.solener.2005.06.010.
[82] Sadio OD, Kouyaté M, Traoré PT, Barro FI. Determination of the Electrical Parameters of a Solar Cell in Steady State. Open Journal of Applied Sciences 2023;13:1834–43. https://doi.org/10.4236/ojapps.2023.1310144.
[83] Akter H, Howlader HOR, Mamud F, Saber AY, Yona A, Senjyu T. Optimal sizing and performance analysis of hybrid microgrid for remote island of developing country: Effect of sustainable parameters, benefits and installation barriers. Franklin Open 2024;6:100074. https://doi.org/10.1016/j.fraope.2024.100074.
[84] Weniger J, Tjaden T, Quaschning V. Sizing of Residential PV Battery Systems. Energy Procedia 2014;46:78–87. https://doi.org/10.1016/j.egypro.2014.01.160.
[85] Psarros GN, Papathanassiou SA. Electricity storage requirements to support the transition towards high renewable penetration levels – Application to the Greek power system. J Energy Storage 2022;55:105748. https://doi.org/10.1016/j.est.2022.105748.
[86] Sun Y, Saxena S, Pecht M. Derating Guidelines for Lithium-Ion Batteries. Energies (Basel) 2018;11:3295. https://doi.org/10.3390/en11123295.
[87] EGING PV. EG-(SERIES) M54-HLV 405Wp Technical Datasheet. Available at: Https://WwwGingroupIt/Prodotto/Eging-Pv-Eg-Seriesm54-Hlv-405wp, [Accessed July 2024] 2024.
[88] EASE. Electrochemical Energy Storage, Lithium-Ion Battery Technical Datasheet. Available at: Https://Www Ease-StorageEu/Wp Content/Uploads/2016/03/EASE_TD_LiIonPdf, [Accessed April 2024] 2024.
[89] Thomas Huld IP-P. Global irradiation and solar electricity potential in Italy. Joint Research Centre Institute for Energy and Transport, Renewable Energy Unit: European Commission; 2025. https://re.jrc.ec.europa.eu/pvg_download/map_pdfs/G_hor_IT.pdf (accessed October 28, 2025.
[90] Shabbir N, Kutt L, Astapov V, Jawad M, Allik A, Husev O. Battery Size Optimization With Customer PV Installations and Domestic Load Profile. IEEE Access 2022;10:13012–25. https://doi.org/10.1109/ACCESS.2022.3147977.
[91] Chatzigeorgiou NG, Theocharides S, Makrides G, Georghiou GE. A review on battery energy storage systems: Applications, developments, and research trends of hybrid installations in the end-user sector. J Energy Storage 2024;86:111192. https://doi.org/10.1016/j.est.2024.111192.
[92] Prezzo Unico Nazionale. Gestore Mercati Energetici (GME) 2023. https://www.mercatoelettrico.org/en/ (accessed May 5, 2025).
[93] Aste N, Leonforte F, Manfren M, Mazzon M. Thermal inertia and energy efficiency – Parametric simulation assessment on a calibrated case study. Appl Energy 2015;145:111–23. https://doi.org/10.1016/j.apenergy.2015.01.084.
[94] Verbeke S, Audenaert A. Thermal inertia in buildings: A review of impacts across climate and building use. Renew Sustain Energy Rev 2018;82:2300–18. https://doi.org/10.1016/j.rser.2017.08.083.
[95] Taylor J, McLeod R, Petrou G, Hopfe C, Mavrogianni A, Castaño-Rosa R, et al. Ten questions concerning residential overheating in Central and Northern Europe. Build Environ 2023;234:110154. https://doi.org/10.1016/j.buildenv.2023.110154.
[96] Darmanis M, Çakan M, Moustris KP, Kavadias KA, Nikas K-S-P. Utilisation of Mass and Night Ventilation in Decreasing Cooling Load Demand. Sustainability 2020;12:7826. https://doi.org/10.3390/su12187826.
[97] Veršić Z, Binički M, Nosil MM. Passive Night Cooling Potential in Office Buildings in Continental and Mediterranean Climate Zone in Croatia. Buildings 2022;12:1207. https://doi.org/10.3390/buildings12081207.
[98] Santamouris M, Kolokotsa D. Passive cooling dissipation techniques for buildings and other structures: The state of the art. Energy Build 2013;57:74–94. https://doi.org/10.1016/j.enbuild.2012.11.002.
[99] Nuytten T, Claessens B, Paredis K, Van Bael J, Six D. Flexibility of a combined heat and power system with thermal energy storage for district heating. Appl Energy 2013;104:583–91. https://doi.org/10.1016/j.apenergy.2012.11.029.
[100] Luo Z, Peng J, Cao J, Yin R, Zou B, Tan Y, et al. Demand Flexibility of Residential Buildings: Definitions, Flexible Loads, and Quantification Methods. Engineering 2022;16:123–40. https://doi.org/10.1016/j.eng.2022.01.010.
[101] International Energy Agency (IEA). The Future of Cooling 2018. https://www.iea.org/reports/the-future-of-cooling (accessed January 11, 2025).
[102] International Energy Agency (IEA). The Future of Heat Pumps 2022. https://www.iea.org/reports/the-future-of-heat-pumps (accessed June 10, 2026).